

EDITORIAL

Celebrating the 50th anniversary
of the Federacion Mexicana de Radiologia e Imagen (p. 135-137)

IN-DEPTH REVIEW

Pulmonary amyloidosis:
clinical, radiological and pathological correlation (p. 138-149)

FULL RESEARCH ARTICLES

Can the absence of breast artery calcifications on mammography
predict the absence of coronary artery calcifications? (p. 150-161)

Multimodality findings of sclerosing adenosis
on mammography, US and MRI in Mexican women (p. 162-174)

Transjugular intrahepatic portosystemic shunt in a private Mexican
medical setting: indications and hemodynamic and technical outcomes (p. 175-181)

Increased incidence of symptomatic venous thrombosis associated with
peripherally inserted central catheter in COVID-19 patients (p. 182-188)

Abnormal US findings of the shoulders in Mexican patients with
end-stage renal disease: association with long-term hemodialysis (p. 189-196)

CASE REPORT

Imaging findings in synchronous bilateral breast cancer:
a case report (p. 197-201)

IMAGES IN RADIOLOGY

Contrast-enhancement CT: aorticaval fistula
secondary to a ruptured abdominal aortic aneurysm (p. 202-203)



PERMANYER
www.permanyer.com

Official Journal of the



FEDERACIÓN MEXICANA DE RADIOLOGÍA E IMAGEN, A.C

A simple step to digital radiography



i550z

Digital Radiography Systems



+52 686-568-1904
 WhatsApp - +520686-606-4076
www.laicoinfo.com
 Mexicali, BC Mexico

The Synergy of Innovation and Health Imaging Solutions

Designed to help you see what matters most



DDR
 DYNAMIC DIGITAL RADIOGRAPHY

Dynamic Digital Radiology (DDR) enables clinicians to observe the dynamic motion of anatomical structures over time, enhancing diagnostic capabilities. **DDR provides a view of anatomy in motion, with a large field of view and low radiation dose.**

DDR is a promising platform for AI (Artificial Intelligence) applications. DDR is not fluoroscopy;

DDR is X-ray that Moves!



xraythatmoves.com

exa

Scalable and customizable to the exact requirements of your practice, our leading IT solutions manage medical imaging and patient data right across the healthcare spectrum, including PACS, RIS, specialty viewers and Billing.

Our Healthcare IT software solutions are packed with the all the speed, security and flexibility you need, anytime/anywhere viewing and a single integrated database across all modules.



KONICA MINOLTA

contact us: kmhalatinoamerica@konicaminolta.com

Learn more about our solutions with Workflow Solutions, Insights and Consulting



Visit <https://radiologia.bayer.com/es> or contact your sales advisor

Clear Direction From Diagnosis to Care

PP-WS-MX-0005-1

MyLab™ OMEGAeXP

Advanced Imaging in Motion



esaote
esaote.com

MedRent
medrent.mx

Carestream

Meet the
NEW
member
of the family

DRX-Rise

It's amazing!



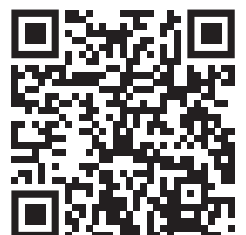
We have **EQUIPMENT** for all **YOUR NEEDS**



Right for **Today...** *Ready for Tomorrow.*



Scan the QR
and visit
the Virtual Hospital





Journal of the Mexican Federation of Radiology and Imaging

J Mex Fed Radiol Imaging

Volume 3. Number 3, July-September 2024

ISSN: 2938-1215

eISSN: 2696-8444

The *Journal of the Mexican Federation of Radiology and Imaging* (JMEXFRI) is the official journal of the Federación Mexicana de Radiología e Imagen. The aim of the journal is to disseminate scientific knowledge and technological developments for innovation in diagnostic and therapeutic radiology with original articles on basic and clinical aspects of modern radiology in an international context with global impact. JMEXFRI is published in American English with 4 issues per year (print and online) and the first issue was published in the first quarter of 2022. Articles undergo a rigorous, double-blind peer-review process. Publication of articles in JMEXFRI is free of charge and all published articles are open access.

The journal publishes the following types of manuscripts: *Full Research Article, Pictorial Essay, Brief Research Article, Technical Note, In-Depth Review, Case Report, Images in Radiology, and Editorial.*

EDITORIAL BOARD

EDITOR-IN-CHIEF

Mauricio Figueroa-Sanchez, M.D.

Department of Radiology, Antiguo Hospital Civil de Guadalajara "Fray Antonio Alcalde", Guadalajara, Jal., Mexico

ASSOCIATE EDITORS

Gerardo E. Ornelas-Cortinas, M.D.

*Centro Universitario de Imagen Diagnostica, Hospital Universitario
"Dr. Jose E. Gonzalez", Monterrey, N.L., Mexico*

Araceli Cue-Castro, M.D.

*Department of Computed Tomography, Hospital General
"Dr. Enrique Cabrera" SEDESA, Mexico City, Mexico*

Oscar A. Chavez-Barba, M.D.

*Department of Radiology,
Antiguo Hospital Civil de Guadalajara "Fray Antonio Alcalde",
Guadalajara, Jal., Mexico*

Ana M. Contreras-Navarro, M.D., M.Sc., Ph.D.

*Scientific Writing Workshop, JMEXFRI,
Zapopan, Jal., Mexico*

David Garza-Cruz, M.D.

*Department of Radiology, Hospital Angeles,
Torreon, Coah., Mexico*

J. Mario Bernal-Ramirez, M.D.

*Department of Medical Clinics, Centro Universitario de
Ciencias de la Salud, Universidad de Guadalajara,
Guadalajara, Jal., Mexico*

SCIENTIFIC TRANSLATOR EDITOR

Sergio Lozano-Rodriguez, M.D.

Research Office of the Vice Dean, Hospital Universitario "Dr. Jose E. Gonzalez", Monterrey, N.L., Mexico

BIostatistics ADVISER

Cesar N. Cristancho-Rojas, M.D., M.Sc.

School of Public Health, Oregon Health & Science University, Portland, OR., USA

DESIGN ADVISER

Jorge Mendez-Palacios, B.Sc.

Design Area, JMEXFRI. Zapopan, Jal., Mexico

NATIONAL EDITORIAL BOARD

HEAD AND NECK RADIOLOGY

Mario A. Campos-Coy, M.D.

*Centro Universitario de Imagen Diagnostica,
Hospital Universitario "Dr. Jose E. Gonzalez",
Monterrey, N.L., Mexico*

Eduardo D. Sarda-Inman, M.D.

*Diagnostico Especializado por Imagen,
Zapopan, Jal., Mexico*

GASTROINTESTINAL RADIOLOGY

Araceli Cue-Castro, M.D.

*Department of Computed Tomography,
Hospital General "Dr. Enrique Cabrera" SEDESA,
Mexico City, Mexico*

Adrian Negreros-Osuna, M.D., Ph.D.

*Departamento de Radiología,
Hospital Regional ISSSTE Monterrey,
Monterrey, N.L., Mexico*

Oscar A. Chavez-Barba, M.D.

*Department of Radiology,
Antiguo Hospital Civil de Guadalajara
"Fray Antonio Alcalde",
Guadalajara, Jal., Mexico*

OBSTETRIC AND GYNECOLOGIC RADIOLOGY

Dante R. Casale-Menier, M.D.

*Department of Radiology and Imaging,
Hospital Angeles,
Ciudad Juarez, Chih., Mexico*

Roberto J. Carrales-Cuellar, M.D.

*Department of Ecographic Diagnosis,
Radiología Especializada,
Guadalajara, Jal., Mexico*

BREAST RADIOLOGY

David F. Perez-Montemayor, M.D.

*General Direction,
Centro de Imagenología Integral IMAX,
Tampico, Tamps., Mexico*

Beatriz Gonzalez-Ulloa, M.D.

*Department of Breast Imaging,
Diagnostico Especializado por Imagen,
Guadalajara, Jal., Mexico*

Margarita L. Garza-Montemayor, M.D.

*Departamento de Imagen Diagnostica,
Centro de Cancer de Mama,
Hospital Zambrano Hellion, Tec Salud,
Monterrey, N.L., Mexico*

Karla M. Nuñez-Barragan, M.D.

*Women's Imaging Department,
Doctors Hospital East Auna
Monterrey, N. L., Mexico*

NUCLEAR AND MOLECULAR MEDICINE

Hugo E. Solis-Lara, M.D.

*Centro de Imagen Molecular,
Hospital Christus Muguerza Alta Especialidad,
Monterrey, N.L., Mexico*

NEURORADIOLOGY

Jorge Paz-Gutierrez, M.D.

*Department of Magnetic Resonance,
Centro Medico Puerta de Hierro,
Zapopan, Jal., Mexico*

Azalea Garza-Baez, M.D.

*Department of Radiology and Imaging,
Hospital Zambrano Hellion,
Tecnologico de Monterrey,
Monterrey, N.L., Mexico*

Perla M. Salgado-Lujambio, M.D.

*Dirección de Enseñanza,
Instituto Nacional de Neurología y
Neurocirugía "Manuel Velasco Suarez"
Mexico City, Mexico*

PEDIATRIC RADIOLOGY

Aida Perez-Lara, M.D.

*Department of Radiology, Hospital Español,
Mexico City, Mexico*

MUSCULOSKELETAL RADIOLOGY

Oscar A. Chavez-Barba, M.D.

*Department of Radiology, Antiguo Hospital Civil
de Guadalajara "Fray Antonio Alcalde",
Guadalajara, Jal., Mexico*

J. Francisco Diaz-Fernandez, M.D.

*Department of Radiology,
Hospital General "Agustin O'Horan",
Merida, Yuc., Mexico*

CHEST AND CARDIOVASCULAR RADIOLOGY

Sergio A. Criales-Vera, M.D.

*Department of Radiology and Imaging,
Instituto Nacional de Cardiología "Ignacio Chavez",
Mexico City, Mexico*

Harold Goerne, M.D.

*Department of Radiology, Hospital de Pediatría,
Instituto Mexicano del Seguro Social,
Guadalajara, Jal., Mexico*

Luis F. Alva-Lopez, M.D.

*Department of Radiology, Hospital Medica Sur,
Mexico City, Mexico*

GENITOURINARY RADIOLOGY

Sergio B. Peregrina-Gonzalez, M.D.

*Consultorio de Imagen,
Guadalajara, Jal., Mexico*

Araceli Cue-Castro, M.D.

*Department of Computed Tomography,
Hospital General "Dr. Enrique Cabrera" SEDESA,
Mexico City, Mexico*

Adrian Negreros-Osuna, M.D.

*Departamento de Radiología,
Hospital Regional ISSSTE Monterrey,
Monterrey, N.L., Mexico*

Benjamin Conde-Castro, M.D.

*Faculty of Medicine,
Universidad Nacional Autónoma de Mexico,
Mexico City, Mexico*

ULTRASOUND

Rosa M. Alanis-Salazar, M.D.

*Departamento de Radiología, UMF Guadalupe, ISSSTE,
Monterrey, NL., Mexico*

Victor M. Rodriguez-Peralta, M.D.

*Department of Radiology,
Fundacion de Cancer de Mama (FUCAM),
Oaxaca, Oax., Mexico*

David Garza-Cruz, M.D.

*Department of Radiology, Hospital Angeles,
Torreon, Coah., Mexico*

Manuel Hernandez-Cruz, M.D.

*Area de Ultrasonido,
Unidad de Ultrasonido Diagnostico,
Puebla, Pue. Mexico*

VASCULAR AND INTERVENTIONAL RADIOLOGY

Guillermo Elizondo-Riojas, M.D., Ph.D.

*Centro Universitario de Imagen Diagnostica,
Hospital Universitario "Dr. Jose E. Gonzalez",
Monterrey, N.L., Mexico*

Raul A. De Luna-Vega. M.D.

*Centro Universitario de Imagen Diagnostica,
Hospital Universitario "Dr. Jose E. Gonzalez",
Monterrey, N.L., Mexico*

ARTIFICIAL INTELLIGENCE

Guillermo Elizondo-Riojas, M.D., Ph.D.

*Centro Universitario de Imagen Diagnostica,
Hospital Universitario "Dr. Jose E. Gonzalez",
Monterrey, N.L., Mexico*

Adrian Negreros-Osuna, M.D.

*Departamento de Radiología,
Hospital Regional ISSSTE Monterrey,
Monterrey, N.L., Mexico*

J. Mario Bernal-Ramirez, M.D.

*Department of Medical Clinics,
Centro Universitario de Ciencias de la Salud,
Universidad de Guadalajara,
Guadalajara, Jal., Mexico*

Benjamin Conde-Castro, M.D.

*Faculty of Medicine,
Universidad Nacional Autónoma de México,
Mexico City, Mexico*

JUNIOR EDITORIAL BOARD

J. Mario Bernal-Ramirez, M.D.

*Department of Medical Clinics,
Centro Universitario de Ciencias de la Salud,
Universidad de Guadalajara,
Guadalajara, Jal., Mexico*

Ana K. Luna-Marroquin, M.D.

*Centro Universitario de Imagen Diagnostica,
Hospital Universitario "Dr. Jose E. Gonzalez",
Monterrey, N.L., Mexico*

M. Lourdes Garcia-Colmenero, M.D.

*Departamento de Radiología,
CID Centro de Imagen y Diagnostico
Guadalajara, Jal., Mexico*

Xavier A. Gonzalez-Ballesteros, M.D.

*Departamento de Radiología,
Hospital San Angel Inn Universidad,
Ciudad de Mexico, Mexico*

Adriana Parada-Gallardo, M.D.

*Department of Radiology,
Hospital General de Zapopan,
Zapopan, Jal., Mexico*

INTERNATIONAL EDITORIAL BOARD

HEAD AND NECK RADIOLOGY

Richard H. Wiggins, M.D.

*Department of Radiology and Imaging Sciences, School
of Medicine, University of Utah,
Salt Lake City, UT., USA*

Amy Juliano, M.D.

*Department of Radiology,
Massachusetts Eye and Ear,
Harvard Medical School,
Boston, MA., USA*

GASTROINTESTINAL RADIOLOGY

Jorge A. Soto, M.D.

*Department of Radiology, Boston Medical Center,
Boston, MA., USA*

Jorge Elias Jr. Ph.D.

*Departamento de Imagenes Medicas,
Oncologia e Hematologia,
Faculdade de Medicina Ribeirao Preto,
Universidade Sao Paulo Ribeirao Preto,
Sao Paulo, Brazil*

Valdair F. Muglia, M.D.

*Faculdade de Medicina de Ribeirão Preto,
Universidade de São Paulo, Ribeirão Preto,
Sao Paulo, Brazil*

Carlo Catalano, M.D.

*Department of Diagnostic Radiology
La Sapienza University of Rome
Rome, Italy*

OBSTETRIC AND GYNECOLOGIC RADIOLOGY

Luciana Pardini Chamie, M.D., Ph.D.
Centro de Diagnostico Ultrasonografico
Especializado en Imagen de la Mujer,
Sao Paulo, Brazil

BREAST RADIOLOGY

Javier Romero-Enciso, M.D.
Department of Radiology,
Fundacion Santa Fe,
Bogota, Colombia

NUCLEAR AND MOLECULAR MEDICINE

Begoña Martinez-Sanchis, M.D.
Department of Nuclear Medicine,
Hospital Universitario y Politecnico La Fe,
Valencia, Spain

Cesar N. Cristancho-Rojas, M.D., M.Sc.
School of Public Health,
Oregon Health & Science University,
Portland, OR., USA

NEURORADIOLOGY

Roy F. Riascos-Castaneda, M.D.
Department of Radiology and Neurosurgery,
Memorial Hermann Hospital System,
Houston, TX., USA

Rafael Rojas-Jasso, M.D.
Department of Radiology, Beth Israel,
Deaconess Medical Center,
Boston, MA., USA

Henrique Carrete Jr., M.D., Ph.D.
Department of Diagnostic Imaging,
Universidade de Sao Paulo,
Sao Paulo, Brazil

Carlos Torres, M.D.
Department of Diagnostic Imaging,
The Ottawa Hospital,
Ottawa, Canada

MUSCULOSKELETAL RADIOLOGY

Javier Fernandez-Jara, M.D.
Department of Radiology,
Hospital Universitario Sanitas La Zarzuela,
Madrid, Spain

Jose Luis del Cura, M.D.
Radiodiagnosis Service,
Hospital Universitario Donostia,
San Sebastian-Donostia, Spain

Diego F. Lemos, M.D.
Department of Radiology,
University of Vermont Medical Center,
Burlington, VT, USA

PEDIATRIC RADIOLOGY

George Bisset, M.D.
Department of Radiology, Children's Hospital
Pennsylvania, PA., USA

Sara Reis Teixeira, M.D., Ph.D.
Department of Radiology, Children's Hospital
Pennsylvania, PA. USA

CHEST AND CARDIOVASCULAR RADIOLOGY

Fernando R. Gutierrez, M.D.
Department of Radiology and Cardiothoracic Imaging,
The Mallinckrodt Institute of Radiology,
St. Louis, MO., USA

Jorge Carrillo-Bayona, M.D.
Department of Radiology,
Hospital Universitario Mayor,
Bogota, Colombia

Carlos S. Restrepo, M.D.
Department of Cardiothoracic Radiology,
Texas University,
San Antonio, TX., USA

Sebastian Rossini, M.D.

Department of Radiology,
Instituto Radiologico Mater Dei,
Buenos Aires, Argentina

Santiago Martinez-Jimenez, M.D.
Department of Radiology,
Saint Luke's Hospital of Kansas City,
Kansas City, KS., USA

L. Antonio Sosa-Lozano, M.D.
Department of Cardiothoracic Radiology,
Medical College of Wisconsin,
Milwaukee, WI., USA

GENITOURINARY RADIOLOGY

Daniela Stoisa, M.D.
Department of Radiology, Diagnostico Medico Oroño,
Rosario, Santa Fe, Argentina

Valdair F. Muglia, M.D.
Faculdade de Medicina de Ribeirao Preto,
Universidade de Sao Paulo Ribeirao Preto,
Sao Paulo, Brazil

ULTRASOUND

Edward G. Grant, M.D.
Department of Radiology, USC Norris Cancer Center,
Los Angeles, CA., USA

Juan P. Niedmann-Espinosa, M.D.
Department of Ecotomography,
Clinica Alemana de Santiago,
Santiago de Chile, Chile

VASCULAR AND INTERVENTIONAL RADIOLOGY

Manuel Cifrian-Perez, M.D., Ph.D.
Imaging Clinic Department,
Hospital Universitario y Politecnico La Fe,
Valencia, Spain

ARTIFICIAL INTELLIGENCE

Leonor Cerda-Alberich, Ph.D.
Imaging Clinic Department,
Hospital Universitario y Politecnico La Fe,
Valencia, Spain

Felipe Campos Kitamura, M.D., Ph.D.
Dasalnova, Dasa,
Sao Paulo, Brazil

GRAPHICAL ABSTRACTS COMMITTEE

Oscar A. Chavez-Barba, M.D.
Department of Radiology,
Antiguo Hospital Civil de Guadalajara
"Fray Antonio Alcalde",
Guadalajara, Jal., Mexico

Adriana Parada-Gallardo, M.D.
Department of Radiology,
Hospital General de Zapopan,
Zapopan, Jal., Mexico

J.M. Ignacio Lopez-Mendez, M.D.
Department of Radiology and Imaging,
Hospital de Especialidades, CMNO
Instituto Mexicano del Seguro Social,
Guadalajara, Jal., Mexico.

Juan Pablo Lopez-Gutierrez, M.D.
Department of Radiology and Imaging,
Hospital General de Zona 3,
Instituto Mexicano del Seguro Social
Aguascalientes, Ags., Mexico

Gerardo Llamas-Linares, M.D.
Centro Universitario de Imagen Diagnostica,
Hospital Universitario "Dr. Jose E. Gonzalez",
Monterrey, N.L., Mexico

Alejandra I. Castillo-Cervantes, M.D.
Centro Universitario de Imagen Diagnostica,
Hospital Universitario "Dr. Jose E. Gonzalez",
Monterrey, N.L., Mexico

A. Sofia Sanchez-Gomez, M.D.

Department of Radiology,
Grupo RIO Centro Integral de Diagnostico Medico.
Guadalajara, Jal., Mexico

SOCIAL MEDIA COMMITTEE

Guillermo Elizondo-Riojas, M.D., Ph.D.
Centro Universitario de Imagen Diagnostica,
Hospital Universitario "Dr. Jose E. Gonzalez",
Monterrey, N.L., Mexico

Oscar A. Chavez-Barba, M.D.
Department of Radiology,
Antiguo Hospital Civil de Guadalajara
"Fray Antonio Alcalde",
Guadalajara, Jal., Mexico

J. Mario Bernal-Ramirez, M.D.
Department of Medical Clinics,
Centro Universitario de Ciencias de la Salud,
Universidad de Guadalajara,
Guadalajara, Jal., Mexico

Adriana Parada-Gallardo, M.D.
Department of Radiology,
Hospital General de Zapopan,
Zapopan, Jal., Mexico

RADIOLOGICAL AND CLINICAL CORRELATION BOARD

GASTROENTEROLOGY

Linda E. Muñoz-Espinosa, M.D., Ph.D.
Liver Unit, Hospital Universitario
"Dr. Jose E. Gonzalez",
Monterrey, N.L., Mexico

David Marti-Aguado, M.D., Ph.D.
Servicio Medicina Digestiva,
Hospital Clinico Universitario,
Valencia, Spain

GASTROINTESTINAL AND GENERAL SURGERY

Carlos Nuño-Guzman, M.D., M.Sc.
Department of Surgery,
Antiguo Hospital Civil de Guadalajara
"Fray Antonio Alcalde",
Guadalajara, Jal., Mexico

OBSTETRICS AND GINECOLOGY

Sergio Fajardo-Dueñas, M.D., M.Sc.
Division of Obstetrics and Gynecology,
Nuevo Hospital Civil de Guadalajara,
Guadalajara, Jal., Mexico

NEUROLOGY

Jose L. Ruiz-Sandoval, M.D., M.Sc.
Department of Neurology,
Antiguo Hospital Civil de Guadalajara
"Fray Antonio Alcalde",
Guadalajara, Jal., Mexico

RHEUMATOLOGY

Monica Vazquez del Mercado-Espinosa,
M.D., Ph.D.
Division of Medicine,
Nuevo Hospital Civil de Guadalajara,
Guadalajara, Jal., Mexico.

CARDIOLOGY-PNEUMOLOGY

Jose M. Hernandez, M.D.
Department of Eocardiography, Doctors Hospital,
Monterrey, N.L., Mexico

PATHOLOGICAL ANATOMY

Marco A. Ponce-Camacho, M.D., Ph.D.
Department of Cytopathology, Doctors Hospital,
Monterrey, N.L., Mexico

ENDOCRINOLOGY

Jesus Zacarias Villarreal-Perez, M.D.
Department of Endocrinology,
Hospital Universitario "Dr. Jose E. Gonzalez",
Monterrey, N.L., Mexico

HEMATOLOGY

Carlos R. Best-Aguilera, M.D.
Department of Hematology,
Hospital General de Occidente. Secretaria de Salud
Zapopan, Jal., Mexico

PEDIATRIC NEUROLOGY

Daniel Perez-Rulfo Ibarra, M.D., Ph.D.
Departamento de Pediatría,
Antiguo Hospital Civil de Guadalajara
"Fray Antonio Alcalde",
Guadalajara, Jal., Mexico

GYNECOLOGICAL UROLOGY

Patricia I. Velazquez-Castellanos, M.D., M.Sc.
Department of Gynecology and Obstetrics,
Antiguo Hospital Civil de Guadalajara
"Fray Antonio Alcalde",
Guadalajara. Jal., Mexico

Follow us



<https://linkedin.com/company/jmexfri>



<https://instagram.com/jmexfri>



<https://facebook.com/jmexfri>



<https://youtube.com/@jmexfri>



<https://x.com/jmexfri>



Original papers should be deposited in their electronic version through the following URL:

<https://publisher.jmexfri.permanyer.com>



PERMANYER
www.permanyer.com

Permanyer Mexico

Temistocles, 315
Col. Polanco, Del. Miguel Hidalgo
11560 Ciudad de Mexico
mexico@permnyer.com

Permanyer

Mallorca, 310 – Barcelona (Cataluña), España
permnyer@permnyer.com

ISSN: 2696-8444

Ref.: 10130AMEX243



www.permanyer.com

Reproductions for commercial purposes:

Without the prior written consent of the publisher, no part of this publication may be reproduced, stored in a retrievable medium or transmitted, in any form or by any means, electronic, mechanical, photocopying, recording or otherwise, for commercial purposes.

Journal of the Mexican Federation of Radiology and Imaging is an open access publication with the Creative Commons license CC BY-NC-ND (<http://creativecommons.org/licenses/by-nc-nd/4.0/>).

The opinions, findings, and conclusions are those of the authors. The editors and publisher are not responsible and shall not be liable for the contents published in the journal.

© 2024 Federacion Mexicana de Radiologia e Imagen, AC. Published by Permanyer.

Celebrating the 50th anniversary of the Federación Mexicana de Radiología e Imagen

Mauricio Figueroa-Sanchez^{1,2,3*} , Gerardo E. Ornelas-Cortinas^{4,5} , and Ana M. Contreras-Navarro⁶ 

¹Radiology and Imaging Department, Antiguo Hospital Civil of Guadalajara “Fray Antonio Alcalde”, Guadalajara, Jalisco; ²University Center of Health Sciences, Universidad of Guadalajara, Guadalajara, Jalisco; ³Laboratorio Vascular S.C., Guadalajara, Jalisco; ⁴Radiology and Imaging Department, Doctors Hospital AUNA; ⁵Centro Universitario de Imagen Diagnostica, Hospital Universitario Dr. Jose E. Gonzalez, Monterrey, Nuevo Leon; ⁶Scientific Writing Editor, Journal of the Mexican Federation of Radiology and Imaging (JMEXFRI), Zapopan, Jalisco. Mexico

In the field of Mexican radiology, the Federación Mexicana de Radiología e Imagen (FMRI) [Mexican Federation of Radiology and Imaging] celebrates the 50th anniversary of its founding on November 23, 1974, in the city of Guadalajara, Jalisco, Mexico. Its original name was the Federación Mexicana de Sociedades de Radiología [Mexican Federation of Radiology Societies]. This organization brought together eight medical societies dedicated to the study of radiology and radiotherapy with the participation of a group of visionary medical radiologists: Ramon Barreda-Ramirez and Jose Manuel Cardoso-Ramon as delegates of the *Sociedad Mexicana de Radiología*, Jose Hugo Arredondo-Galan and Francisco Alanis-Camino as delegates of the *Sociedad Regiomontana de Radiología*, Augusto Reyes-Bolio and William M. Rosado-Nuñez as delegates of the *Sociedad de Radiología del Sureste*, Jose Aguilar-Guerrero and Jorge Falcon-Garcia as delegates of the *Sociedad Poblana de Radiología*, Gregorio Giacinti-Lopez and Ignacio Ramirez-Hernandez as delegates of the *Sociedad de Radiología del Centro*, Arturo Ramos-Echeverria and Mario Cosme Grijalva-Camou as delegates of the *Sociedad de Radiología del Noroeste*, Francisco Meduchi-Meduchi and Lindoro Anguiano-Castañeda as delegates of the *Sociedad Chihuahuense de Radiología*, and Juan Genaro Santoscoy-Gomez and Casimiro Ramirez-Jaime as delegates of the *Sociedad de Radiología de Guadalajara*. During the First General Assembly, Doctor Ramon Barreda-Ramirez was appointed president; Doctor Jose Hugo Arredondo-Galan was vice

president; Doctor Jose Manuel Cardoso-Ramon was secretary; and Doctor Jose Aguilar-Guerrero was treasurer. The statutes, delegates, and foundation of the Mexican Council of Radiodiagnosis and Radiotherapy were established at this first meeting and later renamed the Consejo Mexicano de Radiología e Imagen (CMRI) [the Mexican Council of Radiology and Imaging]. The CMRI certifies the professional knowledge of Mexican radiologists.

The FMRI sponsors many continuing medical education activities to support its associate members:

- Participation in national and international meetings and congresses. Almost every meeting or webinar organized by the FMRI has lectures and round tables with expert and trainee interaction.
- Multidisciplinary participation involving clinicians from other specialties, e.g., surgeons, neurologists, oncologists, gynecologists, etc.
- Dissemination, mainly via the FMRI website (<https://www.fmri.org>), of podcasts, radio programs, and social networks to educate the public and patients about the importance of imaging studies in the context of each patient.
- Promotion of a multidisciplinary approach in radiology programs, emphasizing the importance of radiologists communicating with clinicians who refer patients.
- Participation of radiologists in multidisciplinary teams for diagnosis, management, and development of diagnostic and therapeutic guidelines.

***Corresponding author:**

Mauricio Figueroa-Sanchez

E-mail: figueroa_sanchez@hotmail.com

2696-8444 / © 2024 Federación Mexicana de Radiología e Imagen, A.C. Published by Permanyer. This is an open access article under the CC BY-NC-ND (<https://creativecommons.org/licenses/by-nc-nd/4.0/>).

Received for publication: 21-06-2024

Accepted for publication: 27-06-2024

DOI: 10.24875/JMEXFRI.M24000081

Available online: 03-10-2024

J Mex Fed Radiol Imaging. 2024;3(3):135-137

www.JMEXFRI.com

- Participation in international academic and scientific societies: the Radiological Society of North America (RSNA), the European Society of Radiology (ESR), the International Society of Radiology (ISR), the Sociedad Española de Radiología Médica (SERAM), the French Society of Radiology (SFR), the Sociedad Chilena de Radiología (SOCHRADI), Colegio Brasileño de Radiología y Diagnóstico por Imágenes (CBR), Sociedade Paulista de Radiologia e Diagnóstico por Imagem (SPR), the Asociación Colombiana de Radiología (ACR), the Federación Argentina de Radiología (FAARDIT), the Asociación Costarricense de Radiología e Imágenes Médicas (ACRIM), and the Colegio Interamericano de Radiología (CIR).
- Promote sponsor support for granting scholarships to residents of national radiology programs to participate in national and international conferences and to carry out academic activities in national and international programs.

Radiologists are often isolated in imaging settings, which has led to a loss of visibility on three critical fronts: the patient, the referring clinician, and the hospital or radiology unit authorities¹. FMRI has advocated for the visible radiologist who participates in clinical discussions and collaborates with other specialists to optimize diagnostic and interventional therapeutic procedures by connecting technology with patients, clinicians, and resource management. The visible radiologist represents the roles of a teacher, researcher, and innovator in radiology¹. FMRI promotes their integration and recognition to ensure that the radiologist's visibility is meaningful and impactful.

The FMRI has collaborated with the CMRI to promote certification with additional qualifications in breast imaging, neuroradiology, pediatric radiology, musculoskeletal system, neurological endovascular therapy, and vascular and interventional radiology. Interestingly, in the current field of medicine, interventional radiology has had great growth and technological advances. Up to December 2023, the CMRI has recognized 160 interventional radiologists with additional qualifications. Interventional radiology differs from other radiology subspecialties in its combination of knowledge and ability to apply diagnostic skills with specific requirements for manual dexterity². It has many overlaps with operative surgery, as the work of an interventional radiologist often has a therapeutic aim in addition to the usual diagnostic goal underpinning most radiologists' work².

Radiology is a critical field in modern medicine where medical imaging plays an essential role in the diagnosis

and treatment of most diseases³. Artificial intelligence (AI) is revolutionizing clinical medicine, especially radiology⁴. Every day, more and more research papers are published describing how new deep learning and generative transformer algorithms can be trained to recognize subtle patterns and abnormalities in medical images that may be difficult for the human eye to detect^{3,4}. Radiology benefits from AI's prowess in recognizing imaging patterns, which increases radiologists' skills and optimizes tasks such as scheduling and radiation monitoring, preliminary analysis, and filling out structured reports in radiology units or departments. AI can automate tasks such as image normalization, quality improvement, and noise reduction, leading to better visualization of anatomical structures and lesions. Moreover, AI is now being used to prioritize urgent radiology cases, ensuring timely treatment in life-threatening cases, a crucial improvement in emergency care⁴. While integrating AI into radiology significantly improves diagnostic and operational efficiency, it also poses ethical, legal, and educational challenges⁴. FMRI supports training in residency programs and continuing education courses to achieve an optimal level of AI knowledge to provide patients with dignified, fair, and respectful care and to keep in mind that *"Behind an image is a human being who deserves personalized care with high scientific quality"*⁵.

At the same time that the FMRI was founded, the Sociedad Mexicana de Radiología e Imagen granted the *Revista Mexicana de Radiología* to the FMRI⁶. The last issue of this journal was published in 1991, after which it was discontinued⁶. In the following three decades, the FMRI devoted itself intensively to strengthening training and promoting new groups of radiologists in the country⁶. In 2022, the FMRI launched the *Journal of the Mexican Federation of Radiology and Imaging* (JMeXFRI) to disseminate scientific knowledge and technological developments for innovation in diagnostic and therapeutic imaging with a global impact⁷. The JMeXFRI (www.jmexfri.com) is published in English and has four issues per year. Articles undergo a rigorous, double-blind peer review process before acceptance for publication. The national and international editorial board is composed of renowned experts. The following types of articles are published in the JMeXFRI: Editorials, Full Research Articles, Brief Research Articles, In-Depth Review Articles, Pictorial Essays, Technical Notes, Case Reports, and Images in Radiology.

Medical residency programs in Mexico do not include a program to develop scientific article writing skills; therefore, many health research studies do not culminate in

scientific publication⁷. Approximately 400 theses are concluded yearly in Diagnostic and Therapeutic Imaging residency, subspecialty, and high specialty programs in Mexico⁷. These theses are usually presented at scientific meetings and national and international congresses. Despite offering novel results and noteworthy findings, many of these original research projects have never been published. To address this problem, the FMRI carried out the “*Primera Convocatoria Nacional 2023*” for “*The Best Theses to be Published in the JMeXFRI*,” targeting professors and residents in the field of Diagnostic and Therapeutic Imaging in Mexico⁷. The professors and residents of the selected top-tier theses were supported by the Scientific Writing Workshop (SWW) for optimal writing and publication of original scientific articles in JMeXFRI⁷. The SWW engages participants from all over the country and relies on *virtual interactivity* through distance learning strategies via the Internet⁷.

Since its founding, the FMRI has sought excellence, leadership, and commitment to advancing radiology. Currently, 29 societies and colleges of radiology and imaging in Mexico are affiliated with the FMRI (Supplementary data, Table 1). The FMRI has an unbeatable level of recognition and relationships with major radiology organizations worldwide and actively participates in multinational collaborative committees and forums.

We gather to attend the *National Congress of Diagnostic and Therapeutic Imaging* in the city of Guadalajara Jalisco, Mexico, where the FMRI was founded 50 years ago. We congratulate and recognize all those who have contributed to its success and consolidation, from the founders, who had the vision of unifying the Mexican radiologists with a common goal, to the current members who work with dedication and passion for Mexican radiology. *On behalf of all the members of the Mexican radiology community in Mexico, we congratulate the FMRI on its first 50 years!*

Funding

Not applicable.

Conflicts of interest

The authors disclose no potential conflicts of interest.

Ethical disclosures

Protection of individuals. Not applicable.

Confidentiality of data. Not applicable.

Right to privacy and informed consent. The authors declare no ethical responsibilities as confidential information was not presented.

Use of artificial intelligence for generating text. The authors state that they did not use generative artificial intelligence in preparing this article.

Supplementary data

Supplementary data are available online in the journal, DOI: 10.24875/JMEXFRI.M24000081. These data are provided by the corresponding author and published online for the reader's benefit. The contents of supplementary data are the sole responsibility of the authors.

REFERENCES

1. Dante R. Casale-Menier. The visible radiologist: balancing clinical expertise and technological Advances. *J Mex Fed Radiol Imaging*. 2023; 2(4):223-225 doi:10.24875/JMEXFRI.M23000059.
2. Brady A. Is independent Interventional Radiology the future? *J Mex Fed Radiol Imaging*. 2024;3(2):69-71. doi:10.24875/JMEXFRI.M24000070.
3. Elizondo-Riojas G. Radiologists' empowerment through artificial intelligence. *J Mex Fed Radiol Imaging*. 2023;2(2):79-81. doi: 10.24875/JMEXFRI.M23000044.
4. Elizondo-Riojas G, Negreros-Osuna AA, Bernal-Ramirez JM, Conde-Castro B. Artificial intelligence in radiology. *J Mex Fed Radiol Imaging*. 2024;3(2):72-81. doi:10.24875/JMEXFRI.M24000073.
5. Omelas-Cortinas GE, Cantu-Salinas AC, Luna-Marroquin AK. Knowledge of bioethical principles and elements of responsibility in radiology. *J Mex Fed Radiol Imaging*. 2023;2(2):98-105. doi:10.24875/JMEXFRI.M23000047.
6. Guerrero Avendaño G. Diferencias y similitudes entre la SMRI, CMRI y CNMERI. *Anal Radiol Mex*. 2002;1(3):483-484.
7. Contreras-Navarro AM. What I talk about when I talk about writing scientific articles. *J Mex Fed Radiol Imaging*. 2023;2(3):149-151. doi:10.24875/JMEXFRI.M23000057.

Pulmonary amyloidosis: clinical, radiological, and pathological correlations

Jorge A. Carrillo-Bayona¹*, Paula A. Navarrete-Sosa², Javier L. Galindo-Pedraza²,
Fernando Polo-Nieto³, and Santiago Martinez-Jimenez⁴

¹Radiology Unit, Hospital Universitario Mayor, Mederi, Rosario University, Bogota, Colombia; ²Pneumology Unit, Hospital Universitario Mayor, Mederi, Rosario University, Bogota, Colombia; ³Pathology Unit, Hospital Universitario Mayor, Mederi, Rosario University, Bogota, Colombia; ⁴Department of Radiology, New York University Langone Health, New York, New York, United States of America

ABSTRACT

Amyloidosis is a heterogeneous group of disorders associated with extracellular amyloid deposits. Pulmonary amyloidosis can occur as a localized or systemic disease with amyloid deposits in various lung structures, including the alveolar septum, blood vessel wall, airways, and lymph nodes. The spectrum of amyloidosis-associated lung disease includes nodular amyloidosis (NA), cystic amyloidosis (CA), diffuse alveolar-septal amyloidosis (DASA), and tracheobronchial amyloidosis (TBA). TBA and NA are the most common. Other manifestations in the thorax, including cardiac, mediastinal, and chest wall amyloidosis, are beyond the scope of this review. Various findings on affected lung structures are seen in imaging examinations, especially computed tomography (CT). NA presents as bilateral pulmonary nodules with a peripheral predominance toward the lung bases with smooth, lobulated, or spiculated contours. CA presents bilateral and predominantly peribronchovascular or subpleural multiple cysts of varying size. DASA presents reticulation, thickening of the interlobular septa and the peribronchovascular interstitium, micronodules, ground-glass appearance, and consolidation. TBA presents concentric thickening of the tracheal wall, a long segment with secondary stenosis, nodular thickening of the tracheal wall, calcification, and airway obstruction. Pleural amyloidosis can present diffuse or localized pleural thickening with pleural plaques and/or pleural effusion.

Keywords: Amyloidosis. Amyloid. Amyloidoma. Solitary pulmonary nodule. Interstitial lung disease. Tracheal disease.

INTRODUCTION

Amyloidosis is a large group of multisystemic disorders with heterogeneous clinical presentations characterized by pathological deposition of amyloid fibrils in the extracellular matrix of organs¹. In 1854, the pathologist Rudolf Ludwig Karl Virchow named this deposition material amyloid, which means “starch-like”^{2,3}. The first case of amyloidosis of the lower respiratory tract

was described by Lesser⁴ in 1877 in an autopsy. Congo red staining of amyloid was discovered incidentally in 1922 by Hans Hermann Benhold² while measuring blood volume. It was in the late 1960s when the usefulness of the histopathologic diagnosis of amyloidosis was described. In the second half of the 20th century, with the advent of electron microscopy, it was found that amyloid consists of protein fibrils with wide biochemical heterogeneity³. Amyloid fibrils are formed by

*Corresponding author:

Jorge A. Carrillo-Bayona
E-mail: jorcarbay@hotmail.com

Received for publication: 12-06-2024

Accepted for publication: 23-06-2024

DOI: 10.24875/JMEXFRI.M24000078

Available online: 03-10-2024

J Mex Fed Radiol Imaging. 2024;3(3):138-149

www.JMeXFRI.com

2696-8444 / © 2024 Federación Mexicana de Radiología e Imagen, A.C. Published by Permanyer. This is an open access article under the CC BY-NC-ND (<https://creativecommons.org/licenses/by-nc-nd/4.0/>).

a conformational and metabolic change of proteins (amyloidogenic), which causes their deposition as insoluble aggregates in tissues^{1,3}.

The most representative proteins associated with amyloidosis lung disease are immunoglobulin light-chain-derived amyloid (AL) formerly called *primary amyloidosis*, wild-type transthyretin amyloid (ATTRwt) and its variants (ATTRv), formerly called age-related or senile systemic amyloidosis, and serum apolipoprotein A (AA) amyloidosis, formerly called *secondary amyloidosis*, which is associated with chronic inflammatory diseases that increase this acute phase reactant (e.g., autoimmune diseases, tuberculosis, bronchiectasis, or neoplasms)^{5,6}.

The distinction between localized and systemic amyloidosis depends on the production site of the fibril precursor protein and its deposition⁵. It is considered systemic when the site of synthesis is anatomically distant from the site of deposition⁵. Mortality associated with systemic amyloidosis is commonly attributed to infiltration of the heart, followed by complications arising from pulmonary infiltration⁷. However, pulmonary amyloidosis is not usually diagnosed in the early stages of the disease.

EPIDEMIOLOGY

The number of amyloidosis cases has increased in the United Kingdom, with systemic AL amyloidosis being the most common (55%)⁸. This finding contrasts with a decrease in systemic AA amyloidosis (13% before 2010 to 3% in 2016-2019) and an increase in ATTRwt amyloidosis (less than 3% before 2010 to 25% in 2016-2019)⁸. AL amyloidosis is a rare disease with an incidence of 6-14.3 per million person-years and a prevalence of 8-65 per million person-years in Western countries^{9,10}. In the United States, the incidence of AL amyloidosis has increased^{11,12}. Each year, 3852 new cases are diagnosed, with an incidence of approximately 1.2-1.4% per 100,000 person-years and a mean age of 63 years^{11,12}. ATTR amyloidosis has been found in 15-25% of autopsies in adults over 85 years. The estimated incidence of ATTRwt and ATTRv amyloidosis is 155-191 cases and 5.2 cases per million people/year, respectively^{13,14}.

The prognosis of the entity varies according to the type of amyloidosis and the organ affected. It is estimated that 25% of patients with AL amyloidosis die within 6 months of diagnosis, and 25% of patients with ATTR amyloidosis die within 24 months^{13,14}. The heart and kidneys are the most commonly affected organs in

systemic AL amyloidosis. These presentations have a survival rate of less than 50% five years after diagnosis, a significantly impaired quality of life, and a high financial burden on healthcare systems^{9,10}. In ATTR amyloidosis, the heart is the most affected organ, followed by the peripheral nervous system^{13,14}. The kidney, spleen, adrenal glands, liver, or intestine are organs affected by AA amyloidosis^{15,16}. The prognosis and mortality in these patients correlate with serum amyloid A protein concentration, advanced age, and impaired renal function^{15,16}.

Localized amyloidosis occurs mainly in the mucosa¹⁷. The predominant amyloid type is AL (91%), while a lower percentage of cases are associated with AA (6%) or ATTR amyloidosis (2%)¹⁷. In general, the disease occurs more frequently between the fifth and sixth decades of life and without gender predominance^{17,18}. Localized AL amyloidosis has a better 10-year survival rate (80.3-96.0%) than systemic AL amyloidosis (26.0-51.9%)^{18,19}. Localized amyloidosis rarely progresses to systemic disease, so the clinical manifestations relate to the affected organ. The larynx, trachea, bronchi, and lung parenchyma are commonly affected structures, followed by the skin, the gastrointestinal tract, and the urinary tract^{17,18}.

PHYSIOPATHOLOGY

The International Society of Amyloidosis (ISA) recommends that the term “amyloid” be used for any β -sheet fibril (natural or synthetic, functional or non-functional), and the term “amyloidosis” corresponds to amyloid fibrils in a living organism⁵. Currently, 42 human amyloid fibril proteins are known, of which 14 occur as systemic deposits, 24 as local amyloids, and 4 as systemic or local deposits⁵.

The basic structure of amyloid is the fibril, defined as an aggregate structure of insoluble proteins consisting of protofilaments in a configuration of folded β -sheets that are superimposed and resistant to proteolysis^{5,13}. Approximately 95% of amyloid consists of fibrillar proteins. The remaining 5% is the P component of serum amyloid and other glycoproteins²⁰. Increased synthesis, point mutations, or proteolytic cleavages can induce structural changes in the precursor proteins that predispose to an aggregation state¹. Exposure to denaturing stimuli, such as low pH, elevated temperatures, proteolysis, and ions, causes an unfolding of the polypeptide chains of amyloidogenic proteins, which may be exposed to hydrophobic residues during

refolding that promote the protein's susceptibility to misfolding and self-aggregation^{1,20}. Amyloid fibrils are stabilized by polar hydrogen bonds between parallel chains, and their intermediate aggregates are stabilized by hydrophobic and electrostatic interactions¹.

Amyloid fibril deposition causes cell toxicity, tissue damage, and organ dysfunction through a direct cytotoxic effect, leading to mitochondrial dysfunction, oxidative stress, and apoptosis¹. However, the precise mechanisms of tissue damage are not fully understood. Lysosomal dysfunction appears to be the main cause of impaired autophagy and amyloid-induced proteotoxicity²¹.

DIAGNOSIS

The gold standard for diagnosing amyloidosis is histopathologic confirmation of amyloid fibrils with identification of their crystallographic diffraction patterns using stains such as thioflavin T and Congo red^{5,20}. Amyloid is birefringent with Congo red under polarized light microscopy and produces a mixture of blue-green, yellow-green, or typical "green birefringence," depending on the optical configuration of the filters². Amyloid can also be stained with metachromatic dyes such as crystal violet²⁰.

A biopsy of an organ infiltrated by amyloid carries a high risk of bleeding. An organ biopsy is not considered necessary to confirm AL amyloidosis in the presence of a compatible syndrome and monoclonal gammopathy¹³. If systemic disease is suspected, a biopsy can be performed at various anatomical sites: subcutaneous abdominal fat (sensitivity 78-100%), labial salivary glands (sensitivity 61%), rectal mucosa (sensitivity 75-85%), and bone marrow (sensitivity 57%). A lower diagnostic yield has been described in patients with ATTR amyloidosis^{13,22,23}. Another diagnostic alternative is immunoelectron microscopy, which combines immunohistochemistry and electron microscopy with gold-labeled antibodies^{24,25}. Congo red-based light microscopy and immunoelectron microscopy are equally sensitive for systemic forms (79% and 76.1%, respectively), with the latter being more specific in abdominal fat samples (100% vs. 79.7%, $p < 0.001$)²⁴. The sensitivity for both techniques decreases in AL κ amyloidosis (sensitivity 71%) or ATTR amyloidosis (sensitivity 43%)²⁴.

The amyloid molecule involved in the disease can be identified by immunohistochemistry (AA amyloid and immunoglobulin λ and κ light chains) or mass spectrometry, a technique with a good diagnostic yield, but complex and expensive^{22,24,25}. Immunohistochemistry using immunofluorescence or immunoperoxidase can

Table 1. Types of pulmonary amyloidosis

Description
Nodular amyloidosis (NA)
Cystic amyloidosis (CA)
Diffuse alveolar-septal amyloidosis (DASA)
Tracheobronchial amyloidosis (TBA)

be performed on frozen or paraffin-embedded samples. However, interpretation can be affected by the background staining of the tissue^{20,25}.

Once the diagnosis of amyloidosis is established, the systemic disease should be assessed with a blood count, renal and liver function tests, proteinuria, serum protein electrophoresis, immunofixation, an electrocardiogram, and an echocardiogram²². Scintigraphy with a radiolabeled serum amyloid P component is a sensitive and highly specific method for detecting AA deposits or visceral AL amyloid^{22,26}.

PULMONARY AMYLOIDOSIS

Amyloid deposits are located in various lung structures, including the alveolar septum, blood vessel wall, airways, and lymph nodes. The spectrum of clinical manifestations and imaging findings includes nodular amyloidosis (NA), cystic amyloidosis (CA), diffuse alveolar-septal amyloidosis (DASA), and tracheobronchial amyloidosis (TBA) (Table 1). TBA and NA are the most common²⁷⁻²⁹. NA is commonly associated with localized forms of the entity^{27,29}. DASA is rare and usually associated with systemic amyloidosis^{27,29}. The mean survival after diagnosis is longer in patients with localized disease²⁷.

In general, the prevalence of pulmonary alterations in systemic AL amyloidosis in histopathologic studies is 36-90%⁷. In a Mayo Clinic study of 76 autopsies between 1997 and 2014, AL amyloidosis was described in many patients with amyloidosis and pulmonary disease (76%), with a lower percentage of cases associated with ATTR amyloidosis (22%)⁷. The pattern of pulmonary vascular involvement (97%) and DASA (78%) was more frequent than TBA (29%), mainly in AL amyloidosis and less frequently in ATTRwt amyloidosis.

The Kiel Amyloid Registry of Heidelberg, Germany, in a study of 207 lung samples between 2006 and 2017, reported that AL amyloidosis was the most common type (AL λ in 141 cases and AL κ in 27 cases). Localized amyloidosis was the most common (90.1%) with a predominant NA pattern¹⁹. The mean age was 67 years

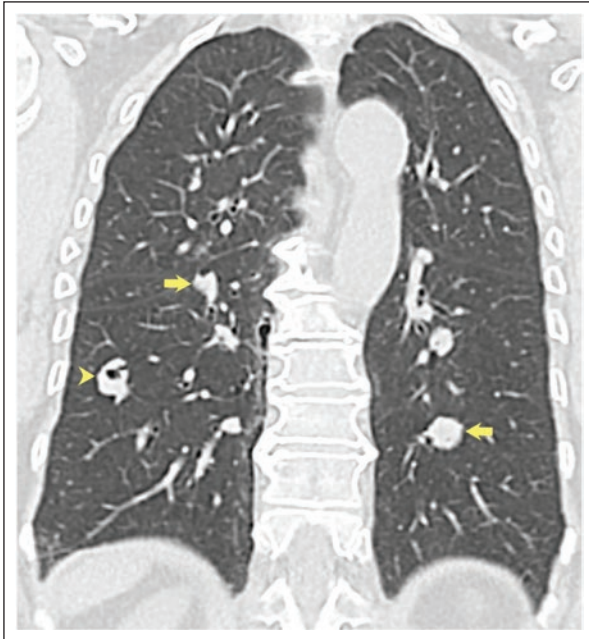


Figure 1. Nodular amyloidosis. A chest CT coronal reconstruction shows solid pulmonary nodules in the lower lobes (arrows) with nodule cavitation in the right lower lobe (arrowhead).

CT: computed tomography.

(range 24-88). Patients with ATTR amyloidosis had a higher mean age (79 years) and it was observed more commonly in men (80%) than those with AL amyloidosis (54.7%).

The type of presentation also varied with age. In a Heidelberg University Hospital cohort study, 67 patients were examined between 2002 and 2018, AL amyloidosis was diagnosed in 61 cases (NA n = 41 and TBA n = 20)²⁸. The mean age for NA, TBA, and systemic pulmonary parenchymal amyloidosis was 67 (range 37-81), 56 (range 39-77), and 58 (range 44-75) years, respectively. In a retrospective review of 55 cases of pulmonary amyloidosis from the Mayo Clinic between 1980 and 1993, imaging findings of a reticulonodular interstitial pattern were found in 35 patients with systemic amyloidosis (mean age 64; range 41-90)²⁷. Localized pulmonary amyloid was found in 11 patients, and 7 (mean age 67 years; range 43-78 years) had amyloidomas. Four TBA cases were reported (mean age 62; range 35-85).

The clinical manifestations of systemic amyloidosis are nonspecific and include fatigue, edema, weight loss, dyspnea, and orthostatic hypotension¹³. Some signs, such as macroglossia and periorbital purpura, may be

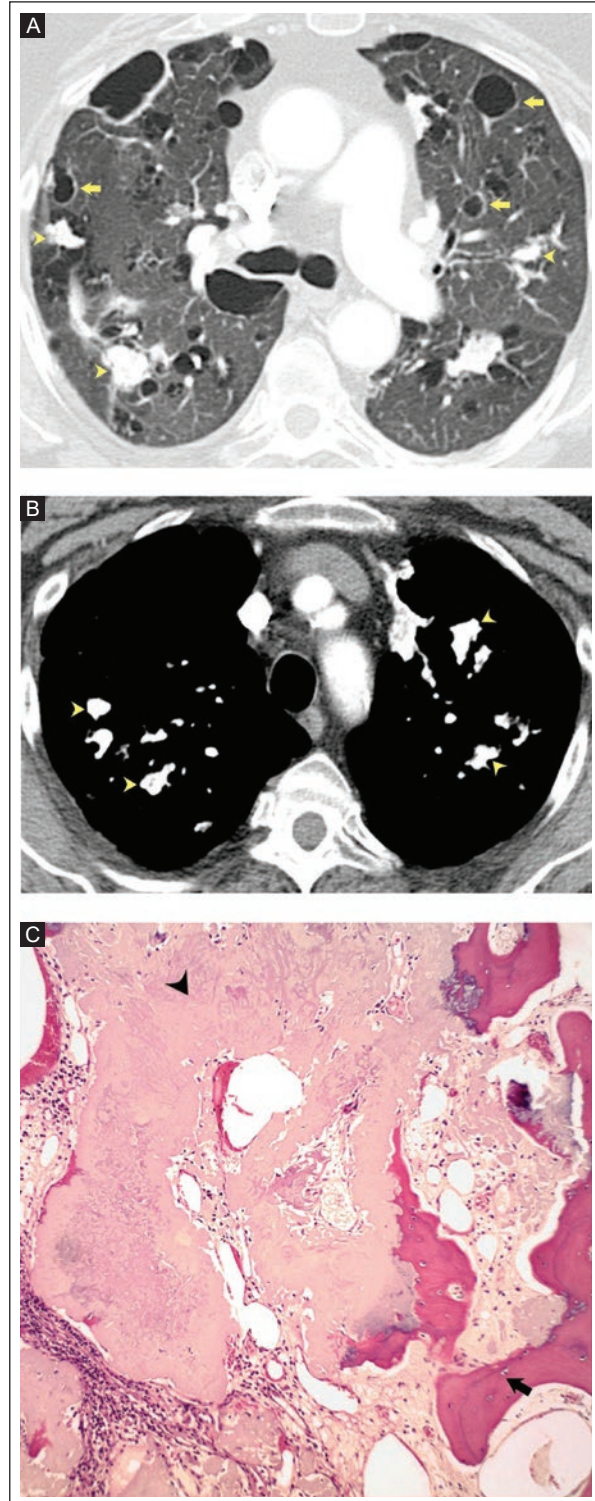


Figure 2. Nodular–cystic calcified amyloidosis. Chest CT axial view. **A:** the lung window shows thin-walled cysts (arrows) in the upper lobes with associated nodules (arrowheads). **B:** the mediastinal window shows calcification of the pulmonary nodules (arrowheads). **C:** the histopathologic findings show amorphous amyloid deposits (arrow) between ossification areas (arrowhead).

CT: computed tomography.

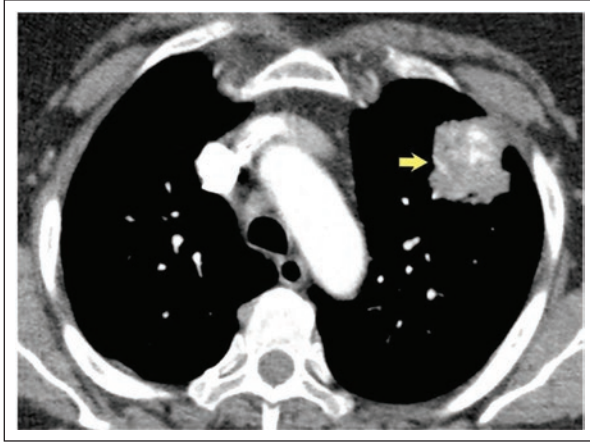


Figure 3. Amyloidoma. Chest CT, axial view, showing subpleural mass in the left upper lobe, solid, irregular contour, with calcifications (arrow).

CT: computed tomography.

specific for AL amyloidosis but occur in only 15% of patients^{13,24}. Non-cardiac signs in ATTR amyloidosis include carpal tunnel syndrome, lumbar spinal stenosis, biceps tendon rupture, small fiber neuropathy, and autonomic dysfunction¹³. Pulmonary disease can be associated with nonspecific respiratory symptoms, particularly cough, which is more common in patients with TBA than in patients with pulmonary parenchymal amyloidosis (90% vs. 46%)²⁸.

NODULAR AMYLOIDOSIS

NA is characterized by localized (single or multiple) tumor-like amyloid deposits in the lung parenchyma²⁰. NA has been described more frequently in patients with localized AL or AL/AH (mixed immunoglobulin light-chain/heavy-chain) amyloidosis and is three times more common in κ -type light-chain immunoglobulins than λ -type light-chain immunoglobulins²⁰. NA is less frequently described in patients with systemic AL or specific types of localized amyloidosis such as AA, ATTRwt, and AB2M/AL (light-chain/mixed immunoglobulin light-chain β 2)²⁰. In a significant percentage of cases, NA is associated with lymphoproliferative disorders, particularly extra-nodal marginal zone lymphoma of mucosa-associated lymphoid tissue (MALT)³⁰⁻³². An association between NA and systemic autoimmune diseases has been demonstrated, most commonly in Sjögren's syndrome³⁰⁻³². These diseases are thought to promote the synthesis and local accumulation of light chains³⁰⁻³².

NA most commonly manifests in the seventh decade of life, with a mean age of 65.5 years (range 36-80 years)¹⁸. The natural history of NA is relatively benign, asymptomatic with slow progression, has no impact on survival, and is often discovered incidentally on imaging examination^{4,18,29}. The behavior of the nodules is variable. They can remain stable, progressively increase in number and size, or sometimes decrease in size³³. NA is the most common form of pulmonary amyloidosis in patients with Sjögren's syndrome. However, it is a rare cause of pulmonary opacities in this population (0-2% of symptomatic patients)³⁴. It occurs almost exclusively in women (96.5%) in the sixth decade of life after the diagnosis of Sjögren's syndrome (median 7 years) and mostly the AL type^{31,34}. Cases with concomitant lymphoma or lymphoid interstitial pneumonia have been described in patients with Sjögren's syndrome and NA³⁴.

Imaging findings

Imaging examination, especially computed tomography (CT), shows bilateral pulmonary nodules (83%) with peripheral predominance toward the lung bases with smooth, lobulated, or spiculated contours^{28,29}. The nodules may have central or punctate calcification (41%) or cavitation (15%)²⁸ (Figure 1). In most cases, lesions are less than 10 mm in diameter, but masses up to 15 cm in diameter have been described²⁷. The nodules are usually numerous, and more than 10 lesions are described in 59% of patients³³. Most nodules are solid, but in multiple nodules, at least one calcified nodule can be found in 82% of cases³³ (Figure 2A-C). Zamora et al.³³ described partially solid or ground-glass nodules in 65% of patients.

The term amyloidoma refers to pseudotumoral amyloid deposits (single or multiple) without systemic amyloidosis. Patients are generally asymptomatic, and deposits are usually incidental findings on imaging³⁵ (Figure 3). Larger amyloidomas may invade adjacent anatomical structures causing secondary clinical manifestations suggesting alternative diagnoses (primary or metastatic neoplasms)³⁵. On magnetic resonance imaging, amyloidomas are isointense to muscle on T1 images and slightly hypointense on T2 images and may show heterogeneous enhancement³⁵. Positron emission tomography (PET) with fluorodeoxyglucose lacks sensitivity and specificity for diagnosing amyloidosis and does not differentiate between amyloidosis and primary or secondary neoplasia^{35,36}.

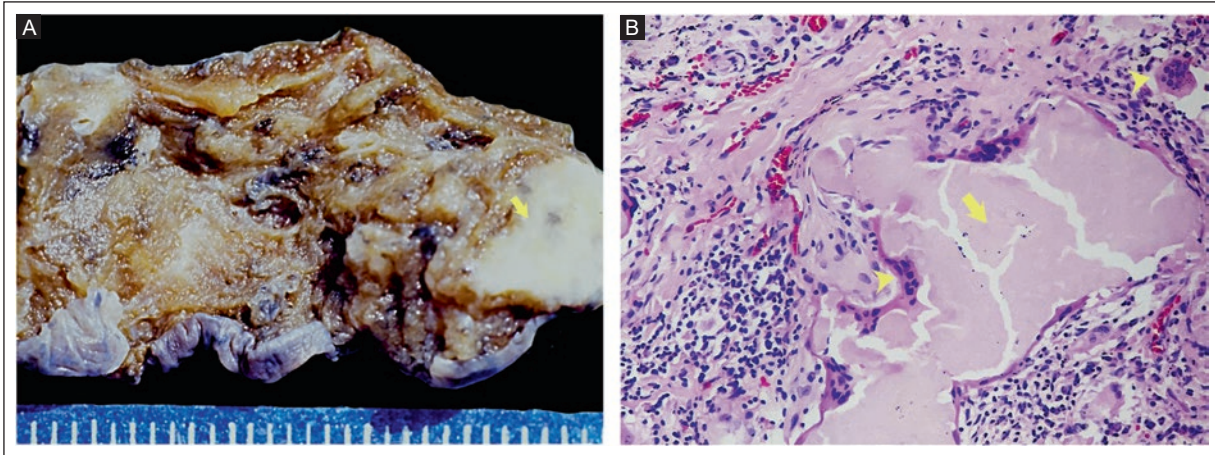


Figure 4. Nodular amyloidosis. **A:** segmentectomy showing lung parenchyma with subpleural nodule 7 mm in diameter, solid, white with irregular borders (arrow). **B:** histopathologic findings (HE 40x): eosinophilic acellular amorphous material (arrow) with multinucleated giant cells (arrowheads) and lymphoplasmacytic inflammation.

HE: hematoxylin and eosin.

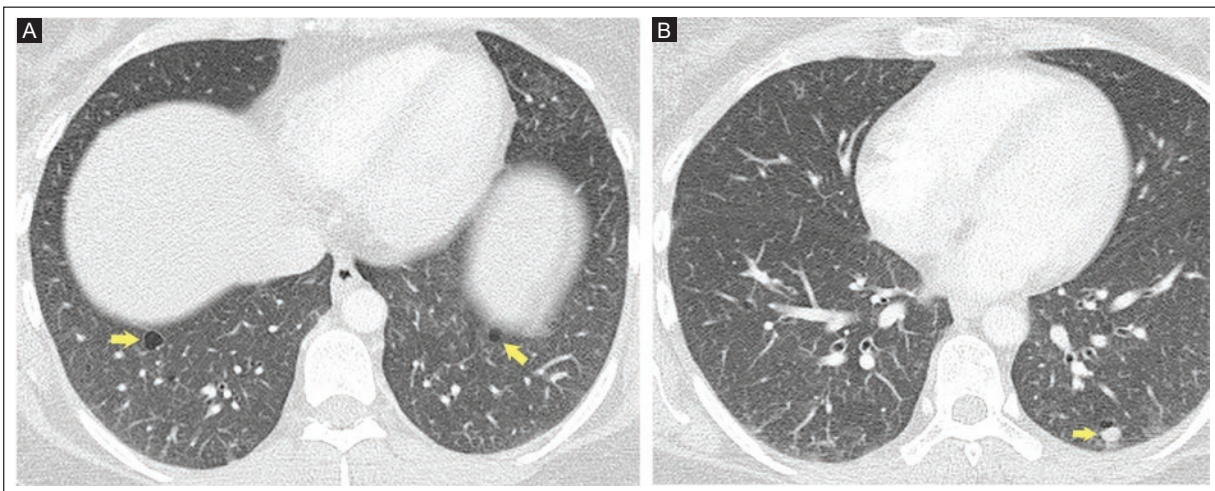


Figure 5. Cystic amyloidosis. Chest CT, axial view. **A:** thin-walled cysts in the lower lobes (arrows). **B:** same patient with a solid nodule in the left lower lobe (arrow).

CT: computed tomography.

The differential diagnosis of NA is broad and includes metastatic disease, multicentric primary lung neoplasms, lymphoproliferative disorders, and granulomatous diseases (tuberculosis and histoplasmosis), among others³⁷.

Histopathologic findings

Macroscopic examination of the lung shows nodules ranging in size from 0.4 to 15 cm (Figure 4A). Histologically, the nodules are well demarcated and consist of homogeneous, acellular, densely eosinophilic

material that may be associated with small clusters of lymphocytes, plasma cells, multinucleated giant cells, calcifications, and bone metaplasia²⁰ (Figure 4B).

CYSTIC AMYLOIDOSIS

CA is rare. In many patients, the cysts are associated with solid nodules (Figures 5A, B and 6). Patients may be asymptomatic, and symptomatic cases present a wide spectrum of clinical manifestations, including cough, dyspnea, and hemoptysis in severe cystic lung disease³³.

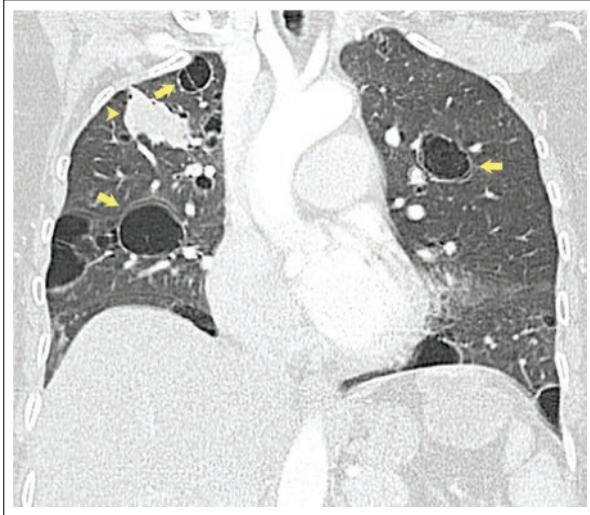


Figure 6. Cystic amyloidosis and amyloidoma. Chest CT coronal reconstruction showing multilobar, bilateral, spherical, thin-walled pulmonary cysts (arrows). Septa in the right apical cyst (arrows). Solid mass in the right upper lobe with lobulated contours corresponding to an amyloidoma (arrowhead).

CT: computed tomography.

Most amyloidosis cases with lung cysts correspond to patients with localized AL amyloidosis and are associated with systemic autoimmune diseases, most commonly Sjögren's syndrome and MALT pulmonary lymphoma^{28,33}. CA and lymphocytic interstitial pneumonia, characteristically also associated with pulmonary cysts, have been described simultaneously in some patients with Sjögren's syndrome^{28,33}. In patients with Sjögren's syndrome and pulmonary cysts, the presence of solid nodules or calcifications is suggestive of CA, and the simultaneous presence of centrilobular ground-glass nodules and cysts is suggestive of lymphocytic interstitial pneumonia³³.

In a cohort of 187 patients with pulmonary amyloidosis from the Mayo Clinic (1997-2010), 11.2% of patients had CA. In the group of patients with cysts, 62% were women with a median age of 61 years (range 26-91) and 57% had associated autoimmune disease, particularly Sjögren's syndrome (83%)³³.

The pathophysiology of pulmonary cysts in amyloidosis is not clear. Some authors postulate that the cysts are formed by a valve mechanism secondary to partial obstruction of the distal airways by amyloid deposits and inflammatory cells, particularly mature lymphocytes and plasma cells³². It has been suggested that amyloid deposition in the pulmonary capillaries may lead to ischemia and destruction of the alveolar wall³⁸. It is also proposed that, similar to light-chain deposition

disease, the recruitment of macrophages induces the production of metalloproteinases that degrade elastic fibers and collagen, leading to the formation of cysts^{39,40}. However, cysts and nodules may have imaging manifestations similar to those of light-chain deposition disease; in the latter, the structure of amyloid fibrils is not recognized on histopathologic examination⁴⁰.

Imaging findings

A report on cystic lung disease associated with amyloidosis (22 patients) describes multiple cysts (more than 10) in 67% of patients, bilateral (100%), predominantly basal (43%), peribronchovascular (90%) or subpleural (90%), spherical (100%) or lobular (95%), with a wall thickness of less than 2 mm (81%), and varying size, <1 cm (100%) and between 1 and 2 cm in 81% of cases³³ (Figure 7A). Solid or calcified nodules related to the cyst wall are described³³. On follow-up, cysts tend to increase in size and number less frequently than nodules³³.

Histopathologic findings

Respiratory epithelium and lymphoid infiltrates line the cysts, and amyloid deposits are found in the wall³¹. The bronchiole wall is dilatated and thickened with eosinophilic material, lymphoid hyperplasia, or follicular bronchiolitis^{31,33} (Figure 7B).

DIFFUSE ALVEOLAR-SEPTAL AMYLOIDOSIS

DASA is related to amyloid deposits in the alveolar septa and blood vessel wall^{20,41}. Most cases are associated with systemic AL amyloidosis and in a much smaller proportion to systemic AA, systemic ATTRwt, and systemic hereditary ATTR amyloidosis^{20,37}. DASA is described in 12% of patients with Sjögren's syndrome in association with different amyloid types (AA and AL)³⁴. The prognosis of patients with DASA is poor, with a median survival of 13 months in untreated patients, and may worsen in patients with heart failure (less than 4 months)⁴¹.

Most patients with DASA have generalized symptoms that reflect the systemic nature of the underlying disease⁴¹. Dyspnea is the most common clinical manifestation. The frequency of respiratory symptoms is lower than expected, as a high percentage of pulmonary infiltration has been described in autopsies of patients with systemic amyloidosis⁴¹. Isolated cases of pulmonary arterial hypertension associated with

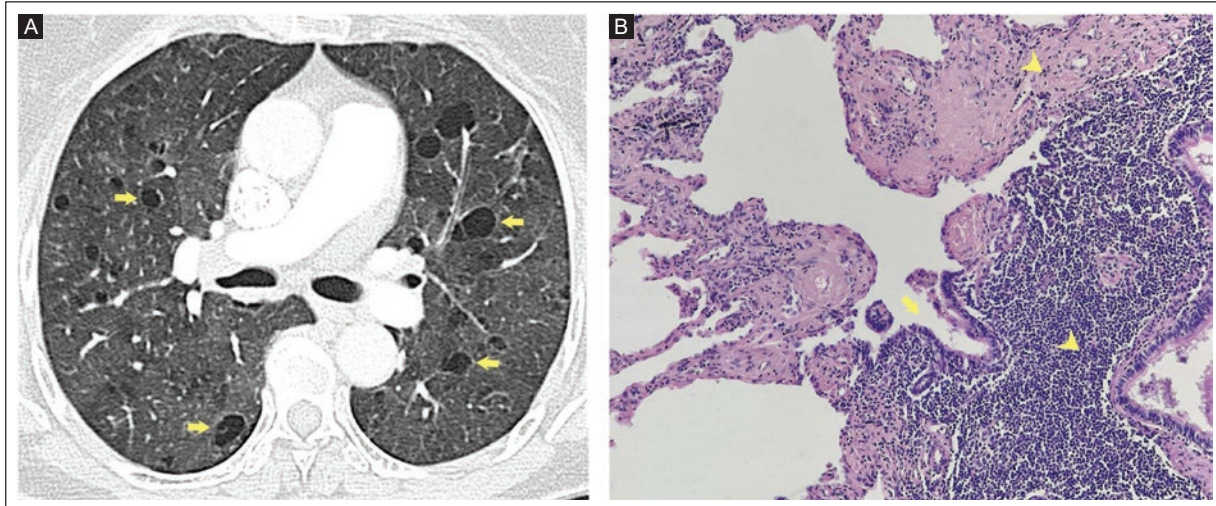


Figure 7. Cystic amyloidosis. Chest CT, axial view. **A:** spherical, smooth-contour, thin-walled lung cysts in the upper lobes (arrows). **B:** histopathologic findings (HE 20 \times). Dilated bronchiole (arrow) with submucosal thickening (arrowheads), lymphoid hyperplasia, and eosinophilic amorphous material. CT: computed tomography; HE: hematoxylin and eosin.

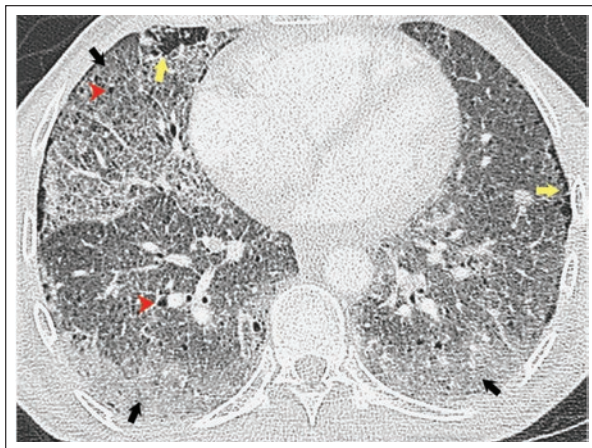


Figure 8. Alveolar hemorrhage associated with amyloidosis. Chest CT axial view showing multilobar ground glass (black arrows), bilateral pulmonary cysts (red arrowheads), and paraseptal emphysema (yellow arrows).

CT: computed tomography.

amyloidosis and related to amyloid deposition in the blood vessels causing vasoconstriction and proliferation of smooth muscle and endothelium have been reported⁴². On the contrary, diffuse alveolar hemorrhage has been described in patients with systemic amyloidosis due to alterations in the alveolar wall caused by amyloid deposition^{37,43} (Figure 8).

Imaging findings

The CT chest findings are extensive and include reticulation, interlobular septa thickening, peribronchovascular

interstitium thickening, micronodules, ground glass, and consolidation⁴¹. Micronodularity may be distributed perilymphatically, similar to that described in patients with lymphangitic carcinomatosis^{29,44} (Figure 9A). Less commonly, cysts, calcifications, pleural effusion, and mediastinal adenomegaly are described in these patients^{41,45}. The associated basal emphysematous changes are explained by damage to the alveolar walls⁴⁶.

The differential diagnosis by imaging is related to radiologic markers such as silicosis, sarcoidosis, lymphangitic carcinomatosis, and entities belonging to the group of interstitial lung disease in patients with reticulation as the most evident abnormality on a CT chest scan⁴¹.

Histopathologic findings

On gross examination, the lung is uniformly rubbery with a sponge-like appearance²⁰. Histology shows eosinophilic amyloid deposits in the alveolar septa^{20,41}. The vessel walls are frequently affected, where small nodules may be formed^{20,41}. Few plasma cells may be present, and multinucleated giant cells are rare^{20,41} (Figure 9B).

TRACHEOBRONCHIAL AMYLOIDOSIS

This form of amyloidosis is characterized by focal, multifocal, or diffuse submucosal deposits of amyloid in the trachea, the main bronchi, and, in exceptional cases, the segmental bronchi^{47,48}. It occurs more frequently

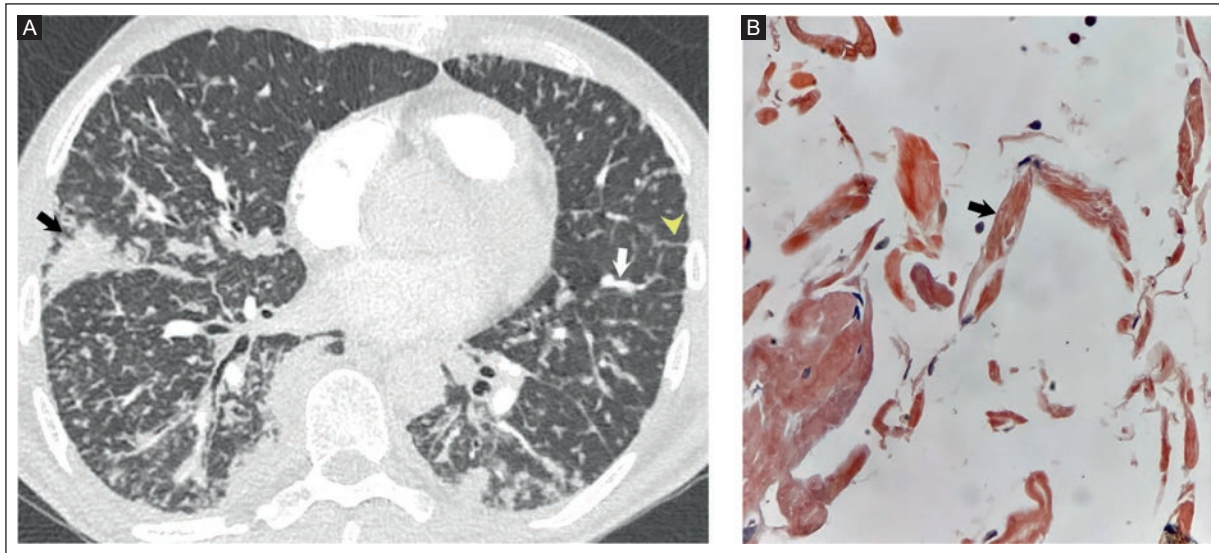


Figure 9. DASA. **A:** chest CT axial view showing periarterolar micronodularity (white arrow), thickening of the peribronchovascular interstitium, nodular thickening of the interlobular septa (arrowhead), and subpleural consolidation (black arrow) in the lateral segment of the middle lobe and the posterior segment of the left lower lobe. **B:** DASA with Congo Red staining (40×) shows septal thickening with salmon-colored amorphous material (black arrow).

CT: computed tomography. DASA: diffuse alveolar–septal amyloidosis.

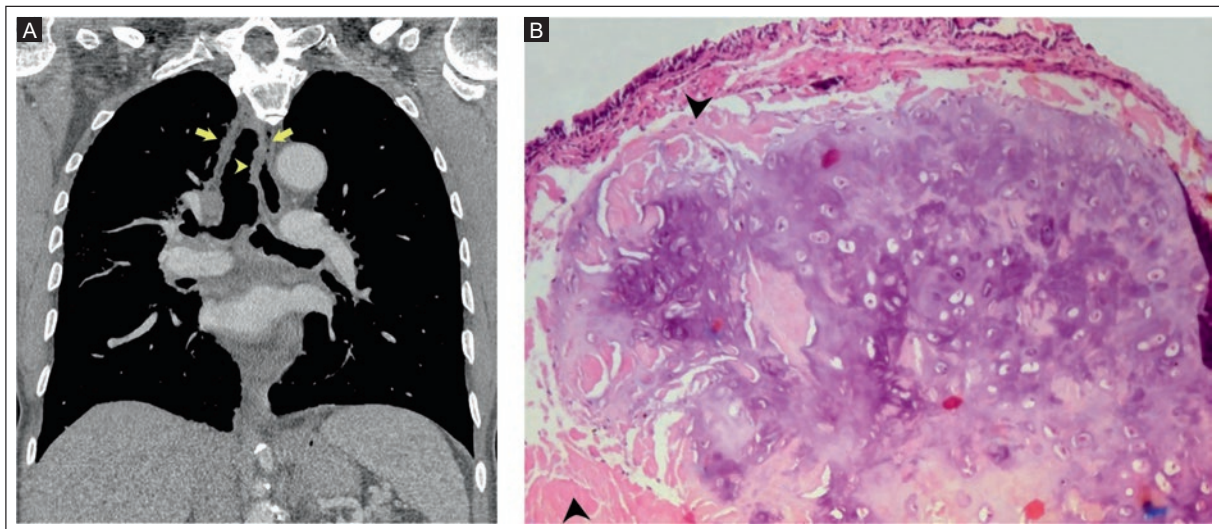


Figure 10. Tracheobronchial amyloidosis. **A:** chest CT coronal reconstruction showing trachea wall (arrows) and large bronchi thickening with nodularity in the tracheal mucosa (arrowhead). **B:** histopathologic findings (HE 4×). Tracheal wall with predominantly submucosal amyloid deposits surrounding the cartilage (arrowheads).

CT: computed tomography; HE: hematoxylin and eosin.

in men than women (1.6:1) between the fifth and sixth decades of life⁴⁷⁻⁵¹. Most cases correspond to localized AL amyloidosis and are less commonly associated with systemic AL amyloidosis or AA^{20,48}. The course of TBA is indolent, and the development of systemic amyloidosis in the natural history of the

entity has not been described⁵². As in other patients with localized AL amyloidosis, clonal proliferation of a small number of B cells has been noted adjacent to light-chain amyloid deposits⁵³.

The clinical manifestations are related to airway narrowing and inflammation, including cough, dyspnea,

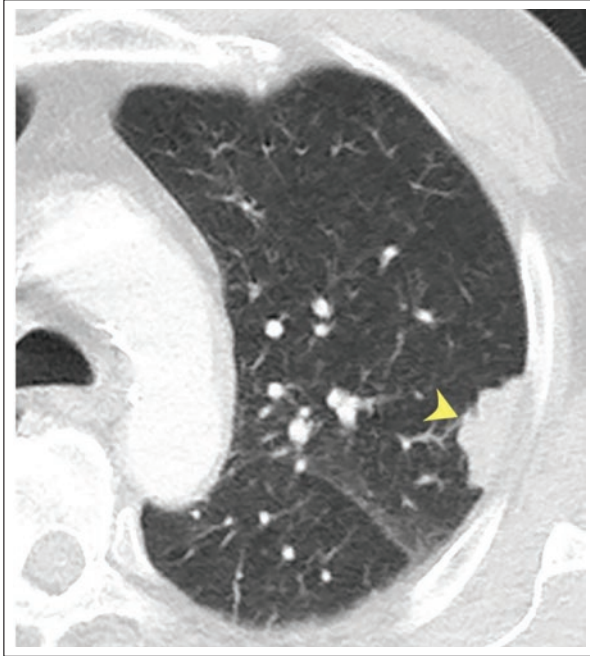


Figure 11. Pleural amyloidosis. Chest CT, axial view showing left apical focal pleural thickening (plaque) with lobulated contours (arrowhead). CT: computed tomography.

hemoptysis, wheezing, chest pain, and stridor^{47,49-51}. Patients are often treated for years with a diagnosis of chronic bronchitis or asthma^{47,52}. Patients with severe proximal disease have airway obstruction requiring dilatation or surgical treatment, and patients with the middle and distal third tracheal or main bronchus have atelectasis or recurrent infections of the lung parenchyma or airways^{47,49-52}.

Bronchoscopy can identify circumscribed yellow plaques, generally multifocal, nodules, or diffuse infiltration⁴⁷. The lesions are predominantly proximal and associated with friable, inflamed, and irregular mucosa^{47,50,52}. A biopsy by bronchoscopy confirms the diagnosis of TBA and is useful in treating stenotic lesions^{47,50,51}.

Laryngeal amyloidosis may coexist in patients with TBA⁵¹. The larynx is the most common site of amyloidosis in the head and neck region. The anatomical structures infiltrated by amyloid include the laryngeal ventricles, vestibule, vocal cords, epiglottis, and arytenoepiglottic folds⁵⁴. Larynx amyloidosis is more common in men, with a mean age of 46 years (range 9-84). It presents with clinical dysphonia (96%) and dyspnea (27%)^{54,55}.

Imaging findings

The main TBA findings on CT examination are concentric thickening of the tracheal wall (>3 mm) and a

long segment with secondary stenosis^{28,48,52}. It is possible to detect nodular thickening of the tracheal wall (60%), calcification (53%), and airway obstruction (47%)^{28,48,52}. Other less common findings on CT are solid pulmonary nodules, mediastinal adenomegaly, atelectasis, and bronchiectasis^{28,48,52} (Figure 10A).

The differential diagnosis of TBA on CT includes granulomatosis with polyangiitis, granulomatous diseases (tuberculosis or sarcoidosis), and inflammatory bowel disease. The alteration of the posterior membrane of the trachea in patients with TBA allows differentiation of this entity from others with similar tomographic findings, such as relapsing polychondritis and osteochondroplastic tracheobronchopathy⁵⁴.

Histopathologic findings

Irregular wall thickening with yellow, gray, or white lesions can be observed macroscopically²⁰. Histologically, the deposits consist of predominantly submucosal eosinophilic material surrounding seromucous glands and cartilage plates, plasma cells, multinucleated giant cells, calcifications, and ossification²⁰ (Figure 10B).

PLEURAL AMYLOIDOSIS

Pleural disease due to amyloidosis is underreported in most series. However, in the work by Brandeliek et al.²⁸, pleural plaques are described in 25% of patients, most without pleural effusion. Pleural amyloidosis is rare in localized forms and is generally associated with systemic amyloidosis⁵⁶. The most common forms of amyloidosis with pleural disease include AL amyloidosis (70.4%), ATTR amyloidosis (16.3%), and AA amyloidosis (8.2%)²¹. The mean age at presentation was 63 years (range 16-92 years), with older patients being more frequently affected (91.9% older than 50 years)⁵⁷. The majority of patients were men (61.2%), with dyspnea, chest pain, and cough as symptoms⁵⁷.

The pleural fluid detected in patients with amyloidosis may be explained by increased pulmonary venous pressure associated with restrictive cardiomyopathy or nephrotic syndrome or by altered fluid reabsorption in the parietal pleura due to amyloid deposition on the surface of the pleura and in lymphatic and blood vessels^{58,59}. In a Boston University study between 1994 and 2001 with 636 patients with AL amyloidosis, 6% had persistent pleural effusion due to pleural amyloid deposits demonstrated in pleural biopsies⁵⁸. The pleural fluid may have characteristics of a transudate (43.4%) or an exudate (42.6%), with a predominance of

lymphocytes⁵⁷. Although rare, pleural effusion may be hemorrhagic or chylous^{60,61}.

The diagnostic yield of closed pleural biopsy and thoracoscopy is 75% and 96.7%, respectively, with a better performance described in patients with unilateral or exudate-like effusion⁵⁷. On thoracoscopy, diffuse inflammation was associated with disseminated light brown nodules in the parietal and visceral pleural sheets and the diaphragmatic surface of the pleura⁵⁹.

Imaging findings

CT findings include pleural fluid characteristically occupying less than one-third of the hemithorax (50%), bilateral (55%) or predominantly right (34%), and diffuse or localized thickening with pleural plaques that may calcify⁵⁶ (Figure 11).

The differential diagnosis of pleural plaques associated with amyloidosis is asbestos-associated pleural disease, and in cases of diffuse pleural thickening, infection (smooth thickening), or primary (mesothelioma) or secondary neoplasia in the case of nodular diffuse thickening^{62,63}. As with NA, PET is of limited use in distinguishing pleural amyloidosis from primary or metastatic pleural neoplasia⁵⁶.

CONCLUSION

Pulmonary and pleural amyloidosis are rare. The nodular form of pulmonary amyloidosis is associated with localized amyloidosis, characteristically has a good prognosis, and should be considered for diagnosing single or multiple pulmonary nodules, especially when calcifications are present and the patient is asymptomatic. CA is rare and usually associated with pulmonary nodules and systemic autoimmune diseases, especially Sjögren's syndrome and MALT-type lymphoma. DASA is a manifestation of systemic amyloidosis with a poor prognosis and nonspecific manifestations on imaging examination, requiring histopathologic confirmation for diagnosis in a significant percentage of patients. Pleural plaques associated with systemic amyloidosis may be more common than traditionally thought, and their differential diagnosis with secondary neoplasms and pleural plaques associated with asbestos exposure represents a diagnostic challenge.

Funding

The authors declare that they received no funding or support for this article.

Conflicts of interest

The authors declare no conflicts of interest.

Ethical disclosures

Protection of individuals. The author declares that no experiments were performed on humans or animals.

Confidentiality of data. The author declares that no patient data are included in this article.

Right to privacy and informed consent. The authors declare that no patient data appear in this article.

Use of artificial intelligence. The authors state that they did not use generative artificial intelligence to prepare this manuscript and/or create tables, figures, or figure legends.

REFERENCES

- Bellotti V, Nuvolone M, Giorgetti S, Obici L, Palladini G, Russo P, et al. The workings of the amyloid diseases. *Ann Med*. 2007;39(3):200-207. doi: 10.1080/07853890701206887.
- Howie AJ. Origins of a pervasive, erroneous idea: The "green birefringence" of Congo red-stained amyloid. *Int J Exp Pathol*. 2019;100(4):208-221. doi: 10.1111/iep.12330.
- Sipe JD, Cohen AS. Review: history of the amyloid fibril. *J Struct Biol*. 2000;130(2-3):88-98. doi: 10.1006/jsbi.2000.4221.
- Thompson PJ, Citron KM. Amyloid and the lower respiratory tract. *Thorax*. 1983;38(2):84-87. doi: 10.1136/thx.38.2.84.
- Buxbaum JN, Dispenzieri A, Eisenberg DS, Fändrich M, Merlini G, Saraiva MJM, et al. Amyloid nomenclature 2022: update, novel proteins, and recommendations by the International Society of Amyloidosis (ISA) Nomenclature Committee. *Amyloid*. 2022;29(4):213-219. doi: 10.1080/13506129.2022.2147636.
- Brunger AF, Nienhuis HLA, Bijzet J, Hazenberg BPC. Causes of AA amyloidosis: a systematic review. *Amyloid*. 2020;27(1):1-12. doi: 10.1080/13506129.2019.
- Ussavarungsi K, Yi ES, Maleszewski JJ, Kurtin PJ, Dasari S, Theis JD, et al. Clinical relevance of pulmonary amyloidosis: an analysis of 76 autopsy-derived cases. *Eur Respir J*. 2017;49(2):1602313. doi: 10.1183/13993003.02313-2016.
- Ravichandran S, Lachmann HJ, Wechalekar AD. Epidemiologic and survival trends in amyloidosis, 1987-2019. *N Engl J Med*. 2020;382(16):1567-1568. doi: 10.1056/NEJMc1917321.
- Kumar N, Zhang NJ, Cherepanov D, Romanus D, Hughes M, Faller DV. Global epidemiology of amyloid light-chain amyloidosis. *Orphanet J Rare Dis*. 2022;17(1):278. doi: 10.1186/s13023-022-02414-6.
- Sabinot A, Ghetti G, Pradelli L, Bellucci S, Lausi A, Palladini G. State-of-the-art review on AL amyloidosis in Western Countries: Epidemiology, health economics, risk assessment and therapeutic management of a rare disease. *Blood Rev*. 2023;59:101040. doi: 10.1016/j.blre.2023.101040.
- Kyle RA, Larson DR, Kurtin PJ, Kumar S, Cerhan JR, Thorneau TM, et al. Incidence of AL amyloidosis in Olmsted county, Minnesota, 1990 through 2015. *Mayo Clin Proc*. 2019;94(3):465-471. doi: 10.1016/j.mayocp.2018.08.041.
- Quock TP, Yan T, Chang E, Guthrie S, Broder MS. Epidemiology of AL amyloidosis: a real-world study using US claims data. *Blood Adv*. 2018;2(10):1046-1053. doi: 10.1182/bloodadvances.2018016402.
- Gertz MA, Dispenzieri A. Systemic amyloidosis recognition, prognosis, and therapy: a systematic review. *JAMA*. 2020;324(1):79-89. doi: 10.1001/jama.2020.5493.
- Antonopoulos AS, Panagiotopoulos I, Kouroutzoglou A, Koutsis G, Toskas P, Lazaros G, et al. Prevalence and clinical outcomes of transthyretin amyloidosis: a systematic review and meta-analysis. *Eur J Heart Fail*. 2022;24(9):1677-1696. doi: 10.1002/ejhf.2589.
- Lane T, Pinney JH, Gilbertson JA, Hutt DF, Rowczenio DM, Mahmood S, et al. Changing epidemiology of AA amyloidosis: clinical observations over 25 years at a single national referral centre. *Amyloid*. 2017;24(3):162-166. doi: 10.1080/13506129.2017.1342235.

16. Lachmann HJ, Goodman HJ, Gilbertson JA, Gallimore JR, Sabin CA, Gillmore JD, et al. Natural history and outcome in systemic AA amyloidosis. *N Engl J Med*. 2007;356(23):2361-2371. doi: 10.1056/NEJMoa070265.
17. Biewend ML, Menke DM, Calamia KT. The spectrum of localized amyloidosis: a case series of 20 patients and review of the literature. *Amyloid*. 2006;13(3):135-142. doi: 10.1080/13506120600876773.
18. Mahmood S, Bridoux F, Venner CP, Sachchithanatham S, Gilbertson JA, Rowczenio D, et al. Natural history and outcomes in localised immunoglobulin light-chain amyloidosis: a long-term observational study. *Lancet Haematol*. 2015;2(6):e241-250. doi: 10.1016/S2352-3026(15)00068-X.
19. Baumgart JV, Stuhlmann-Laeisz C, Hegenbart U, Nattenmüller J, Schönland S, Krüger S, et al. Local vs. systemic pulmonary amyloidosis-impact on diagnostics and clinical management. *Virchows Arch*. 2018;473(5):627-637. doi: 10.1007/s00428-018-2442-x.
20. Khor A, Colby TV. Amyloidosis of the lung. *Arch Pathol Lab Med*. 2017;141(2):247-254. doi: 10.5858/arpa.2016-0102-RA.
21. Guan J, Mishra S, Qiu Y, Shi J, Trudeau K, Las G, et al. Lysosomal dysfunction and impaired autophagy underlie the pathogenesis of amyloidogenic light chain-mediated cardiotoxicity. *EMBO Mol Med*. 2014;6(11):1493-1507. doi: 10.15252/emmm.201404190. Erratum in: *EMBO Mol Med*. 2015 May 04;7(5):688. doi: 10.15252/emmm.201505318.
22. Hachulla E, Grateau G. Diagnostic tools for amyloidosis. *Joint Bone Spine*. 2002;69(6):538-545. doi: 10.1016/s1297-319x(02)00449-9.
23. Mughtar E, Dispenzieri A, Lacy MQ, Buadi FK, Kapoor P, Hayman SR, et al. Overuse of organ biopsies in immunoglobulin light chain amyloidosis (AL): the consequence of failure of early recognition. *Ann Med*. 2017;49(7):545-551. doi: 10.1080/07853890.2017.1304649.
24. Fernández de Larrea C, Verga L, Morbini P, Klersy C, Lavatelli F, Foli A, et al. A practical approach to the diagnosis of systemic amyloidoses. *Blood*. 2015;125(14):2239-2244. doi: 10.1182/blood-2014-11-609883.
25. Wisniowski B, Wechalekar A. Confirming the diagnosis of amyloidosis. *Acta Haematol*. 2020;143(4):312-321. doi: 10.1159/000508022.
26. Hawkins PN, Lavender JP, Pepys MB. Evaluation of systemic amyloidosis by scintigraphy with 123I-labeled serum amyloid P component. *N Engl J Med*. 1990;323(8):508-513. doi: 10.1056/NEJM199008233230803.
27. Utz JP, Swensen SJ, Gertz MA. Pulmonary amyloidosis. The Mayo Clinic experience from 1980 to 1993. *Ann Intern Med*. 1996;124(4):407-413. doi: 10.7326/0003-4819-124-4-199602150-00004.
28. Brandelik SC, Kaussler CP, Kauczor HU, Röcken C, Huber L, Basset M, et al. CT features in amyloidosis of the respiratory system - Comprehensive analysis in a tertiary referral center cohort. *Eur J Radiol*. 2020;129:109123. doi: 10.1016/j.ejrad.2020.109123.
29. Pickford HA, Swensen SJ, Utz JP. Thoracic cross-sectional imaging of amyloidosis. *AJR Am J Roentgenol*. 1997;168(2):351-355. doi: 10.2214/ajr.168.2.9016204.
30. Core JM, Alsaad AA, Jiang L, Patel NM. Nodular pulmonary amyloidosis: a complex disease with malignancy association. *BMJ Case Rep*. 2017;2017:bcr2017220428. doi: 10.1136/bcr-2017-220428.
31. Baqir M, Kluka EM, Aubry MC, Hartman TE, Yi ES, Bauer PR, et al. Amyloid-associated cystic lung disease in primary Sjögren's syndrome. *Respir Med*. 2013;107(4):616-621. doi: 10.1016/j.rmed.2013.01.005.
32. Jeong YJ, Lee KS, Chung MP, Han J, Chung MJ, Kim KI, et al. Amyloidosis and lymphoproliferative disease in Sjögren syndrome: thin-section computed tomography findings and histopathologic comparisons. *J Comput Assist Tomogr*. 2004;28(6):776-781. doi: 10.1097/00004728-20041000-00008.
33. Zamora AC, White DB, Sykes AM, Hoskote SS, Moua T, Yi ES, et al. Amyloid-associated cystic lung disease. *Chest*. 2016;149(5):1223-1233. doi: 10.1378/chest.15-1539.
34. Rajagopala S, Singh N, Gupta K, Gupta D. Pulmonary amyloidosis in Sjögren's syndrome: a case report and systematic review of the literature. *Respirology*. 2010;15(5):860-866. doi: 10.1111/j.1440-1843.2010.01772.x.
35. Crain MA, Vasilakis GM, Adkins JR, Adelanwa A, Hogg JP, Lakhani DA, et al. Primary nodular chest amyloidoma: A case report and review of literature. *Radiol Case Rep*. 2021;17(3):631-637. doi: 10.1016/j.radcr.2021.11.048.
36. Baqir M, Lowe V, Yi ES, Ryu JH. 18F-FDG PET scanning in pulmonary amyloidosis. *J Nucl Med*. 2014;55(4):565-568.
37. Yamada M, Takayanagi N, Yamakawa H, Ishiguro T, Baba T, Shimizu Y, et al. Amyloidosis of the respiratory system: 16 patients with amyloidosis initially diagnosed ante mortem by pulmonologists. *ERJ Open Res*. 2020;6(3):00313-2019. doi: 10.1183/23120541.00313-2019.
38. Ohdama S, Akagawa S, Matsubara O, Yoshizawa Y. Primary diffuse alveolar septal amyloidosis with multiple cysts and calcification. *Eur Respir J*. 1996;9(7):1569-1571. doi: 10.1183/09031936.96.09071569.
39. Colombat M, Caudroy S, Lagonotte E, Mal H, Danel C, Stern M, et al. Pathomechanisms of cyst formation in pulmonary light chain deposition disease. *Eur Respir J*. 2008;32(5):1399-1403. doi: 10.1183/09031936.00132007.
40. Sheard S, Nicholson AG, Edmunds L, Wotherspoon AC, Hansell DM. Pulmonary light-chain deposition disease: CT and pathology findings in nine patients. *Clin Radiol*. 2015;70(5):515-522. doi: 10.1016/j.crad.2015.01.002.
41. Liu Y, Jin Z, Zhang H, Zhang Y, Shi M, Meng F, et al. Diffuse parenchymal pulmonary amyloidosis associated with multiple myeloma: a case report and systematic review of the literature. *BMC Cancer*. 2018;18(1):802. doi: 10.1186/s12885-018-4565-5.
42. Eder L, Zisman D, Wolf R, Bitterman H. Pulmonary hypertension and amyloidosis- an uncommon association: a case report and literature review. *J Gen Intern Med*. 2007;22(3):416-419. doi: 10.1007/s11606-006-0052-9.
43. Sterlacci W, Veits L, Moser P, Steiner HJ, Rüscher S, Jammig H, et al. Idiopathic systemic amyloidosis primarily affecting the lungs with fatal pulmonary haemorrhage due to vascular involvement. *Pathol Oncol Res*. 2009;15(1):133-136. doi: 10.1007/s12253-008-9066-4.
44. Polo-Nieto JF, Quiroga-Dussan MDP, Castañeda-González JP, Fierro-Rodríguez DM, Durán-Acuña R, Carrillo-Bayona JA. Perilymphatic micronodular pattern as a manifestation of pulmonary amyloidosis on high-resolution computed tomography. *Radiol Case Rep*. 2021;16(4):850-854. doi: 10.1016/j.radcr.2021.01.027.
45. Riehani A, Soubani AO. The spectrum of pulmonary amyloidosis. *Respir Med*. 2023;218:107407. doi: 10.1016/j.rmed.2023.107407.
46. Martin MJ, Pennington KM, Skalski JH, Yi ES, Levin DL, Durani U, et al. Emphysematous lung lesions caused by perivascular and alveolar-septal deposition of amyloid light-chain amyloidosis. *Chest*. 2021;160(2):e169-e171. doi: 10.1016/j.chest.2021.03.038.
47. Lu X, He B, Wang G, He B, Wang L, Chen Q. Bronchoscopic diagnosis and treatment of primary tracheobronchial amyloidosis: a retrospective analysis from China. *BioMed Res Int*. 2017;2017:3425812. doi: 10.1155/2017/3425812.
48. Baqir M, Schwegman AR, Maldonado F, Johnson TF, Ryu JH. Airway amyloidosis: a retrospective analysis of 43 patients. *J Bronchology Interv Pulmonol*. 2022;29(4):275-282. doi: 10.1097/LBR.0000000000000836.
49. Chu H, Zhao L, Zhang Z, Gui T, Yi X, Sun X. Clinical characteristics of amyloidosis with isolated respiratory system involvement: A review of 13 cases. *Ann Thorac Med*. 2012;7(4):243-249. doi: 10.4103/1817-1737.102186.
50. Capizzi SA, Betancourt E, Prakash UB. Tracheobronchial amyloidosis. *Mayo Clin Proc*. 2000;75(11):1148-1152. doi: 10.4065/75.11.1148.
51. Ding L, Li W, Wang K, Chen Y, Xu H, Wang H, et al. Primary tracheobronchial amyloidosis in China: analysis of 64 cases and a review of literature. *J Huazhong Univ Sci Technol Med Sci*. 2010;30(5):599-603. doi: 10.1007/s11596-010-0549-7.
52. O'Regan A, Fenlon HM, Beamis JF Jr, Steele MP, Skinner M, Berk JL. Tracheobronchial amyloidosis. The Boston University experience from 1984 to 1999. *Medicine (Baltimore)*. 2000;79(2):69-79. doi: 10.1097/00005792-200003000-00001.
53. Borie R, Danel C, Molinier-Frenkel V, Prevot G, Deslee G, Debray MP, et al. Tracheobronchial amyloidosis: evidence for local B-cell clonal expansion. *Eur Respir J*. 2012;39(4):1042-1045. doi: 10.1183/09031936.00101811.
54. Wang Q, Chen H, Wang S. Laryngo-tracheobronchial amyloidosis: a case report and review of literature. *Int J Clin Exp Pathol*. 2014;7(10):7088-7093.
55. Pai KK, Omiunu AO, Llerena PA, Shave SM, Desai HA, Fang CH, et al. Localized laryngeal amyloidosis: A systematic review. *Am J Otolaryngol*. 2022;43(5):103550. doi: 10.1016/j.amjoto.2022.103550.
56. Kunihiro Y, Onoda H, Aoe K, Furukawa M, Okabe K, Murakami T, et al. A case of localized pleural amyloidosis: multimodality imaging features. *J Thorac Imaging*. 2018;33(6):W54-W56. doi: 10.1097/RTI.0000000000000354.
57. Pou C, Ferreiro L, Suárez-Antelo J, Golpe A, Álvarez-Dobaño JM, Toubes ME, et al. Characteristics of pleural effusion due to amyloidosis. *Ann Thorac Med*. 2023;18(2):53-60. doi: 10.4103/atm.atm_433_22.
58. Berk JL, Keane J, Seldin DC, Sancharawala V, Koyama J, Dember LM, et al. Persistent pleural effusions in primary systemic amyloidosis: etiology and prognosis. *Chest*. 2003;124(3):969-977. doi: 10.1378/chest.124.3.969.
59. Bontemps F, Tillie-Leblond I, Coppin MC, Frehart P, Wallaert B, Ramon P, et al. Pleural amyloidosis: thoracoscopic aspects. *Eur Respir J*. 1995;8(6):1025-1027.
60. Dai Y, Liu C, Chen J, Zeng Q, Duan C. Pleural amyloidosis with recurrent pleural effusion and pulmonary embolism: A case report. *Medicine (Baltimore)*. 2019;98(3):e14151. doi: 10.1097/MD.00000000000014151.
61. George S, Ravindran M, Anandan PT, Kiran VN. Primary systemic amyloidosis: A rare cause for pleural effusion. *Respir Med Case Rep*. 2014;13:39-42. doi: 10.1016/j.rmcr.2014.09.001.
62. Nakano T, Endo S, Tetsuka K, Fukushima N. Asymptomatic localized pleural amyloidosis mimicking malignant pleural mesothelioma: report of a case. *J Thorac Dis*. 2016;8(1):E157-160. doi: 10.3978/j.issn.2072-1439.2016.01.16.
63. Coolbear F, Bilawich AM, Tongson J, Adamo J, Churg A. Pleural amyloidosis imitating pleural malignancy. *Respir Med Case Rep*. 2017;20:195-197. doi: 10.1016/j.rmcr.2017.03.004.

Can the absence of breast arterial calcifications on mammography predict the absence of coronary artery calcifications?

I. Miranda SanchezCarenzo-Velez^{1,2,3} , Sofia Hurtado-Arellano⁴ , Nancy L. Garza-Garcia¹ ,
Mane M. Ayala-Duran¹ , Ilany B. Lopez-Valdivia^{2,3} , Erasmo De la Peña-Almaguer⁵ , and
Margarita L. Garza-Montemayor¹ 

¹Diagnostic Breast Imaging Department, Hospital Zambrano Hellion Tec Salud; ²Department of Radiology and Imaging, Hospital San Jose Tec Salud; ³Department of Radiology and Imaging, Hospital Zambrano Hellion Tec Salud; ⁴School of Medicine and Health Sciences, Tecnológico de Monterrey; ⁵Cardiology Imaging Department, Hospital Zambrano Hellion, Tec Salud. Monterrey, Nuevo Leon, Mexico

ABSTRACT

Introduction: It has been suggested that breast arterial calcifications (BAC) on mammography predict coronary artery calcifications (CAC). However, it has been insufficiently addressed to rule out the presence of CAC. This study aimed to determine whether the absence of BAC on mammography is associated with the absence of CAC using the coronary computed tomography (CT) calcium score in women. **Material and methods:** This retrospective cross-sectional study included asymptomatic women who underwent digital screening mammography and coronary CT calcium score testing. BAC score was grouped into three categories: absence, intermediate, and significant. The Agatston score was used to quantify CAC. The sensitivity, specificity, positive predictive value (PPV), and negative predictive value (NPV) of BAC were calculated to predict CAC. **Results:** We included 611 asymptomatic women with a mean age of 51.3 ± 8.37 years. The prevalence of BAC was 9.1% ($n = 56$), and CAC was 13.4% ($n = 82$). There was a significant association between the absence of BAC and no CAC ($n = 501$, 93.5%; $p < 0.001$). BAC diagnostic performance was stratified by age. In women under 60 years ($n = 525$), specificity was 94.6% (95% CI, 91.4-95.6), and the NPV 92.6% (95% CI, 91.4-95.6) for the absence of BAC in predicting no CAC. In women aged ≥ 60 years ($n = 86$), specificity was 82.6% (95% CI, 68.5-92.1), and the NPV was 60.3% (95% CI, 53.6-66.6). The sensitivity (14.2%, 95% CI, 16.1-35.05) and PPV (18.7%, 95% CI, 25.3-51.02) in women under 60 years were lower than in women ≥ 60 years with a sensitivity of 37.5% (95% CI, 22.7-54.2) and a PPV of 65.2% (95% CI, 47.0-79.8). **Conclusion:** The absence of BAC in screening mammography has the highest diagnostic performance for predicting the absence of CAC, especially in women under 60 years of age.

Keywords: Breast arterial calcification. Coronary artery calcification. Coronary artery disease. Mammography. Coronary computed tomography calcium score.

INTRODUCTION

Screening mammography, used for early detection of breast cancer, allows direct visualization of breast arterial calcifications (BAC)^{1,2}. The Breast Imaging Reporting and Data System (BI-RADS) categorizes BAC as benign and suggests the possibility of not mentioning them on the mammogram report³. Interestingly, some studies

recommend reporting it^{1,4,5} because BAC have been considered surrogate marker for coronary artery calcifications (CAC) and coronary artery disease^{1,6-12}. CAC characterization by the coronary computed tomography (CT) calcium score shows concordance with the total coronary burden of atherosclerosis and the risk of coronary artery disease¹³. Mammography and the coronary CT calcium

*Corresponding author:

Nancy L. Garza-Garcia
E-mail: nancygarza@tec.mx

Received for publication: 20-04-2024

Accepted for publication: 03-08-2024

DOI: 10.24875/JMEXFRI.M24000083

Available online: 03-10-2024

J Mex Fed Radiol Imaging. 2024;3(3):150-161

www.JMeXFRI.com

2696-8444 / © 2024 Federación Mexicana de Radiología e Imagen, A.C. Published by Permanyer. This is an open access article under the CC BY-NC-ND (<https://creativecommons.org/licenses/by-nc-nd/4.0/>).

score are screening methods for breast cancer and coronary artery disease. However, mammography has the advantage of being more accessible, less expensive, and not causing additional radiation exposure⁴.

The prevalence of BAC in screening mammography varies between 3% and 42%^{1,2}. Publications have mostly focused on the sensitivity and positive predictive value (PPV) of the presence of BAC for predicting CAC^{7,10-12,14-19}. However, there are few reports on the specificity and negative predictive value (NPV) of the absence of BAC for predicting the absence of CAC^{11,16,19}. In asymptomatic women, the absence of BAC on screening mammography can indicate a low rate of subclinical coronary artery disease¹⁶. This study aimed to determine whether the absence of BAC on screening mammography could significantly predict the absence of CAC using the coronary CT calcium score in asymptomatic women.

MATERIAL AND METHODS

This retrospective cross-sectional study was conducted from January 2014 to June 2022 in the Department of Radiology and Imaging of the Hospital Zambrano Hellion and the Department of Radiology and Imaging of the Hospital San Jose of the TecSalud System in Monterrey, Nuevo Leon, Mexico. Asymptomatic women with digital screening mammography and a coronary CT calcium score were included. The exclusion criteria were an invalid coronary CT coronary calcium score or no calcium quantification report, a mammography with findings suspicious of malignancy categorized as BI-RADS 4 or 5, a history of mastectomy, radiotherapy, an incomplete electronic record, and a privacy notice without checking the box for consent for research purposes. Written informed consent was obtained from all women, and the institutional ethics and research committees granted study approval.

Study development and variables

Digital mammography and the coronary CT calcium score were performed on women during a routine medical evaluation with an interval of 12 months between the two imaging examinations. The variables age, body mass index (BMI), smoking, and comorbidities such as systemic arterial hypertension, chronic kidney disease, type 2 diabetes, and dyslipidemia were recorded during an electronic medical record review.

Image acquisition and analysis protocol

DIGITAL MAMMOGRAPHY

The Selenia™ Dimensions (HOLOGIC, Inc. Bedford, MA, USA) and the IMS Giotto™ Tomo (Sasso Marconi, BO, Italy) systems were used for digital mammography in mediolateral oblique and craniocaudal projections. The mammograms were assessed visually for the presence and severity of BAC by three breast radiologists: NGG with 15 years of experience, IMSCV with 1 year of experience, and MAD with 1 year of experience. Radiologists were blinded to the CAC results. Different workstations with two 5 MP medical grade monitors (BARCO, Kortrijk, Belgium) were used.

The mammographic calcification severity was determined according to Margolies et al¹⁰. In women with BAC, the number of affected vessels in each breast was coded from 1 to 6; if more than 6 were affected, this was coded as 6. The longest affected length of the affected vessel was scored and coded as none (0 points), less than one-third (1 point), between one-third and two-thirds (2 points), and more than two-thirds (3 points). Calcium density in the most affected segment was recorded as none (0 points), mild with clear visibility of the lumen and/or only one wall of the affected vessel (1 point), moderate with lumen opacity and calcification, both tangential walls (2 points) and severe with no visible light (3 points).

A BAC score between 0 and 12 points was calculated by averaging the scores of the two breasts. The BAC score was classified into three categories according to severity: absence of BAC (0 points), intermediate BAC (1 to 3 points), and significant BAC (4 to 12 points)¹⁰.

CORONARY CT CALCIUM SCORE

A 256-slice SOMATOM™ Definition Flash device (Siemens Healthineers, Erlangen, Germany) was used for image analysis by a cardiologist specializing in cardiovascular imaging with 23 years of experience (EPA) blinded to the BAC results. A medical grade-dual monitor workstation (BARCO, Kortrijk, Belgium) was used.

The Agatston score (AS)²⁰ was used to quantify calcium in the coronary arteries using semi-automated software (syngo CT VC28, Siemens Industry Inc., GA, USA). The AS was determined by multiplying the CAC area by the highest Hounsfield unit (HU) weighted value and summing it with all lesions in all vessels visualized on the CT²⁰. The risk of coronary artery disease was

categorized with the AS as 0, no risk; 1-10 points, minimal risk; 11 to 100 points, slight risk; 101 to 400 points, moderate risk; and > 400 points, severe risk.

STATISTICAL ANALYSIS

Numeric variables were described using central tendency and dispersion measures. Categorical variables were described as absolute numbers and percentages. The association between non-related categorical variables was determined with the chi-square test. The difference in means between numerical variables and categorical groups was analyzed using Student's t-test for two groups and the ANOVA test for more than two groups. Sensitivity, specificity, positive predictive value (PPV), and negative predictive value (NPV), of BAC for predicting CAC were calculated according to age categories < 60 or \geq 60 years. Odds ratios (ORs) were calculated to assess the relationship between BAC and CAC, adjusting other available risk factors such as age, systemic arterial hypertension, chronic kidney disease, type 2 diabetes, and dyslipidemia. A multivariate ordinal regression model analyzed the relationship between multiple variables and a single ordinal variable. A p-value < 0.05 was considered significant for all statistical comparisons. The statistical analysis was performed with SPSS version 29 (IBM Corp. Armonk, NY, USA).

RESULTS

Characteristics of women in relation to the presence or absence of BAC

We included 611 women with a mean age of 51.3 \pm 8.37 years. The characteristics of the women in relation to the presence or absence of BAC are shown in Table 1. BAC were found in 56 of 611 women, with a prevalence of 9.1%. Women with BAC were older (mean age 58.5 \pm 11.5) than women without BAC (mean age 50.6 \pm 7.6 years), indicating a significant association between older age and the presence of BAC ($p < 0.001$). The mean BAC score was 3.6 \pm 2.2 (range, 2-10) in 56 women with intermediate or significant BAC scores. Systemic arterial hypertension was more common in women with BAC than in patients without BAC ($n = 9$, 16.1% and $n = 49$, 8.8%, respectively) ($p = 0.078$). No significant differences were found between the two groups concerning BMI, smoking, chronic kidney disease, Type 2 diabetes, or dyslipidemia. Figure 1 shows the different features of the mammary arteries in digital mammography in the presence or absence of BAC. Figure 2 shows a digital

mammogram in MLO projection of three asymptomatic women of different ages with the three categories of BAC (absent, intermediate, and significant).

Characteristics of women in relation to the presence or absence of CAC

The prevalence of CAC was 13.4% (82/611 women), and the mean Agatston score for CAC was 18.7 \pm 105.9 (range, 0-1494). Women with CAC were older (mean age 61.1 \pm 9.4 years) than women without CAC (mean age 49.8 \pm 7.0 years), indicating a significant association between older age and the presence of CAC ($p < 0.001$) (Table 2). We found a significant risk association between obesity (OR 3.52, 95% CI, 2.13-5.86), systemic arterial hypertension (OR 9.43, 95% CI, 5.24-16.97), and diabetes (OR 2.08, 95% CI, 1.21-3.59) and the presence of CAC, while no differences were found between CAC groups for smoking, chronic kidney disease, or dyslipidemia. Figure 3 shows a coronary CT calcium score of a 42-year-old asymptomatic woman without CAC. In contrast, Figure 4 shows a coronary CT calcium score with significant CAC.

Association of BAC and CAC according to age

Table 3 shows the distribution of BAC and CAC stratified by age. BAC and CAC were found in 21 women, and 15 (71.4%) were women aged \geq 60 years, while only 6 (28.6%) were women under 60 years ($p < 0.001$). The presence of BAC with no CAC ($n = 27$, 77.2%) was significant in women under 60 years compared to women \geq 60 years ($n = 8$, 22.8%) ($p < 0.001$). In contrast, the absence of BAC in the presence of CAC was observed with comparable frequency in both age groups. On the other hand, the absence of BAC and CAC was significant in women under 60 years ($n = 456$, 92.3%) compared to women aged \geq 60 years ($n = 38$, 7.7%) ($p < 0.001$).

Association between the BAC score and the CAC-Agatston categories

Table 4 shows the distribution between the BAC scores and the CAC-Agatston categories in asymptomatic women. There was a significant association between the absence of BAC and no CAC category ($n = 494$, 93.4%) ($p < 0.001$). In contrast, an intermediate BAC score ($n = 25$, 4.7%) or a significant BAC score ($n = 10$, 1.9%) was associated with the absence of CAC in a

Table 1. Characteristics of 611 women in relation to the presence or absence of BAC on mammography

Description	Total (n = 611)	Presence of BAC (n = 56)	Absence of BAC (n = 555)	p-value	OR (95% CI)
Age, years, mean \pm SD	51.3 \pm 8.37	58.5 \pm 11.5	50.6 \pm 7.0	< 0.001	-
BMI					
< 18	4 (0.7)	1 (1.8)	3 (0.5)	0.721	1.08 (0.621-87)
18-24.9	334 (54.6)	29 (51.8)	305 (55.0)		
25-29.9	169 (27.6)	14 (25.0)	155 (27.9)		
30-34.9	77 (12.6)	9 (16.1)	68 (12.3)		
35-39.9	23 (3.8)	3 (5.3)	20 (3.6)		
> 40	4 (0.7)	-	4 (0.7)		
Smoking^a					
Yes	166 (27.2)	20 (37.0)	146 (26.3)	0.091	1.65 (0.92-2.95)
No	443 (72.8)	34 (63.0)	409 (73.7)		
Systemic arterial hypertension					
Yes	58 (9.5)	9 (16.1)	49 (8.8)	0.078	1.97 (0.91-4.27)
No	553 (90.5)	47 (83.9)	506 (91.2)		
Chronic kidney failure^b					
Yes	3 (0.5)	1 (1.8)	2 (0.4)	0.140	5.12 (0.45-57.39)
No	607 (99.5)	54 (98.2)	553 (99.6)		
Type 2 diabetes					
Yes	101 (16.5)	7 (12.5)	94 (16.9)	0.394	0.70 (0.30-1.59)
No	510 (83.5)	49 (87.5)	461 (83.1)		
Dyslipidemia					
Yes	274 (44.8)	27 (48.2)	247 (44.5)	0.595	1.16 (0.67-2.01)
No	337 (55.2)	29 (51.8)	308 (55.5)		

SD: standard deviation; BAC: breast arterial calcifications; BMI: Body Mass Index; OR: Odds Ratio; CI: Confidence Interval. The values refer to absolute frequencies and percentages, unless otherwise stated. ^aThis variable was not specified for two patients; ^bThis variable was not specified for one patient.

small number of women. Women with intermediate and significant BAC scores were about 5 times more likely to have CAC (OR 5.01, 95% CI, 2.73-9.18). Fifty (82.0%) of 61 patients without BAC had minimum or slight CAC-Agatston categories. Nine (69.2%) of 13 patients with a moderate CAC-Agatston category had an intermediate or significant BAC score, while 4 (36.4%) of 11 patients with a severe CAC-Agatston category had an intermediate or significant BAC score.

Four hundred eighty-seven (92.6%) of 525 women under 60 years had a CAC-Agatston category 0 compared to 38 (7.4%) with a non-zero CAC-Agatston category, while 49 (57.0%) of 86 women aged \geq 60 years

had a CAC-Agatston category of 0 compared to 37 (43.0%) with a non-zero CAC-Agatston category ($p < 0.001$). Figure 5 shows a digital mammography and coronary CT calcium score of a 66-year-old, asymptomatic woman without BAC or CAC, respectively. Figure 6 shows an 81-year-old woman with a severe category of CAC and a significant BAC score.

Diagnostic performance of the BAC score for predicting CAC

The diagnostic performance of the BAC score was stratified by age (Table 5). In women under 60 years

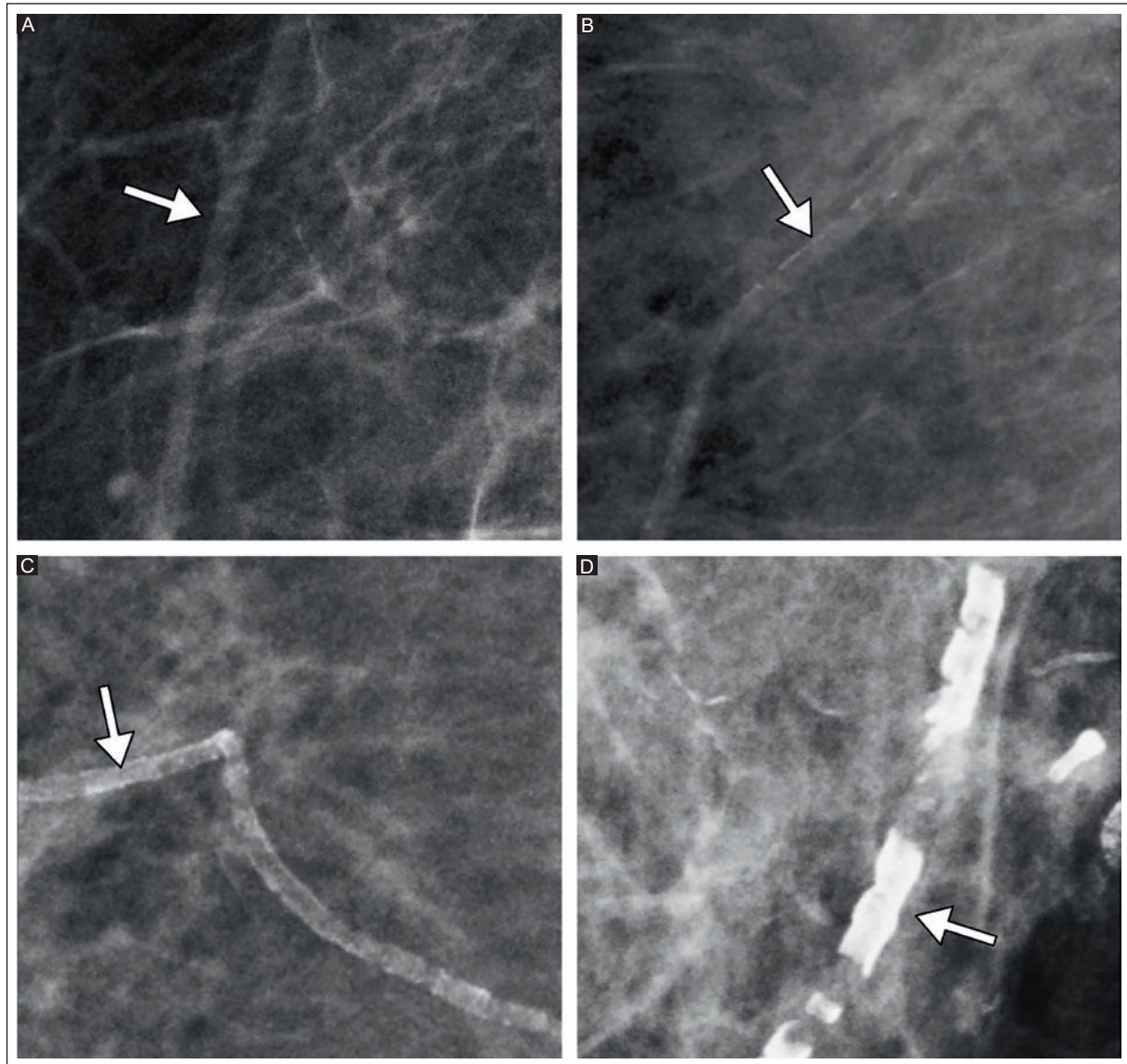


Figure 1. Digital mammography showing a variety of BAC. **A:** breast artery without calcifications (arrow). **B:** breast artery with calcifications in only one wall (arrow). **C:** tram-track-like calcifications (arrow); both walls are calcified, and the lumen is still visible. **D:** extensive BAC without lumen visualization (arrow).

BAC: breast arterial calcification.

(n = 525), we found a high specificity (94.6%, 95% CI, 91.4-95.6) and NPV (92.6%, 95% CI, 86.4-91.6) for the absence of BAC in predicting the absence of CAC. In women aged ≥ 60 years (n = 86), these parameters were intermediate with a specificity of 82.6% (95% CI, 68.5-92.1) and an NPV of 60.3% (95% CI, 53.6-66.6),

The sensitivity (14.2%; 95% CI, 16.1-35.05) and PPV (18.7%, 95% CI, 25.3-51.02) were lower in women under 60 years than in women aged ≥ 60 years, with a sensitivity of 37.5% (95% CI, 22.7-54.2) and a PPV of 65.2% (95% CI, 47.0-79.8).

DISCUSSION

This study shows that the absence of BAC on mammography has a high specificity and NPV for predicting the absence of CAC, especially in women under 60 years of age. To the best of our knowledge, this study is the first that focuses on BAC as an indicator of the absence of CAC. The high NPV of the absence of BAC may suggest that it would not be a cost-effective screening method for coronary artery disease, especially in women under 60 years of age, as CAC testing would result in a large number of negative CAC assessments.

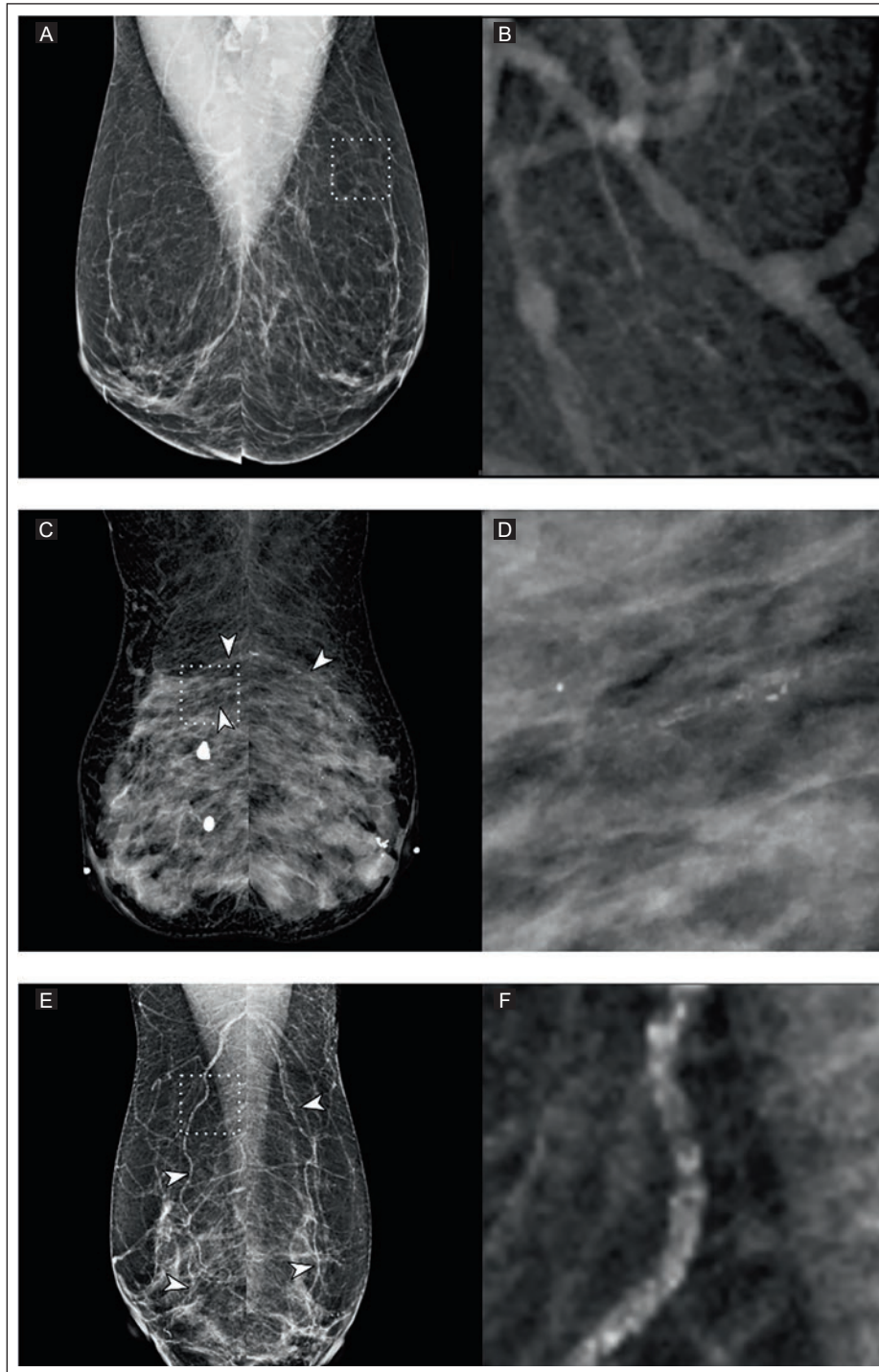


Figure 2. Digital mammography showing the three BAC score categories: A 50-year-old asymptomatic woman. **A:** MLO projections. **B:** magnification (dashed white square) showing breast arteries without calcifications. The BAC score was 0. A 55-year-old woman, asymptomatic, with an Agatston score of 147, class II obesity, dyslipidemia, and smoking. **C:** MLO projection of the right breast showing 2 affected arteries (2 points), a single calcified wall (1 point), and vessel extension less than one-third (1 point). The left breast shows one artery (1 point) with a single calcified wall (1 point) and vessel extension of more than one-third but less than two-thirds (2 points) (arrowheads). The BAC index was 4, and the BAC score was intermediate. **D:** magnification (dashed white square) shows thin arterial calcifications in both the wall and the lumen visible. An 82-year-old asymptomatic woman with an Agatston score of 632, systemic arterial hypertension, and type 2 diabetes. **E:** the MLO projection shows the right breast with 2 affected arteries (2 points), both walls with calcifications, without visible lumen (3 points), and a vessel extension of more than two-thirds (3 points). The left breast shows 2 arteries (2 points) with both walls affected, no visible lumen (3 points), and vessel extension greater than two-thirds (3 points) (arrowheads). The BAC index was 8, and the BAC score was significant. **F:** magnification (dashed white square) shows extensive arterial calcifications on both walls without a visible lumen.

BAC: breast arterial calcifications; MLO: mediolateral oblique.

Table 2. Characteristics of 611 women in relation to the presence or absence of CAC on coronary CT calcium score

Description	Total n = 611	Presence of CAC n = 82	Absence of CAC n = 529	p-value	OR (95% CI)
Age, years, mean ± SD	51.3 ± 8.3	61.1 ± 9.4	49.8 ± 7.0	< 0.001	–
BMI					
< 18	4 (0.7)	2 (2.4)	2 (0.4)	< 0.001	3.52 (2.13-5.86)
18-24.9	334 (54.6)	22 (26.8)	312 (59.0)		
25-29.9	169 (27.6)	35 (42.7)	134 (25.3)		
30-34.9	77 (12.6)	15 (18.3)	62 (11.7)		
35-39.9	23 (3.8)	8 (9.8)	15 (2.8)		
> 40	4 (0.7)	–	4 (0.8)		
Smoking^a					
Yes	166 (27.2)	26 (31.7)	140 (26.6)	0.331	1.65 (0.92-2.95)
No	443 (72.8)	56 (68.3)	387 (73.4)		
Systemic arterial hypertension					
Yes	58 (9.5)	29 (35.4)	29 (5.5)	< 0.001	9.43 (5.24-16.97)
No	553 (90.5)	53 (64.6)	500 (94.5)		
Chronic kidney failure^b					
Yes	3 (0.5)	1 (1.2)	2 (0.4)	0.305	3.29 (0.29-36.74)
No	607 (99.5)	80 (98.8)	527 (99.6)		
Type 2 diabetes					
Yes	101 (16.5)	22 (26.8)	79 (14.9)	0.007	2.08 (1.21-3.59)
No	510 (83.5)	60 (73.2)	450 (85.1)		
Dyslipidemia					
Yes	274 (44.8)	45 (54.9)	229 (43.3)	0.050	1.59 (0.99-2.54)
No	337 (55.2)	37 (45.1)	300 (56.7)		

CAC: coronary artery calcifications; BMI: Body Mass Index; OR: Odds Ratio; CI: Confidence Interval; CT: computed tomography; SD: standard deviation. The values refer to absolute frequencies and percentages, unless otherwise stated. ^aThis variable was not specified for two patients. ^bThis variable was not specified for one patient.

The absence of BAC in screening mammography suggests the absence of CAC and a low risk of sub-clinical coronary artery disease^{1,2,16}. However, there is insufficient data to draw a definitive conclusion about whether women without BAC have a lower risk of cardiovascular events. A study by McLenachan et al.¹⁹ reported that patients without BAC were unlikely to have severe CAC with an NPV of 87%. This result is comparable to a study by Minssen et al¹¹, with a specificity of 87.6% and an NPV of 86.7% for the absence of BAC to predict the absence of CAC in 507 women. Matsumura et al.¹⁶ reported that the absence of BAC was able to accurately define women who did not have

high-risk CAC with an NPV of 99%. Furthermore, in a study conducted on 2100 patients, the specificity was 92%². In our study, the prediction of the absence of CAC by the absence of BAC was significantly associated with age. The highest specificity (94.6%) and NPV (92.6%) were found in asymptomatic women under 60 years, whereas in women aged ≥ 60 years, the specificity was 82.6%, and NPV was 60.3%. Our results suggest that asymptomatic women < 60 years old with an absence of BAC on screening mammography predict the absence of CAC and can be categorized as low-risk and may not need to be tested for CAC.

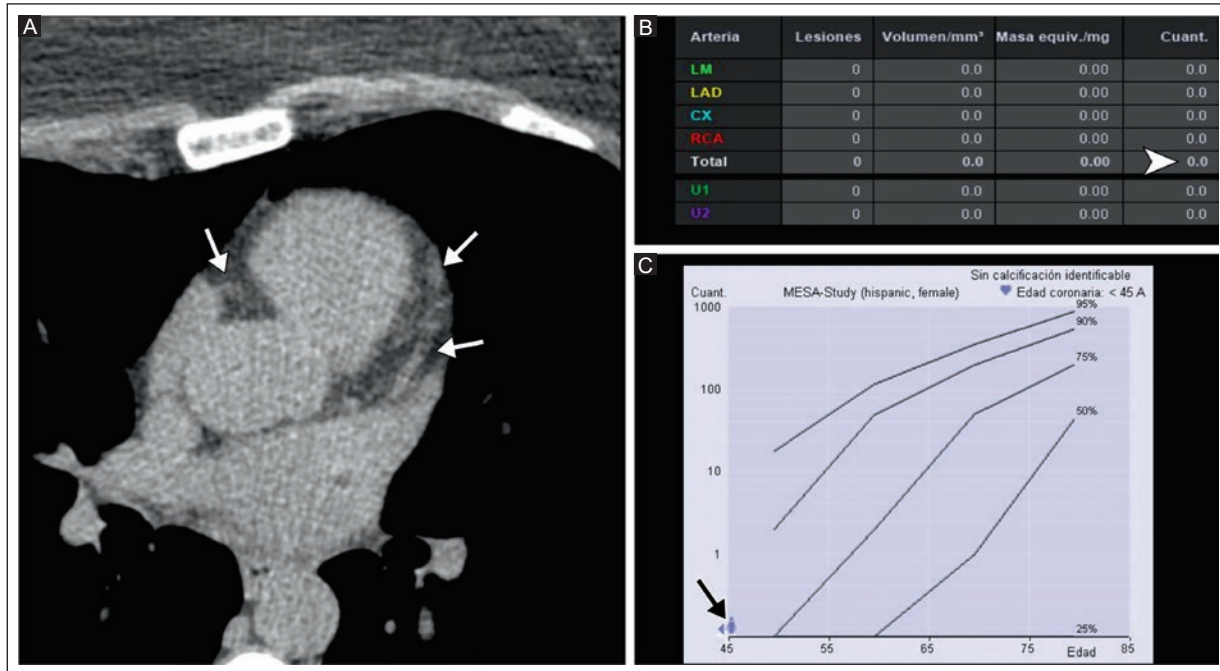


Figure 3. A 42-year-old asymptomatic woman. **A:** axial view of the coronary CT calcium score without CAC (arrows). **B:** table of CAC volume and mass values determined according to AS (arrowhead). **C:** percentile chart with AS by ethnicity and age, with percentiles between 75 and 90% (black arrow) based on MESA.

AS: Agatston score; CAC: coronary artery calcifications; CT: computed tomography; MESA: Multiethnic Study of Atherosclerosis.

Table 3. Association of the presence or absence of BAC with CAC according to age in 611 women

Description	Presence of BAC/ presence of CAC n (%)	Presence of BAC/ absence of CAC n (%)	Absence of BAC/ presence of CAC n (%)	Absence of BAC/ absence of CAC n (%)	Total n = 611
Women under 60 years of age	6 (28.6)	27 (77.2)	36 (59.0)	456 (92.3)	525
Women ≥ 60 years of age	15 (71.4)	8 (22.8)	25 (41.0)	38 (7.7)	86

p < 0.001. BAC: breast arterial calcifications; CAC: coronary artery calcifications.

Table 4. Association between the BAC score^a and the CAC-Agatston categories^b in 611 women

BAC score	CAC-Agatston categories					Total n = 611
	None n = 529	Minimum n = 31	Slight n = 27	Moderate n = 13	Severe n = 11	
Absence, n (%)	494 (93.4)	28 (90.3)	22 (81.5)	4 (30.8)	7 (63.6)	555
Intermediate, n (%)	25 (4.7)	2 (6.5)	2 (7.4)	5 (38.5)	1 (9.1)	35
Significant, n (%)	10 (1.9)	1 (3.2)	3 (11.1)	4 (30.8)	3 (27.3)	21

^aMargolies et al.¹⁰; ^bAgatston et al.²⁰; OR: 5.01 (95% CI, 2.73-9.18, p < 0.001). CAC: coronary artery calcifications; BAC: breast arterial calcifications.

The presence of BAC in screening mammography has been proposed as a non-invasive marker for CAC and coronary artery disease in women^{1,11}. A meta-analysis by Mohammed et al.²¹ evaluated the association

between BAC and CAC and the diagnosis of coronary artery disease by clinical and imaging examinations such as coronary angiography, coronary CT, or stress echocardiography. They found a significant association

Table 5. Diagnostic performance of the BAC score^a for predicting CAC by age

Parameter	Total n = 611	< 60 years n = 525	≥ 60 years n = 86
Sensitivity, % (95% CI)	25.6 (16.1-35.0)	14.2 (16.1-35.05)	37.5 (22.7-54.2)
Specificity, % (95% CI)	93.5 (91.1-95.6)	94.6 (91.4-95.6)	82.6 (68.5-92.1)
PPV, % (95% CI)	38.1 (25.3-51.0)	18.7 (25.3-51.02)	65.2 (47.0-79.8)
NPV, % (95% CI)	89.0 (86.4-91.6)	92.6 (86.4-91.6)	60.3 (53.6-66.6)

^aMargolies et al.¹⁰. BAC: breast arterial calcifications; CAC: coronary artery calcifications; CI: Confidence Interval; PPV: positive predictive value; NPV: negative predictive value.

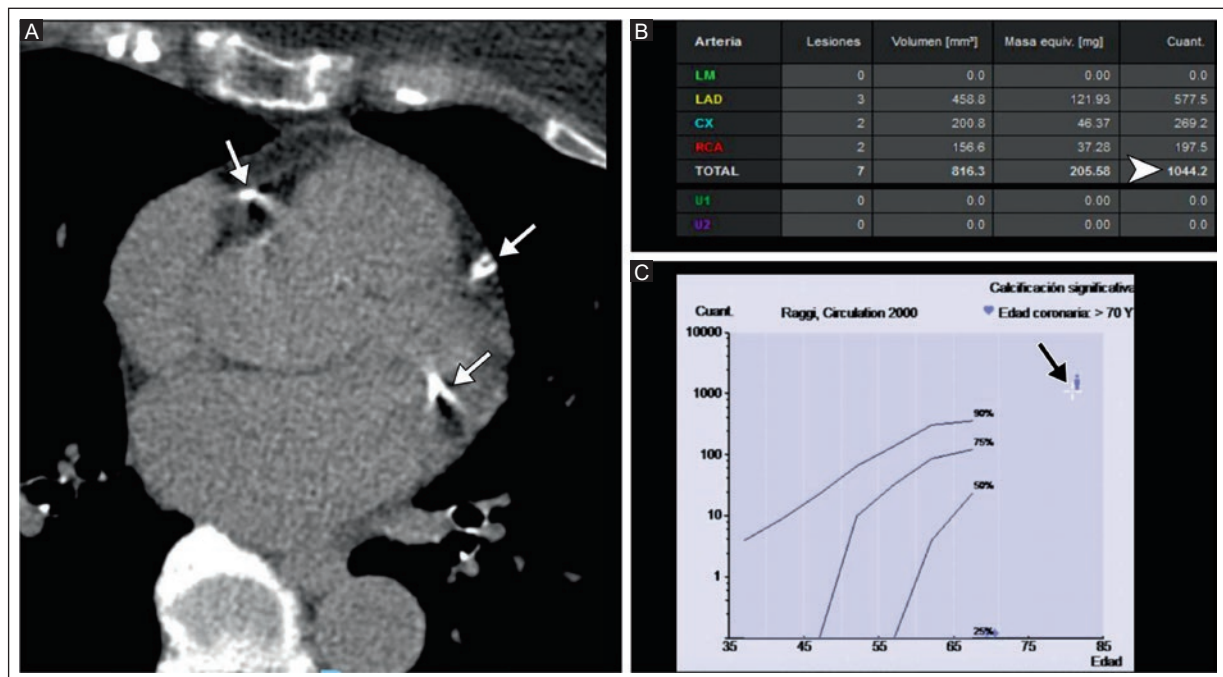


Figure 4. A 76-year-old asymptomatic woman with type 2 diabetes, dyslipidemia, and smoking. **A:** axial view of coronary CT calcium score with CAC (arrows). **B:** table of CAC volume and mass values determined by AS (arrowhead). **C:** the percentile chart shows AS with significant CAC by ethnicity and age, with percentiles above 90% (black arrow) based on MESA.

AS: Agatston score; CAC: coronary artery calcifications; CT: computed tomography; MESA: Multiethnic Study of Atherosclerosis.

between the presence of BAC and CAC (OR 2.14, 95% CI, 1.63-2.81). However, the diagnostic accuracy of BAC for predicting CAC was low, with a sensitivity of 33% and a PPV of 9%. Margolies et al¹. reported a sensitivity of 63% and a PPV of 70% in women regardless of age in 292 asymptomatic women. In comparison, the highest sensitivity of 75% and PPV of 86% for detecting CAC was found in the older age group (70 to 92 years). On the other hand, the lowest sensitivity of 50% and PPV of 53% for the presence of CAC was found in women aged between 39 and 59 years¹. Of note, a study conducted in 2100 patients

reported a sensitivity of 23% for BAC to detect CAC. Therefore, the low sensitivity of BAC to detect CAC implies that the absence of BAC does not effectively rule out coronary artery disease. In our study, women with intermediate and significant BAC scores were five times more likely to have CAC (OR 5.01, CI: 2.73-9.18) than women without BAC. We found a sensitivity (25.6%) and PPV (38.1%) of the presence of BAC to predict the presence of CAC in women regardless of age, whereas in women aged ≥ 60, sensitivity increased to 37.5% and the PPV to 65.3%. The CAC burden in patients with and without BAC by age

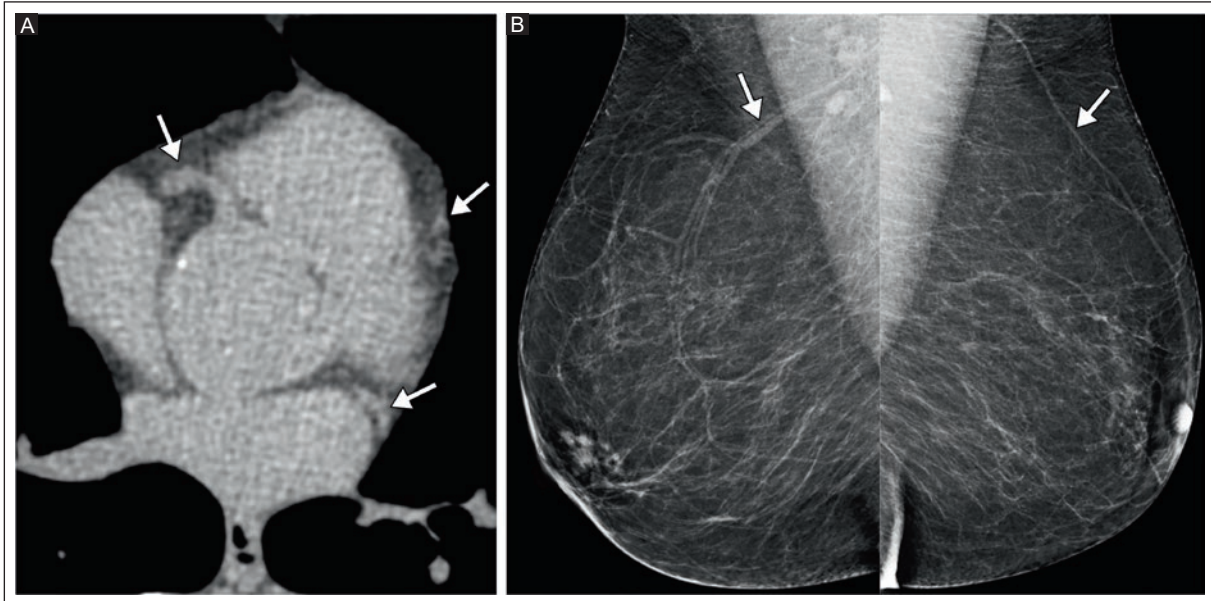


Figure 5. A 66-year-old asymptomatic woman. **A:** coronary CT artery calcium scan, axial view, without calcifications (arrows), AS was 0. **B:** digital mammography in MLO projection of both breasts shows bilateral breast arteries without calcifications (arrows). The BAC score was 0, and the BAC category was 0 (absence).

AS: Agatston score; BAC: breast arterial calcifications; CT: computed tomography; MLO: mediolateral oblique.

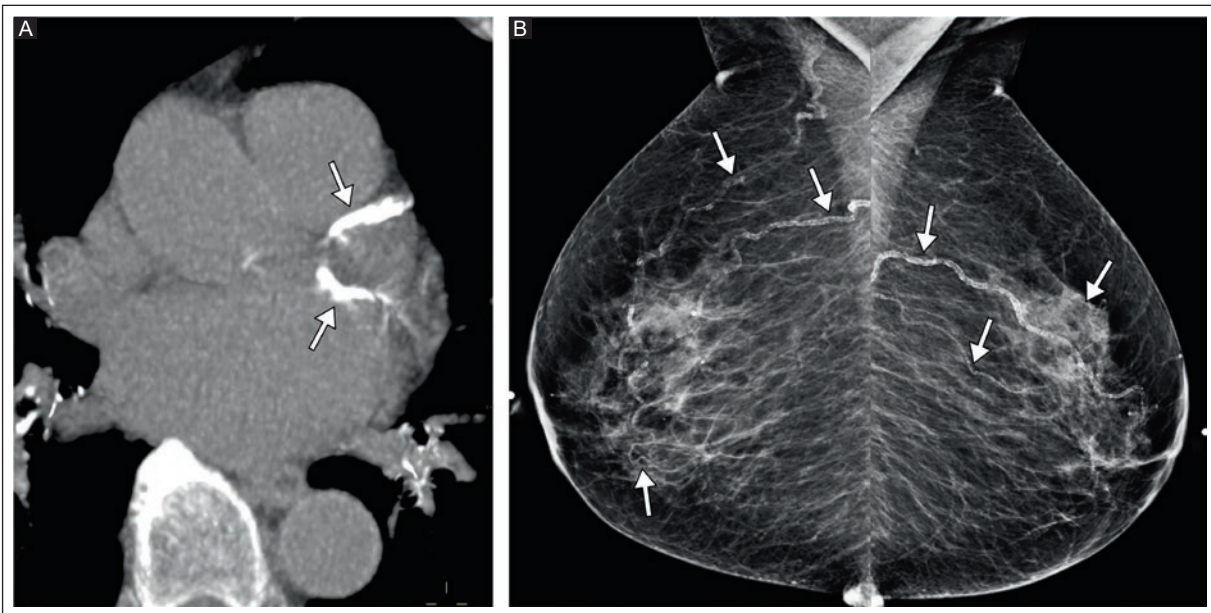


Figure 6. An 81-year-old asymptomatic woman with dyslipidemia. **A:** MIP reconstruction, axial view of coronary CT calcium score with significant CAC (arrows). AS was 1,494, and AC was severe. **B:** digital mammography in MLO projection of both breasts shows 3 arteries (3 points) (arrows) with tram-track calcifications (2 points) and vessel length extension greater than two-thirds (3 points) in each breast. The BAC score was 8 in the BAC category of 4 to 12 (significant).

AC: Agatston category; AS: Agatston score; BAC: breast arterial calcifications; CAC: coronary artery calcifications; CT: computed tomography; MIP: maximum intensity projection; MLO: mediolateral oblique.

distribution reveals the increasing frequency of both BAC and CAC with increasing age and the increasing CAC in those with BAC in each age group. A proposal to optimize the diagnostic performance of BAC could be to target a specific older age group with a better diagnostic performance of BAC for predicting CAC.

Chronic metabolic diseases are associated with CAC and BAC. There are two types of risk factors for coronary artery disease in women. Traditional risk factors include diabetes, smoking, overweight/obesity, sedentarism, systemic arterial hypertension, and dyslipidemia. In contrast, non-traditional factors, such as preterm labor, gestational diabetes, autoimmune disease, radiation and chemotherapy for breast cancer, depression, and early menopause, are unique to women⁶. Margolies et al.¹ reported that BAC was significantly more common in older women and those with systemic arterial hypertension and chronic kidney failure but not in hyperlipidemia and diabetes and that it was less common in smokers. In contrast, Minssen et al.¹¹ reported that diabetes was more common in patients with CAC but not BAC. In our study, obesity, systemic arterial hypertension, and diabetes were significantly associated with the presence of CAC. In contrast, there was no significant association between smoking, systemic arterial hypertension, chronic kidney disease, diabetes, and dyslipidemia, and the presence of BAC. There is no clear explanation for these varying associations. It may be due to differences in the histologic location of BAC, which is in the media of vessels, and CAC, which is located in the intima¹¹.

The issue of systematically reporting BAC on mammograms is open¹¹. Many physicians are unaware of the clinical significance of BAC in screening mammograms, and there is no standard reporting format related to BAC²². Reporting BAC could be considered additional information on mammograms. In one study, physicians from Canada were asked about BAC, and it was found that only 17% were previously aware of the association between BAC and increased cardiovascular risk; 51% preferred the inclusion of BAC in the mammography report, 63% would inform their patients that their mammogram showed evidence of BAC, and 71% agreed that there is a need for guidelines⁵ which emphasizes the importance of integrating BAC into routine mammographic assessment⁴. BAC should be actively sought in all mammograms. Therefore, we recommend that the presence or absence of BAC be routinely reported in mammographic screening.

The strength of our study stems from the systematic quantification of BAC, which allows an objective assessment, and the use of the Agatston score as a quantitative and objective parameter to assess CAC and as a reference for risk stratification in most databases and publications. There are some limitations of the study. First, the retrospective design is subject to selection bias. Second, the patients in this study were not followed, so their clinical evolution is unknown. Third, non-traditional risk factors in women were not recorded. Fourth, intra- and interobserver variability was not assessed. Fifth, the study population consists of a group of Mexican women with a high socioeconomic status, a high educational level, and a healthy lifestyle, which corresponds to a minority group of the Mexican population.

CONCLUSION

In our study, the absence of BAC in screening mammography was linked to the absence of CAC in asymptomatic women, especially in women <60 years of age. These results show another face of the diagnostic possibilities of BAC in mammography. However, no definitive conclusions can be drawn about the clinical benefit of the absence of BAC in women for predicting low risk of subclinical coronary artery disease. Further large randomized controlled trials in patients undergoing screening mammography are needed to assess whether and what role BAC can play in predicting cardiovascular risk in asymptomatic women.

Acknowledgments

The authors thank Professor Ana M. Contreras-Navarro for her guidance in preparing and writing this scientific paper. This original paper in the Radiology Specialty field was an awarded thesis at the Segunda Convocatoria Nacional 2023-2024, "*Las Mejores Tesis de Radiología para Publicar en el JMeXFRI.*"

Funding

This research received no external funding.

Conflicts of interest

The authors declare that they have no conflicts of interest.

Ethical disclosures

Protection of individuals. This study complied with the Declaration of Helsinki (1964) and subsequent amendments.

Confidentiality of data. The authors declare they followed their center's protocol for sharing patient data.

Right to privacy and informed consent. Informed consent was not required for this observational study of information collected during routine clinical care.

Use of artificial intelligence. The authors did not use generative artificial intelligence to prepare this manuscript and/or create tables, figures, or figure legends.

REFERENCES

- Margolies LR, Yip R, Hwang E, Oudsema RH, Subramaniam VR, Hecht H, et al. Breast Arterial Calcification in the Mammogram Report: The Patient Perspective. *Am J Roentgenol.* 2019;212(1):209–214. doi: 10.2214/AJR.18.20171.
- Hendriks EJ, de Jong PA, van der Graaf Y, Mali WP, van der Schouw YT, Beulens JW. Breast arterial calcifications: a systematic review and meta-analysis of their determinants and their association with cardiovascular events. *Atherosclerosis.* 2015;239(1):11–20. doi: 10.1016/j.atherosclerosis.2014.12.035.
- American College of Radiology. (2013). ACR Breast Imaging Reporting and Data System (BIRADS). Reston, VA: American College of Radiology.
- Bui QM, Daniels LB. A Review of the Role of Breast Arterial Calcification for Cardiovascular Risk Stratification in Women. *Circulation.* 2019;139(8):1094–1101. doi: 10.1161/CIRCULATIONAHA.118.038092.
- Zaki-Metias KM, McKee H, Applewhaite C, Davis MK, Keyes M, LeVasseur N. Breast Arterial Calcifications on Mammography: Awareness and Reporting Preferences Amongst Referring Physicians in Canada. *Can Assoc Radiol J.* 2024;8465371241262292. doi: 10.1177/08465371241262292.
- Garcia M, Mulvagh SL, Bairey Merz CN, Buring JE, Manson JE. Cardiovascular Disease in Women. *Circ Res.* 2016;118(8):1273–1293. doi: 10.1161/CIRCRESAHA.116.307547.
- Iribarren C, Chandra M, Lee C, Sanchez G, Sam DL, Azamian FF, et al. Breast Arterial Calcification: a Novel Cardiovascular Risk Enhancer Among Postmenopausal Women. *Circ Cardiovasc Imaging.* 2022;15(3):e013526. doi:10.1161/CIRCIMAGING.121.013526.
- Maas AH, van der Schouw YT, Atsma F, Beijerinck D, Deurenberg JJ, Mali WP, et al. Breast arterial calcifications are correlated with subsequent development of coronary artery calcifications, but their aetiology is predominantly different. *Eur J Radiol.* 2007;63(3):396–400. doi: 10.1016/j.ejrad.2007.02.009.
- Suh J-W, Yun B La. Breast Arterial Calcification: A Potential Surrogate Marker for Cardiovascular Disease. *J Cardiovasc Imaging.* 2018;26(3):125–134. doi: 10.4250/jcvi.2018.26.e20.
- Margolies L, Salvatore M, Hecht HS, Kotkin S, Yip R, Baber U, et al. Digital Mammography and Screening for Coronary Artery Disease. *JACC Cardiovasc Imaging.* 2016;9(4):350–360. doi: 10.1016/j.jcmg.2015.10.022.
- Minssen L, Dao TH, Quang AV, Martin L, Andureau E, Luciani A, et al. Prevalence of Coronary Artery Disease Evaluated by Coronary CT Angiography in Women with Mammographically Detected Breast Arterial Calcifications. *PLoS One.* 2015; 10(4):e0122289. doi: 10.1371/journal.pone.0122289.
- Newallo D, Meinel FG, Schoepf UJ, Baumann S, De Cecco CN, Leddy RJ, et al. Mammographic detection of breast arterial calcification as an independent predictor of coronary atherosclerotic disease in a single ethnic cohort of African American women. *Atherosclerosis.* 2015;242(1):218–221. doi: 10.1016/j.atherosclerosis.2015.07.004.
- Matsumura ME, Maksimik C, Martinez MW, Weiss M, Newcomb J, Harris K, et al. Breast artery calcium noted on screening mammography is predictive of high-risk coronary calcium in asymptomatic women: a case control study. *Vasa.* 2013;42(6):429–433. doi: 10.1024/0301-1526/a000312.
- Chadashvili T, Litmanovich D, Hall F, Slanetz PJ. Do breast arterial calcifications on mammography predict elevated risk of coronary artery disease? *Eur J Radiol.* 2016;85(6):1121–1124. doi: 10.1016/j.ejrad.2016.03.006.
- Moradi M, Adibi A, Abedi M. Relationship between breast arterial calcification on mammography with CT Calcium scoring and coronary CT angiography results. *Adv Biomed Res.* 2014;3:79. doi: 10.4103/2277-9175.127992.
- McLenachan S, Camilleri F, Smith M, Newby DE, Williams MC. Breast arterial calcification on mammography and risk of coronary artery disease: a SCOT-HEART sub-study. *Clin Radiol.* 2019;74(6):421–428. doi: 10.1016/j.crad.2019.01.014.
- Agatston AS, Janowitz WR, Hildner FJ, Zusmer NR, Viamonte M, Detrano R. Quantification of coronary artery calcium using ultrafast computed tomography. *J Am Coll Cardiol.* 1990;15(4):827–832. doi: 10.1016/0735-1097(90)90282-T.
- Osman M, Regner S, Osman K, Shahan C, Kheiri B, Kadiyala M. Association Between Breast Arterial Calcification on Mammography and Coronary Artery Disease: A Systematic Review and Meta-Analysis. *J Womens Health (Larchmt).* 2022;31(12):1719–1726. doi: 10.1089/jwh.2020.8733.
- Elizondo Riojas G. [Mamografía Más Allá del Cáncer: Las Calcificaciones Arteriales y su Relevancia] [Internet]. Monterrey (MX): Universidad Autónoma de Nuevo Leon; 2024 Jul 25 [cited 2024, Jul 27]. Podcast: 19 min. Available from: <https://open.spotify.com/episode/4S9Eghkg7J2Tn0urOwBLGv?si=J7IH2ejAQPCKSSG2-U-j8sg&nd=1&dlsi=fc6e1a9a308f4a50>.

Multimodality findings of sclerosing adenosis on mammography, US, and MRI in Mexican women

Karen L. Ceballos-Martinez¹, Yesika J. Davila-Zablah^{1*}, Miguel A. Hinostrroza-Sanchez¹,
Maria Guerra-Ayala¹, Mariana del Rio-Gonzalez¹, Laura A. Ortiz-Arizmendi¹,
Gabriela S. Gomez-Macias¹, Daniel F. Lopez-Altamirano¹, and Margarita L. Garza-Montemayor¹

Diagnostic Breast Imaging Center, Hospital Zambrano Hellion, TecSalud. Monterrey, Nuevo Leon, Mexico

ABSTRACT

Introduction: Sclerosing adenosis is a benign, proliferative breast disease. Few reports of imaging findings exist in the world literature, and none exists in Mexican literature. This study describes the mammography, ultrasound (US), and magnetic resonance imaging (MRI) findings of histopathologically confirmed sclerosing adenosis in Mexican women. **Materials and Methods:** This retrospective cross-sectional study was conducted in two private medical centers from January 2006 to July 2022. Adult women with a histopathologic diagnosis of sclerosing adenosis and an imaging examination, mammography, breast (US), and/or MRI were included. **Results:** A total of 169 women with a median age of 47.0 ± 8.4 years were included. Screening was the main indication for the imaging examination ($n = 130, 76.9\%$). Of the 169 patients, 25 (14.8%) had a relative with a history of breast cancer, whereas 23 (13.6%) had a personal history of breast cancer. Mammography was performed on 155 (91.7%) patients. The most common finding was the grouping of amorphous and pleomorphic calcifications ($n = 55, 44.7\%$). Breast US was performed in 147 (86.9%) patients, with an oval, circumscribed, hypoechoic, avascular mass being the most common findings ($n = 61, 41.5\%$), followed by architectural distortions ($n = 32, 21.8\%$). Breast MRI was performed in 17 women; non-mass enhancement was the most common finding ($n = 8, 47.0\%$). **Conclusion:** Our study comprehensively describes sclerosing adenosis multimodality imaging findings with mammography, US, and MRI. We found no specific imaging feature.

Keywords: Sclerosis adenosis. Multimodal imaging. Mammography. Ultrasound. Magnetic resonance imaging.

INTRODUCTION

Sclerosing adenosis, first described in 1968¹, is a benign proliferative breast disease that occurs more frequently in women of reproductive age and during perimenopause². This non-atypical proliferative lesion involves the epithelial (terminal duct lobular unit) and mesenchymal components of the breast³. Sclerosing adenosis is associated with benign (cystic changes, apocrine metaplasia, fibroadenoma, and intraductal

papilloma) and malignant (carcinoma in situ and invasive ductal carcinoma) lesions^{1,3}. It occurs in 12-28% of benign lesions and 5-7% of malignant lesions at histopathologic diagnosis⁴. Although it is not considered a premalignant lesion, it represents a relative risk (1.7-3.7) for the development of invasive carcinoma. It can simulate malignancy on imaging examination, which is why it is clinically significant^{1,3}. Due to its similarity to breast cancer, it is usually categorized as BI-RADS 4 or 5⁵.

*Corresponding author:

Yesika J. Davila-Zablah
E-mail: yesikadavila@gmail.com

Received for publication: 13-02-2024

Accepted for publication: 23-04-2024

DOI: 10.24875/JMEXFRI.M24000080

Available online: 03-10-2024

J Mex Fed Radiol Imaging. 2024;3(3):162-174

www.JMeXFRI.com

2696-8444 / © 2024 Federación Mexicana de Radiología e Imagen, A.C. Published by Permanyer. This is an open access article under the CC BY-NC-ND (<https://creativecommons.org/licenses/by-nc-nd/4.0/>).

Mammography and ultrasound (US) are common methods for evaluating breast lesions^{1,2,5,6}. Mammograms may show focal asymmetry, calcifications, or architectural distortion as sclerosing adenosis findings². It may appear as a mass, architectural distortion, or non-mass lesion on US^{3,5}, as a mass, non-mass enhancement, or focus on contrast-enhanced breast magnetic resonance imaging (MRI)⁶. Few authors have described mammography, US, and MRI features^{3,5-7}, and there are no reports on Mexican women. This study aimed to describe the mammography, US, and MRI findings of histopathologically confirmed sclerosing adenosis in Mexican women.

MATERIALS AND METHODS

This retrospective cross-sectional study was conducted in the Breast Imaging Department of the San José Hospital and Zambrano Hellion Hospital, TecSalud in Monterrey, Nuevo Leon, Mexico, from January 2006 to July 2022. We included all cases of sclerosing adenosis diagnosed by percutaneous or excisional biopsy during the study period. Patients who had no imaging record in PACS or with an association with other benign breast lesions or malignancies were excluded. Informed consent was not required for this retrospective data analysis obtained during routine medical care. The institutional ethics and research committees approved this study.

Study development and variables

We reviewed the pathology database to identify all sclerosing adenosis cases. Age, family history of breast cancer, personal history of breast cancer, the reason for the imaging examination (screening or diagnosis), and clinical signs such as a palpable breast mass, pain, telorrhea, and telorrhagia were recorded for each case.

Image acquisition and analysis

Images were stored in a Picture Archiving and Communication System (PACS) (Carestream, Phillips, Rochester, NY, USA). Radiologists (YDZ) with 14 and (MGM) 25 years of experience in breast imaging performed the image analysis.

Mammography

Craniocaudal, mediolateral oblique, and magnified images of each breast were obtained using a Selenia Dimensions™ (Hologic, Inc., Bedford, MA, USA) or an

Table 1. Characteristics and clinical manifestations of 169 patients with sclerosing adenosis

Description	n (%)
Age, years mean ± SD	47.0 ± 8.4
Family history of breast cancer	
Yes	25 (14.8)
Mother	5 (20.0)
Sister	8 (32.0)
Grandmother	3 (12.0)
Aunt	3 (12.0)
Daughter	2 (8.0)
Two or more ^a	4 (16.0)
No	144 (85.2)
Personal history of breast cancer	
Yes	23 (13.6)
No	146 (86.4)
Indication for imaging examination	
Screening	130 (76.9)
Diagnosis	39 (23.1)
Clinical manifestations	
Palpable lump	35 (89.7)
Telorrhea	2 (5.1)
Pain	1 (2.6)
Telorrhagia	1 (2.6)

^aTwo or more relatives.

IMS Giotto Tomo (Sasso Marconi BO, Italy) digital mammography system. The breast characteristics were assessed according to the BI-RADS⁸.

Breast US

US examination was performed with iU22, EPIC7g, or EPIC 7w equipment (Phillips Co. Bothell, WA, USA) with a linear 14-, 17.2-, and 18.4-MHz multifrequency transducer in grayscale, color Doppler, and power Doppler. Ultrasonographic features were evaluated according to the BI-RADS⁸.

Contrast-enhanced breast MRI

A 1.5-T Magnetom Aera and a 3T Espree MRI (Siemens Medical Solutions, Erlangen, Germany) were used.

Table 2. Mammography findings of 155 women with sclerosing adenosis by BI-RADS

Description	n (%)
Normal mammography ^a	32 (20.6)
Abnormal mammography	123 (79.4)
Mass	18 (14.5)
Asymmetry	14 (11.3)
Architectural distortion	22 (17.8)
Calcifications	55 (44.7)
Mass and calcifications	4 (3.6)
Architectural distortion and calcifications	10 (8.1)
Size of lesions ^b	109
< 0.5 cm	6 (5.6)
0.5-2 cm	80 (73.3)
2-5 cm	18 (16.5)
> 5 cm	5 (4.6)

^aIn total, 32 patients with normal mammography showed abnormal findings in breast ultrasound; ^bAsymmetry was not considered (n = 14).

BI-RADS: Breast Imaging-Reporting and Data System.

Sequences were performed in T1-weighted without contrast and TIRM. A gadolinium-based contrast agent was injected at a dose of 0.1 mL/kg at a rate of 2 mL/s with the acquisition of five post-contrast T1-weighted series with subtraction and subsequent multiplanar reformatting and maximum intensity projection (MIP). MRI characteristics were assessed according to the BI-RADS⁸.

Percutaneous and excisional breast biopsy

A BARD Magnum Disposable Core Biopsy Instrument, 12G x 10 cm needle (BARD, Tempe, AZ, USA), was used for percutaneous biopsy of the breast lesion. In some patients, an excisional biopsy was performed by a surgeon in the operating room. This was done before placing a BARD DuaLok (Tempe, AZ, USA) US breast localization wire 20G x 5.5 cm and 20G x 7.7 cm. Complete removal of the lesion was confirmed by mammography or US. Breast biopsies were evaluated by a breast pathology specialist with 12 years of experience (GG).

Statistical analysis

Data are presented as frequencies, percentages, means, and standard deviation. Excel version 18.0 (Microsoft Co. Seattle, WA, USA) was used.

Table 3. Mammography findings of 155 women with sclerosing adenosis by BI-RADS

Breast composition	n (%)
a. Almost entirely fatty	1 (0.6)
b. Scattered densities	27 (17.4)
c. Heterogeneously dense	90 (58.1)
d. Extremely dense	37 (23.9)
Descriptors	
Mass ^a	22
Shape	
Oval	12 (54.5)
Round	6 (27.3)
Irregular	4 (18.2)
Margin	
Circumscribed	12 (54.6)
Not circumscribed	
Obscured	3 (13.6)
Microlobulated	4 (18.2)
Indistinct	2 (9.1)
Spiculated	1 (4.5)
Density	
High	10 (45.5)
Equal	12 (54.5)
Asymmetry	14 (9.0)
Architectural distortion ^b	22 (14.2)
Low density	18 (56.3)
High density	14 (43.7)
Calcifications ^c	n = 69
Amorphous	42 (60.9)
Coarse heterogeneous	10 (14.5)
Fine pleomorphic	13 (18.8)
Fine linear	4 (5.8)
Associated features	
Skin retraction	2 (1.0)
Axillary adenopathy	2 (1.0)

^aIncluded 18 masses and 4 masses + calcifications; ^bincluded 22 architectural distortions and 10 architectural distortions + calcifications; ^cincluded 55 calcifications, 4 masses + calcifications, and 10 architectural distortions + calcifications.

BI-RADS: Breast Imaging-Reporting and Data System.

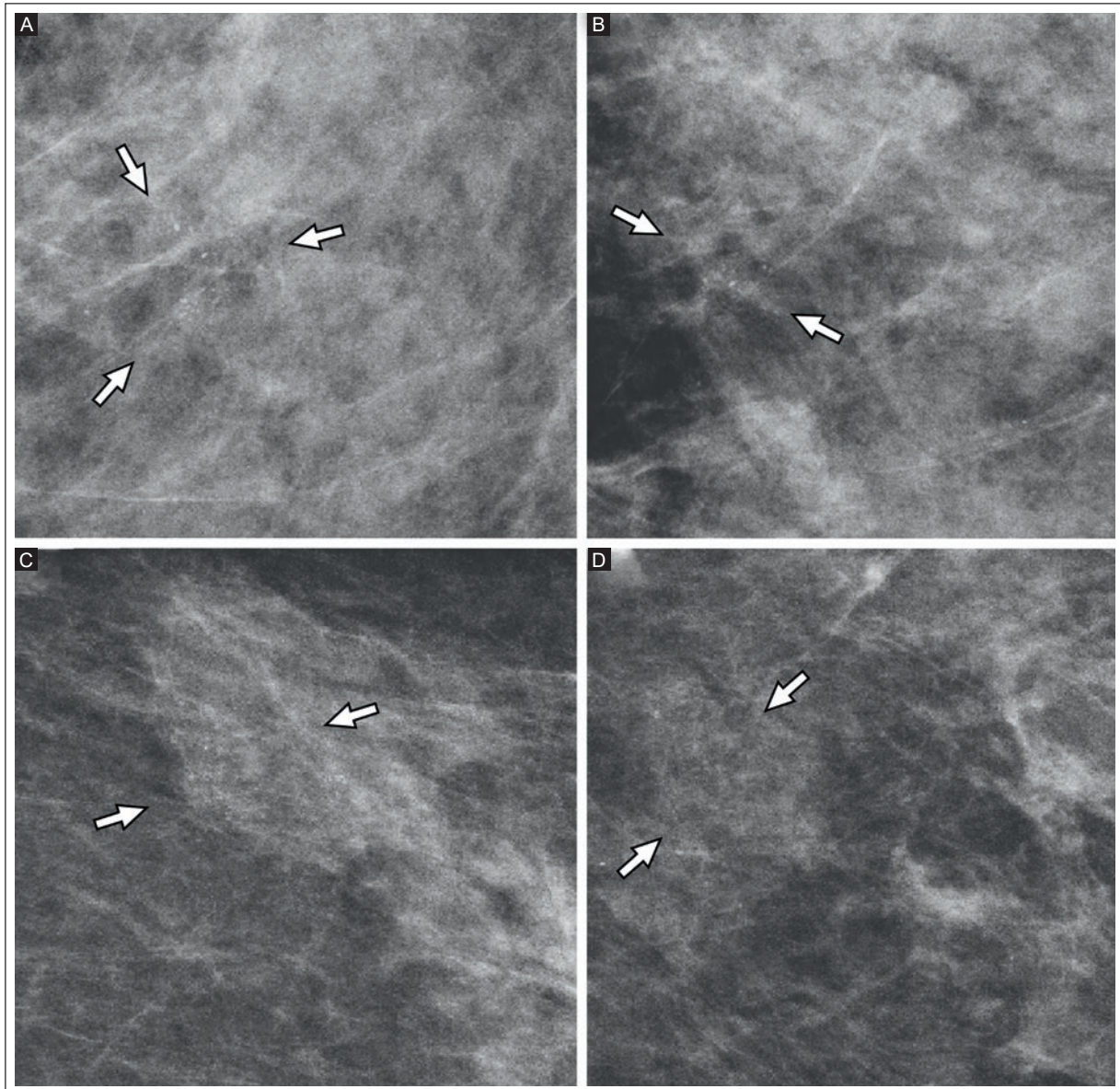


Figure 1. Screening mammography of a 44-year-old woman. **A:** magnified CC projection. **B:** magnified lateral projection shows fine pleomorphic calcifications (arrows) with focal distribution at the junction of the inner quadrants in the left breast, in an area of 7 mm, and not associated with any mass or distortion. The histopathologic diagnosis was sclerosing adenosis. Screening mammogram of a 40-year-old woman. **C:** magnified CC projection. **D:** magnified lateral projection of a group of amorphous calcifications (arrows) with focal distribution in the upper outer quadrant of the left breast in an area of 18 mm, not associated with a mass or distortion. The histopathologic diagnosis was sclerosing adenosis.

CC: craniocaudal.

RESULTS

In total, 205 women with a histopathological diagnosis of sclerosing adenosis were identified; 36 were excluded due to missing images in PACS, leaving a final sample of 169 women with at least one imaging study such as mammography ($n = 155$), breast US ($n = 147$), and breast MRI ($n = 17$). All women were between 28 and 73 years of age (mean 47.0 ± 8.4). Nearly 25 (14.8%) of the 169

patients had a relative with a history of breast cancer and 23 (13.6%) had a personal history of breast cancer (Table 1). The most common indication for examination was screening in 130 (76.9%) patients. The number of women who underwent diagnostic examinations was $n = 39$ (23.1%). The most common clinical finding was a palpable lump ($n = 35$, 89.7%) and telorrhea, pain, and telorrhagia in others.

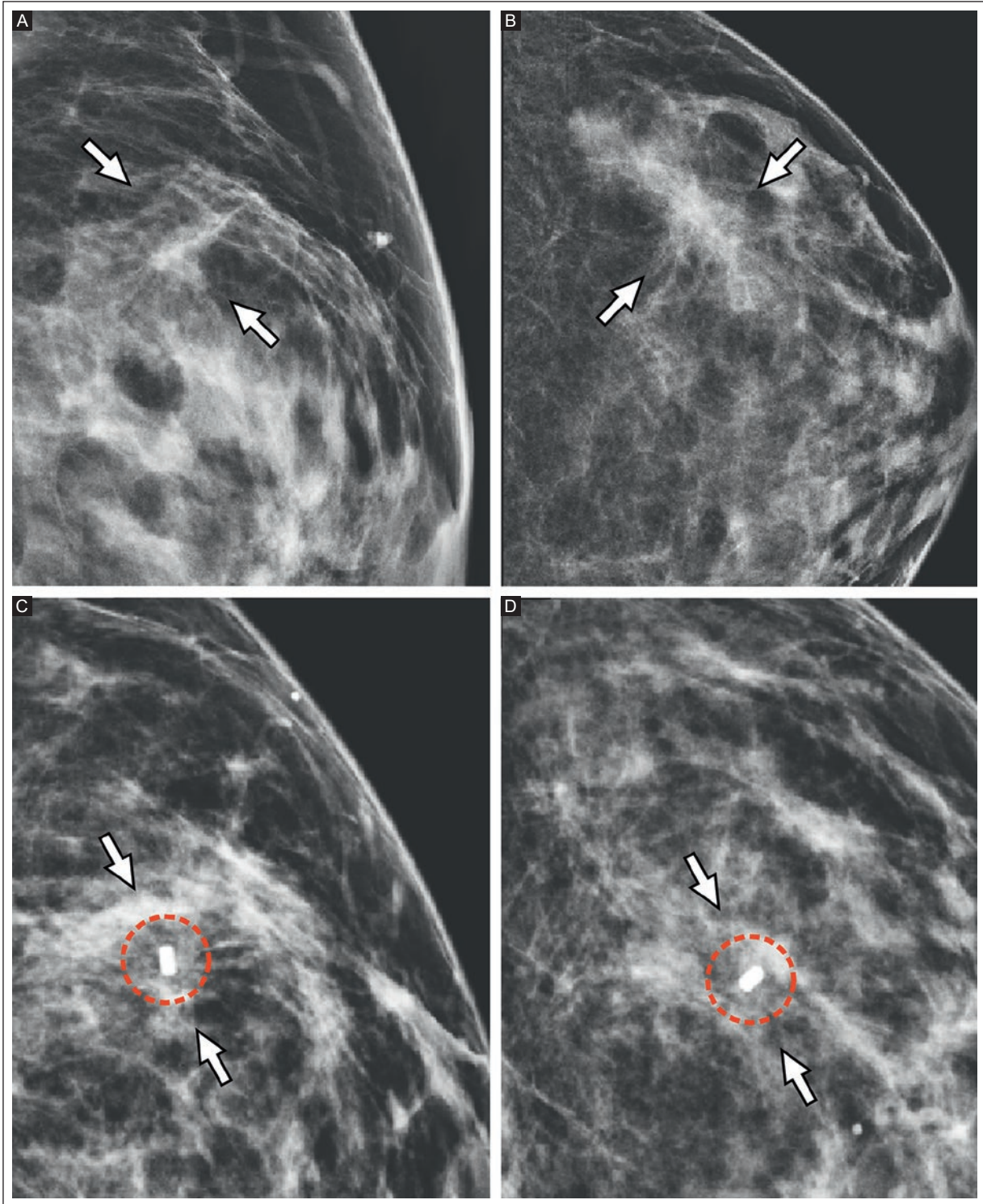


Figure 2. Screening mammogram of a 39-year-old woman. **A:** magnified lateral projection. **B:** magnified CC projection showing an architectural distortion area (arrows) in the upper outer quadrant of the left breast. The histopathologic diagnosis was sclerosing adenosis. Screening mammogram of a 39-year-old woman. **C:** lateral projection. **D:** CC projection showing an architectural distortion area (arrows) in the upper outer quadrant of the left breast. Biopsy markers can also be seen (circles). The histopathologic diagnosis was sclerosing adenosis. CC: craniocaudal.

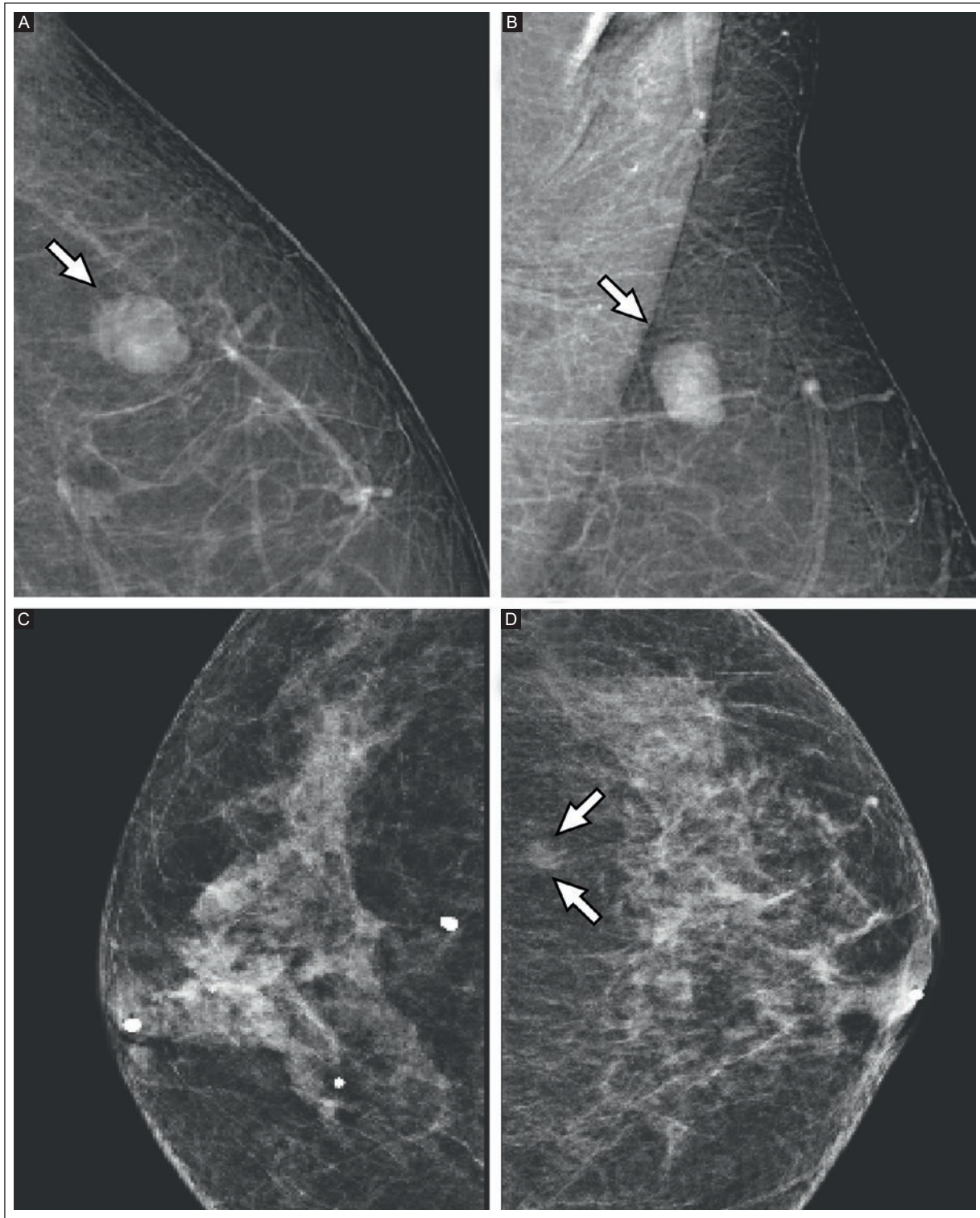


Figure 3. Diagnostic mammogram of a 44-year-old woman. **A:** CC projection. **B:** MLO projection of an oval, circumscribed, high-density mass in the upper outer quadrant of the left breast (arrows). The histopathologic diagnosis was sclerosing adenosis. A screening mammogram of a 59-year-old woman. **C** y **D:** CC projections of both breasts. Asymmetry (arrows) in the outer quadrant is seen in the left breast. The histopathologic diagnosis was sclerosing adenosis.

CC: craniocaudal; MLO: mediolateral oblique.

Table 4. US findings of 147 women with sclerosing adenosis

Description	n (%)
Normal US ^a	20 (13.6)
Abnormal US	127 (86.4)
Size of the lesions ^b	
< 0.5	4 (3.2)
0.5-2 cm	99 (79.9)
2.1-5 cm	16 (12.9)
> 5 cm	5 (4.0)

^aIn total, 20 women with normal US showed abnormal findings in mammography;

^bductal changes were not considered.

US: ultrasound.

Mammography findings

Mammograms were normal in 32 (20.6%) of 155 (Table 2). In those with an abnormal examination, 123 (79.4%), the findings were a mass (n = 18, 14.5%), asymmetry (n = 14, 11.3%), architectural distortion (n = 22, 17.8%), calcifications (n = 55, 44.7%), a mass and calcifications (n = 4, 3.6%), and architectural distortion and calcifications (n = 10, 8.1%). The lesion size was between 0.5 and 2 cm (n = 80, 73.3%).

The most common breast composition was category c (n = 90, 58.1%) (Table 3). In 22 masses, the most common shape was oval (n = 12, 54.5%) with a circumscribed margin (n = 12, 54.6%) and equal density (n = 12, 54.5%). Asymmetry was found in 14 (9.0%), architectural distortion was found in 22 (14.2%), and low density was the most common. In total, 69 calcifications were found; amorphous (n = 42, 60.9%) and fine pleomorphic (n = 13, 18.8%) morphologies were the most common. Other rare associated findings were skin retraction (n = 2, 1.0%) and axillary adenopathy (n = 2, 1.0%).

Figure 1 shows pleomorphic and amorphous calcifications on screening mammograms. Figure 2 shows an architectural distortion on screening mammograms. Figure 3 shows an oval circumscribed mass and asymmetry on diagnostic and screening mammograms.

US findings

US findings were normal in 20 (13.6%) and abnormal in 127 (86.4%) of 147 women (Table 4). The most common lesion size was 0.5-2 cm (n = 99, 79.9%). Table 5 shows the most common breast composition, category c (n = 92, 62.6%). We found 61 (41.5%) masses. The most common shape was oval (n = 44, 72.1%), with a

Table 5. US findings of 147 women with sclerosing adenosis by BI-RADS

Breast composition	n (%)
a. Homogeneous background echotexture fat	0
b. Homogeneous background echotexture fibroglandular	55 (37.4)
c. Heterogeneous background echotexture	92 (62.6)
Descriptors	
Mass	61 (41.5)
Shape	
Oval	44 (72.1)
Round	3 (4.9)
Irregular	14 (23.0)
Orientation	
Parallel	59 (96.7)
Not parallel	2 (3.3)
Margin	
Circumscribed	32 (52.5)
Not circumscribed	
Indistinct	9 (14.7)
Angular	5 (8.2)
Microlobulated	15 (24.6)
Echo pattern	
Anechoic	3 (4.9)
Hyperechoic	1 (1.6)
Complex cystic and solid	5 (8.2)
Hypoechoic	44 (72.1)
Isoechoic	4 (6.6)
Heterogeneous	4 (6.6)
Posterior features	
Enhancement	13 (21.3)
Shadowing	8 (13.1)
Combined pattern	7 (11.5)
None	33 (54.1)
Vascularity	
Yes	29 (19.7)
No	118 (80.3)
Architectural distortion	32 (21.8)
Non-mass lesion	31 (21.1)
Duct changes	3 (2.04)

^aBI-RADS: Breast Imaging-Reporting and Data System; US: ultrasound.

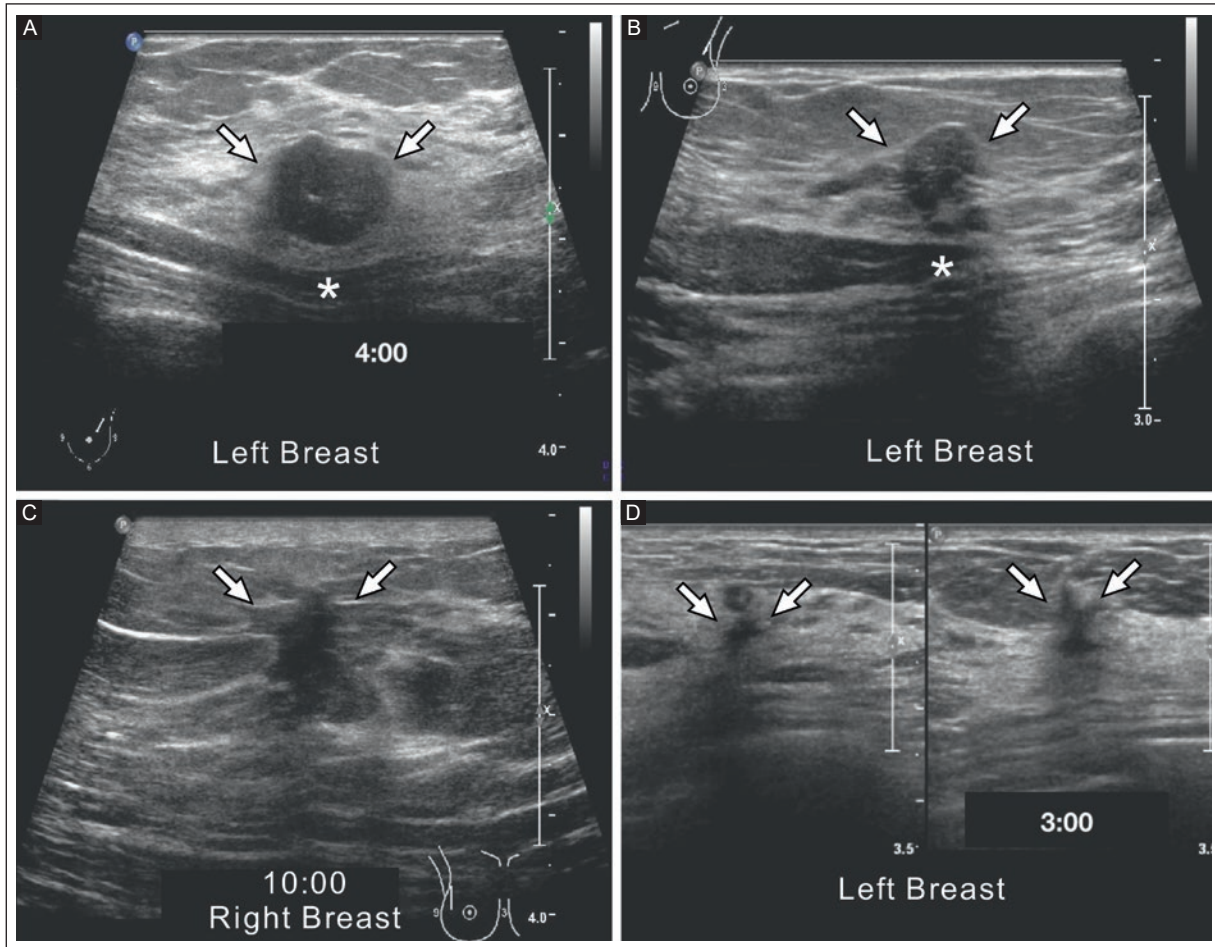


Figure 4. A: diagnostic grayscale US of a 47-year-old woman shows an oval, parallel, circumscribed, hypoechoic mass (arrows) with posterior shadowing (asterisk). The histopathologic diagnosis was sclerosing adenosis. **B:** diagnostic grayscale US of a 52-year-old woman shows an oval, parallel mass (arrows) with lobulated margins, posterior shadowing (asterisk), and ductal changes. The histopathologic diagnosis was sclerosing adenosis. **C:** diagnostic grayscale US of a 33-year-old woman shows architectural distortion (arrows). The histopathologic diagnosis was sclerosing adenosis. **D:** diagnostic grayscale US in a 41-year-old woman shows architectural distortion (arrows). The histopathologic diagnosis was sclerosing adenosis.

US: ultrasound.

parallel orientation ($n = 59$, 96.7%), circumscribed margin ($n = 32$, 52.5%), and a hypoechoic pattern ($n = 44$, 72.1%), without posterior features ($n = 33$, 54.1%) and vascularity ($n = 118$, 80.3%). Other findings were duct changes ($n = 3$, 2.04%), non-mass lesions ($n = 31$, 21.1%), and architectural distortion ($n = 32$, 21.8%).

Figure 4 shows an oval mass and architectural distortion on a diagnostic breast US examination. Figure 5 shows a non-mass lesion and a conglomerate of prominent ducts on a screening US examination.

MRI findings

Breast MRI was performed in 17 patients (Table 6). The most common breast composition categories

were b and c, equally ($n = 6$, 35.3%). Background enhancement of the parenchyma was minimal or mild ($n = 5$, 29.4%). The findings were masses ($n = 6$, 35.2%) with an oval shape ($n = 3$, 50.0%) as the most common, a circumscribed margin ($n = 4$, 66.7%), and homogeneous internal enhancement ($n = 2$, 33.3%).

The most common MRI finding was non-mass enhancement ($n = 8$, 47%) with focal distribution ($n = 6$, 75.0%). Internal enhancement was equally homogeneous and heterogeneous ($n = 4$, 50.0%). A focus was found in 3 (17.6%); the most common sizes were 0.5-2 cm ($n = 12$, 70.6%).

Figure 6 shows an irregular enhancement mass on a diagnostic contrast-enhanced breast MRI.

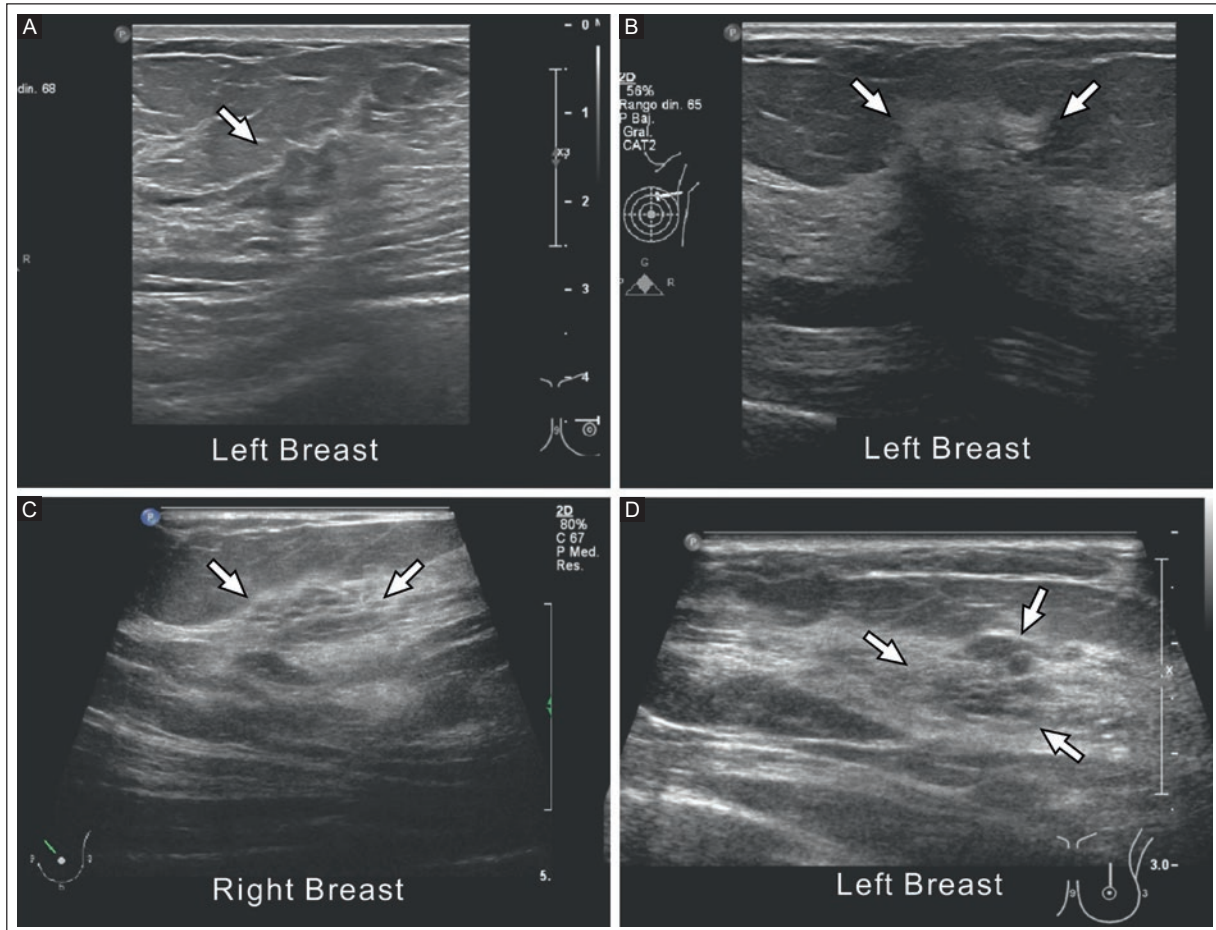


Figure 5. A: screening grayscale US of a 47-year-old woman shows a non-mass, hypoechoic, irregular lesion (arrow). The histopathologic diagnosis was sclerosing adenosis. **B:** diagnostic grayscale US of a 38-year-old woman with a non-mass, isoechoic, irregular lesion (arrows). The histopathologic diagnosis was sclerosing adenosis. **C:** screening grayscale US of a 51-year-old woman with a conglomerate of prominent ducts (arrows). The histopathologic diagnosis was sclerosing adenosis. **D:** screening grayscale US of a 47-year-old woman with a conglomerate of prominent ducts (arrows). The histopathologic diagnosis was sclerosing adenosis. US: ultrasound.

Figure 7 shows non-mass enhancement and a scattered focus on a diagnostic contrast-enhanced breast MRI.

cell layer. Figure 8 shows stromal sclerosis of the terminal duct lobular unit compressing and distorting the acini on histologic sections.

Histologic diagnosis

Sclerosing adenosis was diagnosed by percutaneous biopsy in 149 patients and by excisional biopsy in 20. Sclerosing adenosis affects the components of the terminal duct lobular unit, increasing the number and size of acini. Sclerosis of the periacinar stroma compresses and distorts the acini, resulting in the characteristic swirling image and preserving the lobular-centric architecture. This finding may be associated with calcifications. The affected acinus preserves its epithelial lining by a luminal and a myoepithelial

DISCUSSION

Our study comprehensively describes the multimodality imaging findings of sclerosing adenosis using mammography, US, and MRI. We did not find a specific imaging feature in our population. Radiologists need to know how sclerosing adenosis behaves in multimodality images to be aware of these findings to make an accurate radiologic–pathologic correlation of sclerosing adenosis.

Sclerosing adenosis on mammograms may appear as a focal or diffuse lesion with various features, including

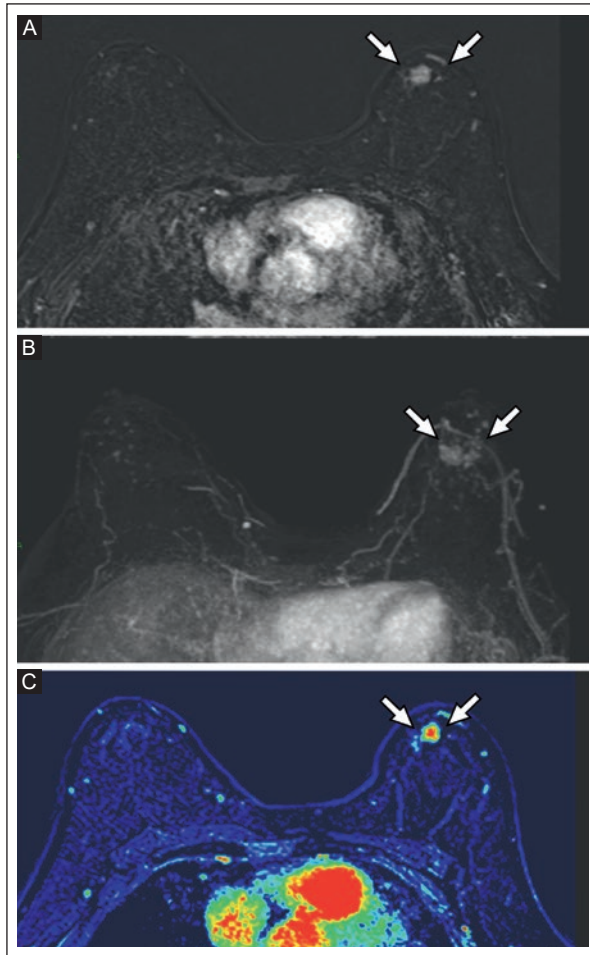


Figure 6. Diagnostic contrast-enhanced breast MRI of a 52-year-old woman. **A:** contrast-enhanced subtracted image. **B:** maximum intensity projection. **C:** PEI color map showing an irregularly shaped mass (arrows) with margin and homogeneous enhancement in the upper inner quadrant of the left breast. The histopathologic diagnosis was sclerosing adenosis.

MRI: magnetic resonance imaging. PEI: positive enhancement integral.

calcification, mass, focal asymmetry, and architectural distortion^{2,5,9}. The combination of imaging features in mammography can mimic breast carcinoma^{3,4,7}. According to our study, calcifications were the most common abnormal mammographic finding in sclerosing adenosis ($n = 55$, 44.7%). This result is consistent with Ling et al.⁵, in which calcifications were found in 43 (31.6%) of 136 mammograms, and with Günhan-Bilgen et al.⁴, in which microcalcifications were present in 24 (55.8%) of 43 mammograms of histopathologically proven sclerosing adenosis cases. Both authors concluded that the accuracy of mammograms and their ability to differentiate sclerosing adenosis from malignancy is limited or unreliable. In our study, areas of architectural distortion were found in 14.2% of our

Table 6. MRI findings of 17 women with sclerosing adenosis by BI-RADS

Breast composition	n (%)
a. Almost entirely fat	0
b. Scattered fibroglandular tissue	6 (35.3)
c. Heterogeneous fibroglandular tissue	6 (35.3)
d. Extremely fibroglandular tissue	5 (29.4)
Background parenchymal enhancement	
Minimal	5 (29.4)
Mild	5 (29.4)
Moderate	7 (41.2)
Masses	
Shape	
Oval	3 (50.0)
Round	2 (33.3)
Irregular	1 (16.7)
Margin	
Circumscribed	4 (66.7)
Not circumscribed	
Irregular	2 (33.3)
Internal enhancement characteristics	
Homogeneous	2 (33.3)
Heterogeneous	1 (16.7)
Rim enhancement	3 (50.0)
Non-mass enhancement	
Distribution	
Focal	6 (75.0)
Linear	2 (25.0)
Internal enhancement pattern	
Homogeneous	4 (50.0)
Heterogeneous	4 (50.0)
Focus	3 (17.6)
Size of the lesions	
< 0.5	3 (17.6)
0.5-2 cm	12 (70.6)
2.1-5 cm	2 (11.8)

^aBI-RADS: Breast Imaging-Reporting and Data System; MRI: magnetic resonance imaging.

patients ($n = 22/155$), and a normal mammogram was found in 20.6% ($n = 32/155$). The presence of architectural distortion in our population was less frequent than

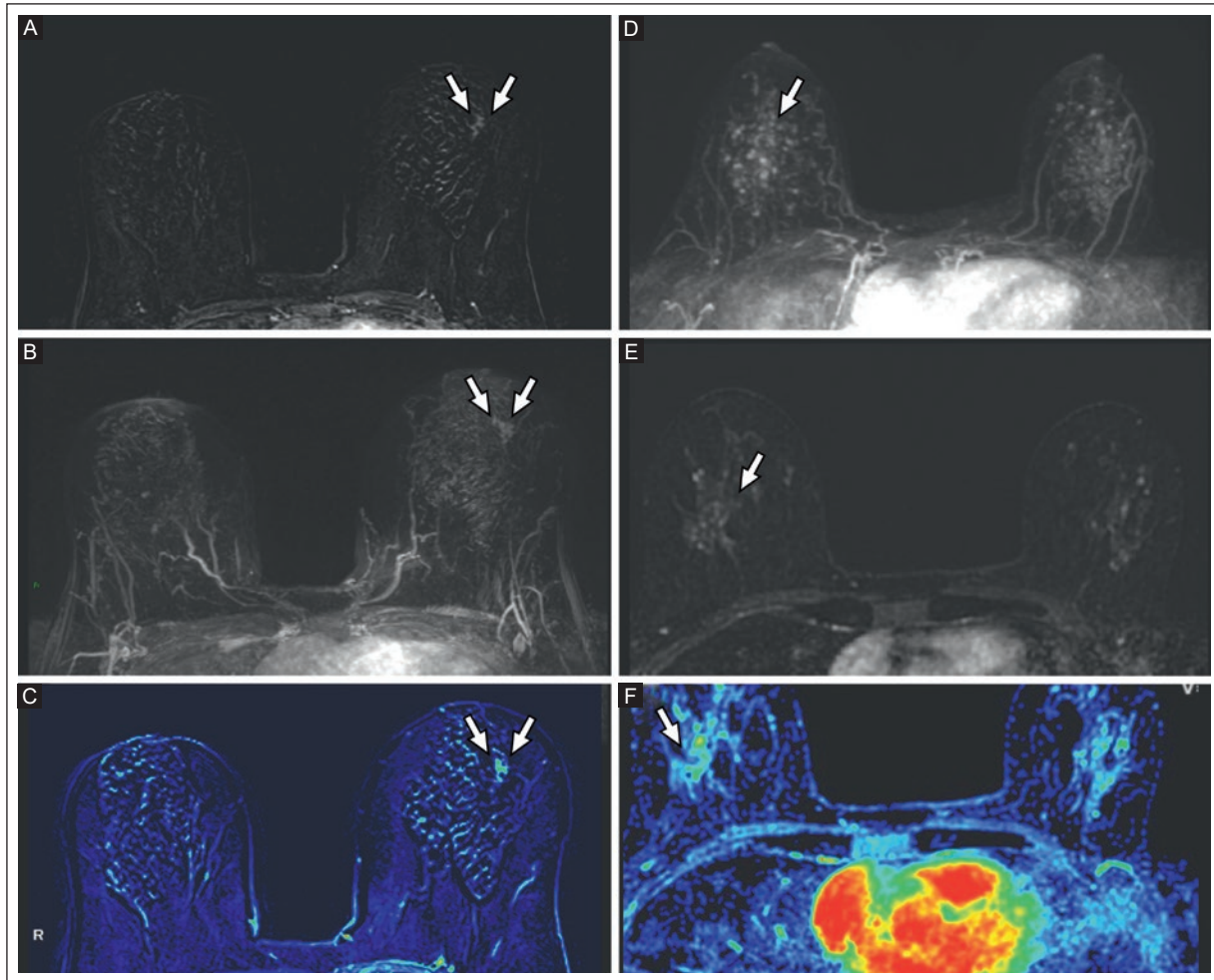


Figure 7. Diagnostic contrast-enhanced breast MRI of a 60-year-old woman. **A:** contrast-enhanced subtracted image. **B:** maximum intensity projection. **C:** PEI color map showing a non-mass enhancement, focal with homogeneous enhancement (arrows) at the junction of the outer quadrants in the left breast. The histopathologic diagnosis was sclerosing adenosis. Diagnostic contrast-enhanced breast MRI in a 57-year-old woman. **D:** contrast-enhanced subtracted image. **E:** maximum intensity projection. **F:** PEI color map showing scattered foci in both breasts, predominantly in the right breast (arrows). The histopathologic diagnosis was sclerosing adenosis.

MRI: magnetic resonance imaging. PEI: positive enhancement integral.

in the study by Ozturk et al.⁹ in which architectural distortion was a common mammographic feature of sclerosing adenosis. It was observed in 21% of mammograms (n = 5/26). Higher rates of architectural distortion have been described, as in the study by Tan H et al.², who reported a 30.8% rate of this mammography feature (n = 12/39), which was the most common. Sclerosing adenosis has several mammography features, with calcifications and architectural distortion being the most common. Although the features of sclerosing adenosis on mammography are not reliable enough to rule out or confirm the diagnosis of cancer, they do raise the radiologist's suspicion of an underlying malignancy; thus, mammography remains an essential imaging modality for breast lesions.

US examination is a common method for diagnosing breast lesions. Compared to mammography, it can provide detailed images of sclerosing adenomatous lesion morphology and internal features. However, the overall appearance of sclerosing adenosis on US examination is also non-specific and includes oval, hypoechoic, non-shadowing masses with circumscribed, indistinct, or microlobulated margins. It may appear as a solid or complex cyst. Several authors have described a mass appearance as the main finding in US breast examination, ranging from 51.7 to 87.5%^{2,3,5,9}. In our study, a mass was the most common lesion detected (n = 61, 41.5%) on US examination in 147 women, with 54.6% (n = 32/61) having a circumscribed margin. These findings are consistent

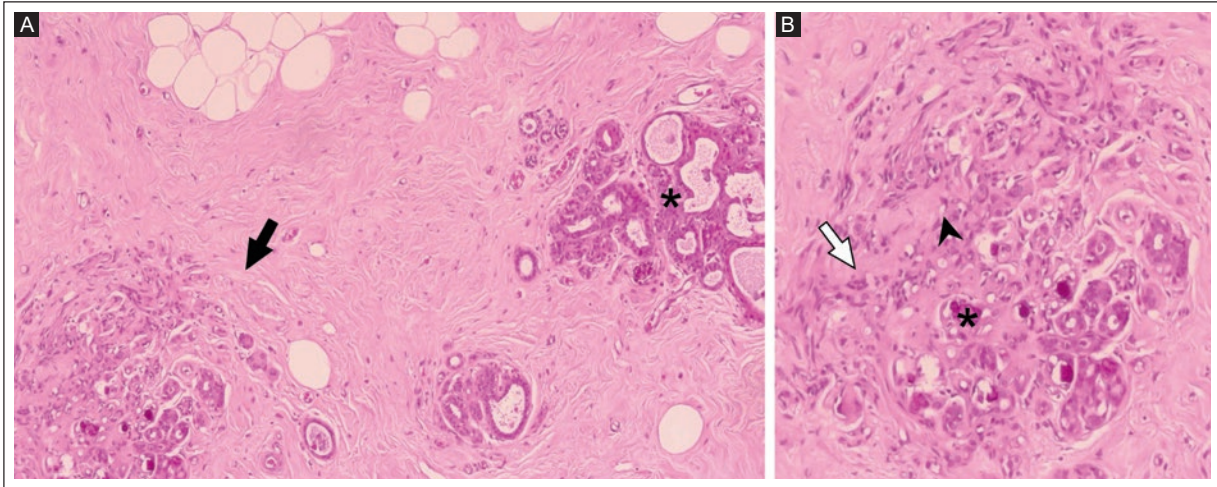


Figure 8. Histology findings. **A:** sclerosing adenosis with calcifications. The adenosis shows a lobulocentric architecture with increased acini embedded in a sclerotic stroma (black arrow). There are also changes and hyperplasia of the columnar cells (asterisk) adjacent to the lobule (hematoxylin and eosin stain 10x). **B:** at higher magnification, the stromal sclerosis of the terminal duct lobular unit compresses and distorts the affected acini (white arrow). The lesion preserves epithelial and myoepithelial cells (black arrowhead) with calcifications (asterisk) associated with sclerosing adenosis (hematoxylin and eosin stain 20x).

with Tan H et al.², who described a well-defined margin in 60% (21 of 35 women). Acoustic shadowing was found in 13.1% (n = 8) of the masses in our study. Acoustic shadowing was found by Taskin et al.¹⁰ in 5% (2 of 37 women) and Günhan-Bilgen et al. in 10% (3 of 30 women)⁴. The US appearance of sclerosing adenosis is highly variable, and our study agrees with other reports stating mass appearance features as the most common finding. Nevertheless, other US features are not specific to sclerosing adenosis.

MRI continues to be addressed in the literature with new approaches to imaging protocols and artificial intelligence. Sclerosing adenosis has a wide spectrum of features, such as enhanced mass, non-enhanced mass, architectural distortion, and no findings at all, as in other imaging modalities⁷. The most common finding on MRI in our study of sclerosing adenosis was non-mass enhancement, which occurred in 8 (47%) of 17 cases. This contrasts with Panourgias et al.⁷, who described a mass-type lesion as the main finding, occurring in 19 (73%) of 26 patients. Enhancing mass-type lesions were the main MRI findings in our study in 35% (n = 6) of the 17 cases. Similar studies have reported enhancing mass-type lesions as a common finding in sclerosing adenosis on MRI, ranging from 52 to 82.4%^{2,6,11}. Interestingly, Ruan et al.¹² suggest that further applications, such as radiomics based on dynamic contrast-enhanced MRI, which provides

higher diagnostic accuracy than BI-RADS analysis alone (AUCs 0.92, 95% CI 0.75-0.97, vs 0.71, 95% CI 0.60-0.80, respectively) can be used to distinguish sclerosing adenosis and ductal carcinoma in situ. Most MRI studies refer to mass-type enhancement as a common finding of sclerosing adenosis^{2,6,7,11}. This is inconsistent with our study results, which opens the possibility of considering MRI findings of sclerosing adenosis as variable as those previously reported on US and mammography; therefore, the presence or absence of any of these features does not exclude its diagnosis.

The strength of this study is related to the sample size, which is comparable to and even higher than in the literature^{2,4,7,9,10,13}. On the contrary, this study was coordinated by experienced radiologists specializing in breast imaging and conducted in two academic centers specifically focused on breast pathology. The limitations were the retrospective study design and the small number of MRI studies.

CONCLUSION

Using mammography, US, and MRI, we comprehensively describe sclerosing adenosis multimodality imaging findings. Despite being a common incidental finding and because of its similarity with breast cancer, histopathologic analysis is still needed for diagnosis.

Because of sclerosing adenosis's variable behavior and its different image appearance in all modalities, better insight regarding its imaging findings is important to achieve an accurate histopathological correlation and decide the patient's treatment.

Acknowledgments

The authors thank Professor Ana M. Contreras-Navarro for her guidance in preparing and writing this scientific paper. This original research in the Radiology Specialty field was an awarded thesis at the Segunda Convocatoria Nacional 2023–2024, “*Las Mejores Tesis de Radiología para Publicar en el JMeXFRI.*”

Funding

This research received no external funding.

Conflicts of interest

The authors declare no conflicts of interest.

Ethical disclosures

Protection of individuals. This study complies with the Declaration of Helsinki (1964) and its amendments.

Confidentiality of data. The authors declare that they followed their center's protocol for sharing patient data.











Right to privacy and informed consent. Informed consent was not required for this observational study of information collected during routine clinical care.

Use of artificial intelligence. The authors state that they did not use generative artificial intelligence to prepare this manuscript and/or create tables, figures, or figure legends.

REFERENCES

- Huang N, Chen J, Xue J, Yu B, Chen Y, Yang W, et al. Breast Sclerosing Adenosis and Accompanying Malignancies: A Clinicopathological and Imaging Study in a Chinese Population. *Medicine*. 2015;94(49):e2298. doi:10.1097/MD.0000000000002298.
- Tan H, Zhang H, Lei Z, Fu F, Wang M. Radiological and clinical findings in sclerosing adenosis of the breast. *Medicine*. 2019;98(39):e17061. doi:10.1097/MD.00000000000017061.
- Liu W, Li W, Li Z, Shi L, Zhao P, Guo Z, et al. Ultrasound characteristics of sclerosing adenosis mimicking breast carcinoma. *Breast Cancer Res Treat*. 2020;181(1):127-134. doi: 10.1007/s10549-020-05609-2.
- Günhan-Bilgen I, Memiş A, Ustün EE, Ozdemir N, Erhan Y. Sclerosing adenosis: mammographic and ultrasonographic findings with clinical and histopathological correlation. *Eur J Radiol*. 2002;44(3):232-238. doi:10.1016/s0720-048x(02)00020-7.
- Liang T, Cong S, Yi Z, Liu J, Huang C, Shen J, et al. Ultrasound-Based Nomogram for Distinguishing Malignant Tumors from Nodular Sclerosing Adenoses in Solid Breast Lesions. *J Ultrasound Med*. 2021;40(10):2189-2200. doi: 10.1002/jum.15612.
- Cao RL, Scaranelo AM. Magnetic resonance imaging of “pure” sclerosing adenosis of the breast with surgical pathology correlation. *Breast J*. 2019;25(1):143-144. doi: 10.1111/tbj.13178.
- Panourgias E, Bourgioti C, Skountzos G, Koutoulidis V, Mouloupoulos L. MRI manifestations of sclerosing adenosis of the breast: a single institution experience. *Hell J Radiol*. 2020; 5(4):2-7. doi: 10.36162/hjr.v5i4.363.
- D’Orsi C, Sickles EA, Mendelsohn EB, moors EA. *Breast Imaging Reporting and Data system: ACR BI-RADS breast imaging atlas*. 5th Edition. Reston: American College of Radiology, 2013.
- Ozturk E, Yucesoy C, Onal B, Han U, Seker G, Hekimoglu B. Mammographic and Ultrasonographic Findings of Different Breast Adenosis Lesions. *J Belg Soc Radiol*. 2015;99(1):21-27. doi: 10.5334/jbr-btr.850.
- Taşkin F, Köseoğlu K, Unsal A, Erkuş M, Özbaş S, Karaman C. Sclerosing adenosis of the breast: radiologic appearance and efficiency of core needle biopsy. *Diagn Interv Radiol*. 2011;17(4):311-316. doi: 10.4261/1305-3825.DIR.3785-10.2.
- Gity M, Arabkheradmand A, Taheri E, Shakiba M, Khademi Y, Bijan B, et al. Magnetic Resonance Imaging Features of Adenosis in the Breast. *J Breast Cancer*. 2015;18(2):187-194. doi: 10.4048/jbc.2015.18.2.187.
- Ruan M, Ding Z, Shan Y, Pan S, Shao C, et al. Radiomics Based on DCE-MRI Improved Diagnostic Performance Compared to BI-RADS Analysis in Identifying Sclerosing Adenosis of the Breast. *Front Oncol*. 2022;12:888141. doi: 10.3389/fonc.2022.888141.
- Chen YL, Chen JJ, Chang C, Gao Y, Wu J, Yang WT, et al. Sclerosing adenosis: Ultrasonographic and mammographic findings and correlation with histopathology. *Mol Clin Oncol*. 2017;6(2):157-162. doi: 10.3892/mco.2016.1108.

Transjugular intrahepatic portosystemic shunt in a private Mexican medical setting: Indications and hemodynamic and technical outcomes

Mariana del Rio-Gonzalez^{1*}, Miguel A. Carrillo-Martinez¹, Francisco E. Puente-Gallegos¹, Samuel E. Kettenhofen-Jimenez¹, Laura E. Cisneros-Garza², Carlos A. Rodriguez-Montalvo³, Eduardo Flores-Villalba³, Maria E. Diaz-Sanchez⁴, Adriana E. Flores-Gonzalez⁵, and Monica M. Contreras-Rivera⁶

¹Department of Interventional Radiology, Hospitales San Jose and Zambrano Hellion, TecSalud; ²Department of Gastroenterology, Hospital Mugerza, Alta Especialidad; ³Department of Surgery, Centro de Enfermedades Hepaticas y Nutricion, Hospital Angeles Valle Oriente; ⁴Department of Radiology, Hospital San Jose and Zambrano Hellion, TecSalud; ⁵Department of Radiology, Hospital Zambrano Hellion, TecSalud; ⁶Department of Radiology, Hospital San Jose, TecSalud. Monterrey, Nuevo Leon. Mexico

ABSTRACT

Introduction: Transjugular intrahepatic portosystemic shunt (TIPS) is a procedure for portal hypertension complications. However, regional geographical differences pose a particular challenge. This study analyzed the indications and the hemodynamic and technical outcomes of TIPS in patients with liver cirrhosis in a private medical setting in northern Mexico.

Material and Methods: Three interventional radiologists conducted this cross-sectional study in two private Mexican hospitals between March 2004 and March 2024. Age, gender, etiology of cirrhosis, indications for TIPS, Child–Pugh score, and model for end-stage liver disease (MELD) were recorded electronically. The hemodynamic and technical outcomes of the TIPS were also recorded. **Results:** In total, 85 TIPS procedures were performed, 76.5% ($n = 65$) were performed in the last 10 years. The indications for TIPS were mainly secondary prevention of recurrent variceal bleeding in 47 (55.3%) patients, followed by refractory ascites in 35 (41.1%). Hemodynamic success was achieved in 73.7% from 2004 to 2013 and increased to 95.2% from 2014 to 2024, with a mean final portosystemic pressure gradient (PSPG) of 9 mmHg. Technical success, completing the shunt on the first attempt, was 100% over two decades. The most common etiology of cirrhosis was metabolic-associated fatty liver disease (MAFLD) ($n = 29$ patients, 34.1%). **Conclusion:** The main indication for TIPS in our study was secondary prevention of recurrent variceal bleeding, and hemodynamic and technical success was high. This study is the first in Mexico to analyze the indications and hemodynamic and technical outcomes of patients undergoing TIPS.

Keywords: Cirrhosis. Portal hypertension. Variceal hemorrhage. TIPS.

INTRODUCTION

Transjugular intrahepatic portosystemic shunt (TIPS) is a key procedure for the treatment of liver cirrhosis. It is the most effective solution for reducing portal hypertension by creating a shunt that lowers portal venous pressure (PVP)¹⁻³, which depends on splenic blood inflow and flow resistance. A normal portosystemic

pressure gradient (PSPG) is between 1 and 5 mmHg in healthy individuals and exceeds 5 mmHg in portal hypertension⁴⁻⁷. An increase in hepatic pressure depends on the pathology, and it is categorized as prehepatic before entering the liver, hepatic, and post-hepatic, with increased blood resistance at the level of the hepatic veins depending on the site of obstruction⁸.

*Corresponding author:

Mariana del Rio-Gonzalez
E-mail: marianadelrio@me.com

Received for publication: 13-02-2024

Accepted for publication: 18-05-2024

DOI: 10.24875/JMEXFRI.M24000077

Available online: 03-10-2024

J Mex Fed Radiol Imaging. 2024;3(3):175-181

www.JMeXFRI.com

2696-8444 / © 2024 Federación Mexicana de Radiología e Imagen, A.C. Published by Permanyer. This is an open access article under the CC BY-NC-ND (<https://creativecommons.org/licenses/by-nc-nd/4.0/>).

The first hepatic shunt in animals was performed in 1969 by Joseph Rösch using balloon angioplasty⁹. In 1988, Richter and Palmaz et al.¹⁰ performed the first TIPS on a male patient in Freiburg, Germany, using the expandable Palmaz metal stent to keep the shunt open. Since its introduction, the use of TIPS has increased exponentially^{11,12}. It is a minimally invasive procedure primarily used to treat portal hypertension complications, such as refractory ascites, variceal bleeding, and hepatic gastropathy¹³⁻¹⁶. In addition, TIPS is a recommended treatment for Budd–Chiari syndrome, hepatic hydrothorax, and select cases of non-cirrhotic portal hypertension¹⁷. This procedure improves renal function and prevents variceal bleeding by decompressing the portal vein system¹⁷.

Although TIPS has become a cornerstone in treating liver disease worldwide, reduction of portal hypertension, uptake, and regional outcomes vary due to different demographic and socioeconomic factors. A high success rate of TIPS has been reported in international publications^{17,18}. In contrast, there is a lack of local or national reports on the indications and outcomes of patients undergoing TIPS in the Mexican population. This information is essential to optimize the allocation of health resources and tailor patient care. This study analyzed the indications and hemodynamic and technical outcomes of TIPS in patients with liver cirrhosis in a private medical setting in northern Mexico.

MATERIAL AND METHODS

Three interventional radiologists affiliated with the Department of Interventional Radiology and the Department of Radiology of the San Jose and Zambrano Hellion Hospitals, TecSalud, a private institution in Monterrey, Nuevo Leon, Mexico, conducted this retrospective, observational, cross-sectional study, which ran from March 2004 to March 2024 and included all patients, over the age of 18 years with portal hypertension, who underwent a TIPS. Patients with procedures performed by interventional radiologists outside the group were excluded. Informed consent was not required for data collection as part of routine medical care. The study protocol was approved by the institutional ethics and research committees.

Study development and variables

Physical and electronic medical records, radiology reports, and treatment protocols were analyzed. Age, gender, etiology of cirrhosis, indications for TIPS,

Child–Pugh score, and model for end-stage liver disease (MELD) were recorded.

For patients for whom Child–Pugh and MELD scores were not reported, laboratory parameters from the day of the procedure were obtained and calculated. Patients underwent previous clinical examinations by a hepatologist, including laboratory analysis and/or histopathology results, to determine the etiology of cirrhosis.

Indications for TIPS were jointly determined by the referring hepatologist and/or surgeon and the interventional radiologist: variceal bleeding (secondary prevention), refractory ascites, refractory hydrothorax, and hepatopulmonary syndrome. Procedural TIPS outcomes and baseline and final PSPG were recorded.

Definitions

Hemodynamic success of TIPS: Reduction of PSPG to ≤ 12 mmHg¹⁹.

Technical success: The ability of the radiologist to create the TIPS by bridging the portal and hepatic veins with a stent¹⁹.

TIPS attempt: A separate visit to the interventional radiology angiography suite¹⁹.

Secondary prophylaxis with TIPS: Treatment in patients who rebleed despite conventional non-selective beta-blockers or carvedilol and endoscopic variceal ligation³.

TIPS technical procedure

The TIPS procedure was performed according to the standardized approach²⁰ by a team of three interventional radiologists with 30 years (MCM), 10 years (FPG), and 1 year (SKJ) of experience.

A RUPS-100 Transjugular Liver Access Set (Cook Medical, Bloomington, IN, USA) was used with each patient. Corrected sinusoidal pressure was calculated as the difference between the wedged and free hepatic venous pressure. The wedged hepatic venous pressure (WHVP) was measured at the right hepatic vein by advancing the sheath or catheter until no venous reflux occurred during contrast injection.

The intrahepatic puncture was performed through the right hepatic vein toward the right portal vein. Splenoportography and balloon/stent measurements were performed using a 4-5F pigtail sizing catheter. The shunt was then predilated with 6-8 mm diameter angioplasty balloons (Figure 1). Bare metal stents were used from 2004 to 2011. Since its introduction in 2012, the ViatorTM (W.L. Gore & Associates, Inc. Newark, DE,

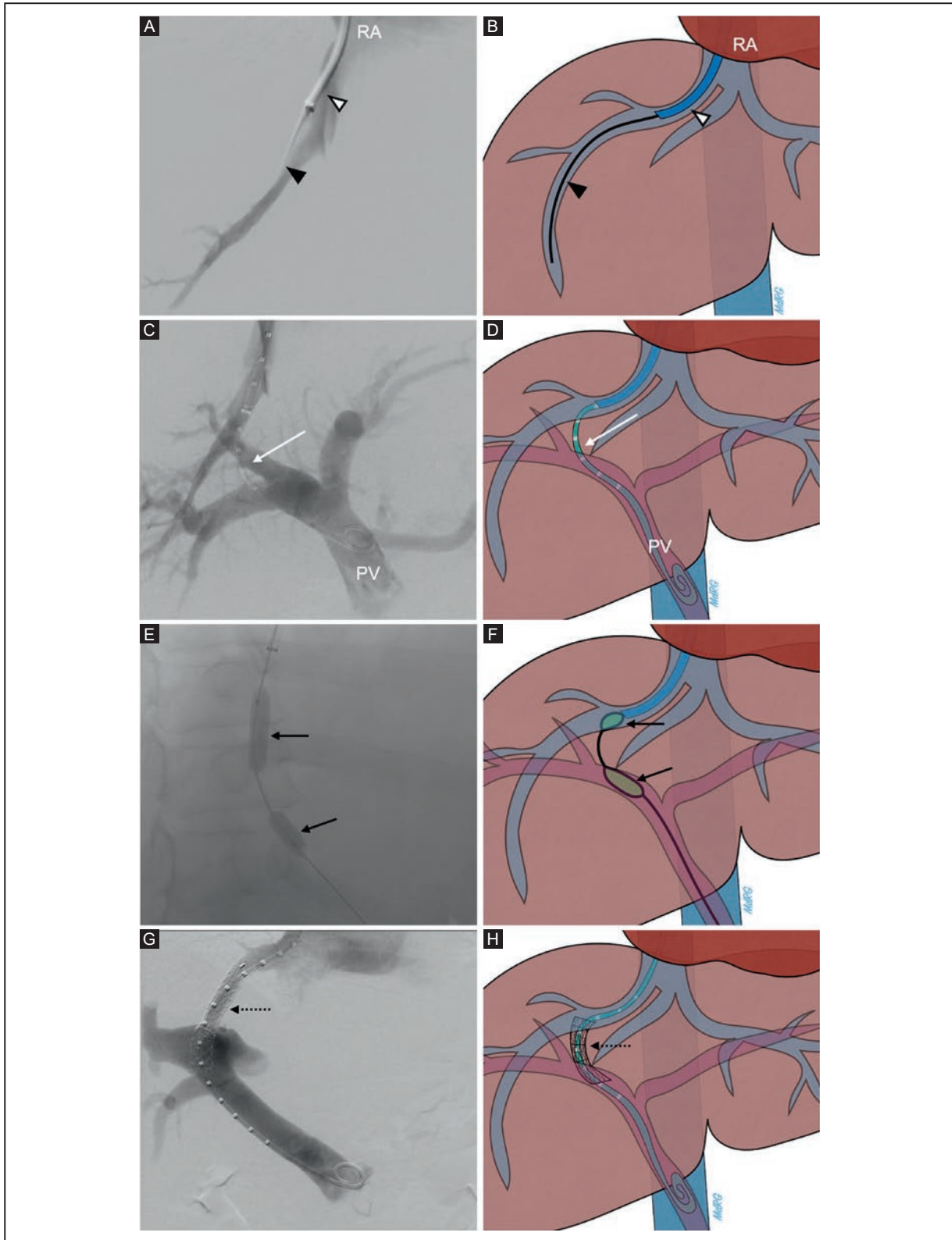


Figure 1. TIPS procedure. **A:** digital subtraction venogram. **B:** graphic representation through the 10F sheath (white arrowhead) in the right hepatic vein, visualizing the guidewire (black arrowhead) and the sheath where the WHVP is measured. **C:** digital subtraction portography. **D:** graphic representation with a pigtail catheter (white arrow) after successful puncture of the right PV. **E:** fluoroscopic image. **F:** graphic representation during TIPS creation and predilatation of the shunt with an angioplasty balloon (black arrows) showing the size of the required stent. **G:** digitally subtracted portogram. **H:** graphic representation showing the final appearance of the shunt and stent (dashed arrow).

PSPG: portosystemic pressure gradient; PV: portal vein; RA: right atrium; TIPS: transjugular intrahepatic portosystemic shunt; WHVP: wedged hepatic vein pressure.

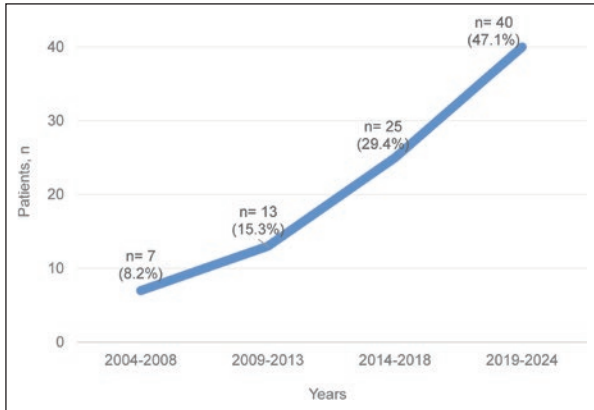


Figure 2. Total number of patients who underwent the TIPS procedure between March 2004 and March 2024, with an increase in the last 10 years. Patients were grouped every 5 years with an exponential increase, starting with 7 (8.2%) in 2009 and 40 (47.1%) in the last 5 years. TIPS: transjugular intrahepatic portosystemic shunt.

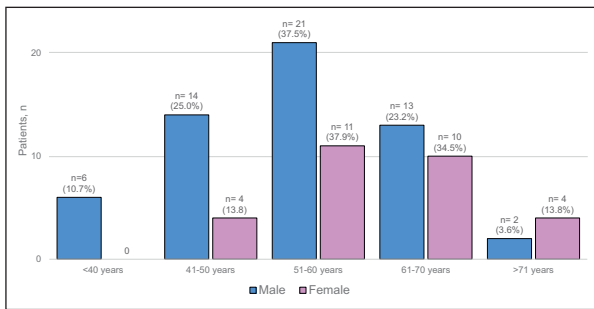


Figure 3. Distribution of patients who underwent TIPS by age and gender. The age distribution was comparable for both genders, with most in the third group (51-60 years), with 21 (37.5%) male and 11 (37.9%) female patients. TIPS: transjugular intrahepatic portosystemic shunt.

USA) expanded polytetrafluoroethylene-lined stent-graft endoprosthesis has been used. After stent placement, 8-10-mm high-pressure angioplasty balloons were used until the measured PSPG was satisfactory. The PSPG was measured between the portal and hepatic veins. The inferior vena cava and right atrial pressures were also measured before sheath removal. Venous hemostasis was achieved with manual compression. In patients with ascites, a large-volume paracentesis was performed after the procedure.

Statistical analysis

Descriptive statistics were used to summarize the data. Quantitative variables were expressed as means, standard deviation (SD), and range. After all the information

was collected and coded in Excel for Mac version 16.83 (Microsoft Corporation, Redmond, WA, USA), it was exported to SPSS version 29 (IBM Corp., Armonk, NY, USA) for analysis.

RESULTS

In total, 85 patients underwent TIPS, 20 (23.5%) between 2004 and 2013 and 65 (76.5%) between 2014 and 2024 (Figure 2). Five groups were defined by age and gender distribution, starting with patients <40 years and every 10 years until the last group was classified as >71 years. The mean \pm SD was 56.2 ± 11.9 years (range, 22-88), with 56 (65.9%) males and 29 (34.1%) females (Figure 3).

Figure 4 shows the indications for TIPS. The most common was secondary prevention of recurrent variceal bleeding in patients who rebleed despite non-selective beta-blockers or carvedilol and endoscopic variceal ligation, with a total of 47 (55.3%) patients, followed by refractory ascites in 35 (41.1%) patients, refractory hydrothorax in two (2.4%), and one (1.2%) patient with hepatopulmonary syndrome.

Hemodynamic success was achieved in 14 (73.7%) of 19 patients from 2004 to 2013 (data not available in one patient) and increased to 59 (95.2%) of 62 patients from 2014 to 2024 (data not available in three patients). The final mean PSPG was 9 mmHg. Technical success with the completion of the shunt was achieved in 85 patients (100%) on the first attempt in both periods. The records showed no complications throughout the procedure.

Table 1 shows the etiology of cirrhosis. The main cause was MAFLD in 29 (34.1%) patients, followed by 14 (16.5%) patients with chronic hepatitis C and 13 (15.3%) with cirrhosis due to alcohol-related liver disease. Regarding the Child-Pugh score at the time of the TIPS procedure, most participants were Child B (n = 31, 36.5%), followed by Child C (n = 24, 28.2%) and Child A (n = 12, 14.1%). Insufficient data in the medical records precluded the Child classification for 18 (21.2%) patients. The mean MELD score was 16.3 ± 6.7 points.

DISCUSSION

The main indication for TIPS in our study was secondary prevention of recurrent variceal bleeding, and a high hemodynamic and technical success was achieved. This study is the first in Mexico to analyze the indications and hemodynamic and technical outcomes in patients undergoing TIPS procedures. Identifying the most common

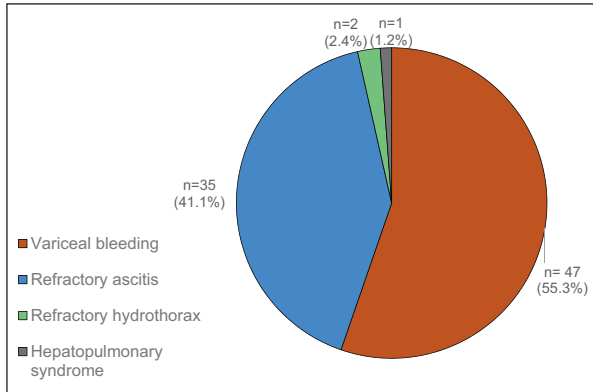


Figure 4. The indications for performing TIPS. Most of the patients had variceal bleeding (47 patients, 55.3%) and refractory ascites (35 patients, 41.1%).

TIPS: transjugular intrahepatic portosystemic shunt.

Table 1. Etiology of cirrhosis in 85 Mexican patients who underwent TIPS

Description	n (%)
Metabolic-associated fatty liver disease (MAFLD)	29 (34.1)
Chronic hepatitis C	14 (16.5)
Alcohol-related liver disease	13 (15.3)
Autoimmune hepatitis (AH)	8 (9.4)
Non-cirrhotic portal hypertension (NCPH)	5 (5.9)
Primary biliary cholangitis (PBC)	3 (3.5)
Overlap syndrome ^a	1 (1.2)
Idiopathic cirrhosis	1 (1.2)
Not classified ^b	11 (12.9)

^aPrimary biliary cholangitis and autoimmune hepatitis; ^bPatients still under clinical investigation or with incomplete records.

TIPS: transjugular intrahepatic portosystemic shunt.

indications and reporting the success rate may encourage more medical practitioners in Mexico to consider TIPS as a treatment so that more patients can benefit from this procedure.

There is a consensus for using TIPS in treating complications of portal hypertension and managing complications such as variceal bleeding, for which international guidelines recommend TIPS³. Steib et al.¹⁷ surveyed 43 national hospitals by mail. In total, 19 responses came from the radiology departments, and 24 from the hepatology/gastroenterology departments, all included TIPS patients. The number of TIPS per year and the main indications were recorded. Their survey showed that refractory ascites

or hydrothorax was the predominant indication ($69 \pm 13.4\%$), followed by preventing recurrent variceal bleeding ($21.2 \pm 11.7\%$). Buttner et al.¹⁸ conducted a retrospective analysis of 835 patients who underwent TIPS over 25 years from 1993 to 2018. They reported that the most common indications were refractory ascites ($n = 464, 55.6\%$) and secondary prevention of variceal bleeding ($n = 183, 22\%$). Other less common indications were hepatorenal syndrome ($n = 24, 2.9\%$) and rescue TIPS ($n = 10, 1.3\%$). In a meta-analysis²¹ that included 507 articles, refractory ascites and prevention of recurrent variceal bleeding were identified as the most common indications. Diffuse hepatic vein thrombosis and progressive liver failure were also documented. Refractory ascites are the most common indication for the TIPS procedure reported in international publications^{17,21}. In contrast, secondary prophylaxis of variceal bleeding was the most common in our population. This finding sheds light on the fact that ascites is a common symptom of portal hypertension. However, TIPS may not be offered as a therapeutic option for Mexican patients.

Lowering portal pressure in patients with compensated or decompensated cirrhosis reduces the risk of developing further complications. Varices do not form at a PSPG <12 mmHg. In contrast, a PSPG of 20 mmHg indicates endoscopic and/or pharmacological therapy¹⁹. In a retrospective analysis of 835 German patients, Buttner et al.¹⁸ documented hemodynamic success in up to 77.9% ($n = 650$), which increased to 84.9% ($n = 708$) with a second procedure. In our study, TIPS had a comparable success rate with a hemodynamic success rate of up to 95.2% in lowering PSPG to ≤ 12 mmHg and a 100% technical success rate of TIPS with completion of the procedure in a single TIPS procedure. On the contrary, a retrospective study by Saad et al.¹⁹ compared the functional and anatomic outcomes of TIPS created with a specialized stent (ViatorrTM) with the generic stent WallstentTM (Boston Scientific Natick, MA, USA) or FluencyTM (Bard Peripheral Vascular Inc., Tempe, AZ, USA). They included 172 patients who underwent TIPS over 54 months. They reported a hemodynamic success of 93% and 98% in the generic and Viatorr groups, respectively. Technical success was achieved in 164 (95%) patients on the first attempt, 171 (99%) patients on the second attempt, and 172 (100%) patients on the third attempt. Our study showed an exponential growth in TIPS procedures over the last decade, with 65 patients (76.5%) in the last 10 years compared to 20 (23.5%) in 2004-2013. The implantation of Viatorr stents

for TIPS has increased in Mexico, with 95 procedures reported from 2016 to 2019 and 181 from 2020 to 2023 (personal communication from the provider). The increase in the total number of patients over the past decade in our population can be attributed to greater awareness among physicians, the increasing efficacy of the procedure, and favorable patient outcomes.

A variety of liver cirrhosis etiologies are found in the literature. In a retrospective, multicenter, cross-sectional study by Mendez-Sanchez et al.²² of eight Mexican hospitals with 1210 patients, the main cause of cirrhosis in 438 (36.2%) patients was chronic hepatitis C, followed by alcohol-related liver disease in 337 (27.8%), and MAFLD in 281 (23.2%) patients. The number of patients with cirrhosis associated with MAFLD has increased worldwide²³⁻²⁷. In 2022, Younossi et al.²⁴ conducted a retrospective study in the United States using data from the Scientific Registry of Transplant Recipients (SRTR), which included 116,292 patients who underwent liver transplantation between 2013 and 2022. They found that the most common etiology was alcohol-related liver disease, increasing from 23% in 2013 to 48% in 2022, while MAFLD was the second most common, increasing from 19% (2013) to 27% (2022). Our study highlights MAFLD over chronic hepatitis C and alcohol-related liver disease as the etiology for cirrhosis. On the other hand, the predominant male gender and age are consistent with the existing literature, but MAFLD as a primary etiology represents a notable departure from traditional reports. A comprehensive understanding of epidemiologic and demographic patterns holds the potential to refine patient care strategies and expand the range of treatment options for patients with cirrhosis.

The strength of this study is that the most common indications and cirrhotic etiology in the literature were included in our study. This study has several limitations, including the cross-sectional, retrospective, single-center study design and small sample size. In addition, the focus of the study included interventions in private healthcare facilities, and the etiology of cirrhosis was obtained from medical records rather than as a standardized assessment. These factors can lead to distribution bias since access to diagnosis and treatment may vary for patients in remote areas or be influenced by socioeconomic factors. This situation has been linked to increased inequality in treatment access based on socioeconomic status and ethnicity; therefore, this procedure may not be available in Mexican public health facilities due to its high cost.

CONCLUSION

This study showed that secondary prevention of recurrent variceal bleeding was a major indication for TIPS with a high hemodynamic and technical success rate. We believe that understanding our patients' epidemiologic landscape and technical outcomes could refine patient care in our population. TIPS is costly but also cost-effective²⁸. While the use of TIPS is increasing, this study emphasizes the need for a comprehensive look at potential candidates in the Mexican population. Future analysis of short- and mid-term clinical and hemodynamic outcomes following TIPS is warranted and may provide insight into areas where patient care can be improved. We advocate for expanding this research and including data from multiple medical centers nationwide.

Acknowledgments

The authors thank Professor Ana M. Contreras-Navarro for her guidance in preparing and writing this scientific paper.

Funding

This research received no external funding.

Conflicts of interest

The authors declare no conflicts of interest.

Ethical disclosures

Protection of individuals. This study complies with the Declaration of Helsinki (1964) and its amendments.

Confidentiality of data. The authors declare that they followed their center's protocol for sharing patient data.

Right to privacy and informed consent. Informed consent was not required for this observational study of information collected during routine clinical care.




Use of artificial intelligence. The authors state that they did not use generative artificial intelligence to prepare this manuscript and/or create tables, figures, or figure legends.

REFERENCES

1. Villanueva C. The hidden face of preemptive TIPS. *Hepatology*. 2024;79(3):535-537. doi: 10.1097/HEP.0000000000000714.
2. García-Pagán JC, Caca K, Bureau C, Laleman W, Appenrodt B, Luca A, et al. Early TIPS (Transjugular Intrahepatic Portosystemic Shunt) Cooperative Study Group. Early use of TIPS in patients with cirrhosis and variceal bleeding. *N Engl J Med*. 2010;362(25):2370-2379. doi: 10.1056/NEJMoa0910102.

3. de Franchis R, Bosch J, Garcia-Tsao G, Reiberger T, Ripoll C. Baveno VII Faculty. Baveno VII - Renewing consensus in portal hypertension. *J Hepatol.* 2022;76(4):959-974. doi:10.1016/j.jhep.2021.12.022.
4. Kaplan DE, Ripoll C, Thiele M, Fortune BE, Simonetto DA, Garcia-Tsao G, et al. AASLD Practice Guidance on risk stratification and management of portal hypertension and varices in cirrhosis. *Hepatology.* 2024;79(5):1180-1211. doi: 10.1097/HEP.0000000000000647.
5. Iwakiri Y. Pathophysiology of portal hypertension. *Clin Liver Dis.* 2014;18(2):281-291. doi: 10.1016/j.cld.2013.12.001.
6. Sass DA, Chopra KB. Portal hypertension and variceal hemorrhage. *Med Clin North Am.* 2009;93(4):837-853, vii-viii. doi: 10.1016/j.mcna.2009.03.008.
7. Bochnakova T. Hepatic Venous Pressure Gradient. *Clin Liver Dis (Hoboken).* 2021;17(3):144-148. doi: 10.1002/cld.1031.
8. Gupta TK, Chen L, Groszmann RJ. Pathophysiology of portal hypertension. *Baillieres Clin Gastroenterol.* 1997;11(2):203-219. doi: 10.1016/s0950-3528(97)90036-1.
9. Röscher J, Hanafee WN, Snow H. Transjugular portal venography and radiologic portacaval shunt: an experimental study. *Radiology.* 1969;92(5):1112-1114. doi:10.1148/92.5.1112.
10. Richter GM, Palmaz JC, Nöldge G, Rössle M, Siegerstetter V, Franke M, et al. The transjugular intrahepatic portosystemic stent-shunt. A new non-surgical percutaneous method. *Radiologie.* 1989;29(8):406-411.
11. Rössle M. TIPS: 25 years later. *J Hepatol.* 2013;59(5):1081-1093. doi: 10.1016/j.jhep.2013.06.014.
12. Lee EW, Kuei A, Saab S, Busuttill RW, Durazo F, Han SH, et al. Nationwide trends and predictors of inpatient mortality in 83884 transjugular intrahepatic portosystemic shunt. *World J Gastroenterol.* 2016;22(25):5780-5789. doi: 10.3748/wjg.v22.i25.5780.
13. Nicoară-Farcău O, Han G, Rudler M, Angrisani D, Monescillo A, Torres F, et al. Preemptive TIPS Individual Data Meta-analysis, International Variceal Bleeding Study and Baveno Cooperation Study groups. Effects of Early Placement of Transjugular Portosystemic Shunts in Patients With High-Risk Acute Variceal Bleeding: a Meta-analysis of Individual Patient Data. *Gastroenterology.* 2021;160(1):193-205.e10. doi: 10.1053/j.gastro.2020.09.026.
14. Abraides JG, Caraceni P, Ghabril M, Garcia-Tsao G. Update in the Treatment of the Complications of Cirrhosis. *Clin Gastroenterol Hepatol.* 2023;21(8):2100-2109. doi: 10.1016/j.cgh.2023.03.019.
15. Attila T, Kolbeck KJ, Bland ZM, Wang A, Rodriguez SA. Duodenal variceal bleeding successfully treated with transjugular intrahepatic portosystemic shunt: a case report and review of the literature. *Turk J Gastroenterol.* 2008;19(4):284-290.
16. Alqadi MM, Chadha S, Patel SS, Chen YF, Gaba RC. Transjugular Intrahepatic Portosystemic Shunt Creation for Treatment of Gastric Varices: Systematic Literature Review and Meta-Analysis of Clinical Outcomes. *Cardiovasc Intervent Radiol.* 2021;44(8):1231-1239. doi: 10.1007/s00270-021-02836-y.
17. Steib CJ, Li H, Zhang J, Mayerle J, Ricke J, Gerbes AL, et al. Transjugular intrahepatic portosystemic shunt for patients with liver cirrhosis: survey evaluating indications, standardization of procedures and anticoagulation in 43 German hospitals. *Eur J Gastroenterol Hepatol.* 2020;32(9):1179-1185. doi: 10.1097/MEG.0000000000001628.
18. Büttner L, Aigner A, Pick L, Brittinger J, Steib CJ, Böning G, et al. 25 years of experience with transjugular intrahepatic portosystemic shunt (TIPS): changes in patient selection and procedural aspects. *Insights Imaging.* 2022;13(1):73. doi: 10.1186/s13244-022-01216-5.
19. Saad WE, Darwish WM, Davies MG, Waldman DL. Stent-grafts for transjugular intrahepatic portosystemic shunt creation: specialized TIPS stent-graft versus generic stent-graft/bare stent combination. *J Vasc Interv Radiol.* 2010;21(10):1512-1520. doi:10.1016/j.jvir.2010.06.009.
20. Walker TG, Thabet A, Baccin CE, Crim J, Salazar GM, Gangull S, et al. Diagnostic Imaging: Interventional Procedures. 1ST ed. Lippincott Williams & Wilkins. Philadelphia, USA. 2012, pp. 870-890.
21. Qi X, Yang M, Fan D, Han G. Transjugular intrahepatic portosystemic shunt in the treatment of Budd-Chiari syndrome: a critical review of literatures. *Scand J Gastroenterol.* 2013;48(7):771-784. doi: 10.3109/00365521.2013.777775.
22. Méndez-Sánchez N, Zamarripa-Dorsey F, Panduro A, Purón-González E, Coronado-Alejandro EU, Cortez-Hernández CA, et al. Current trends of liver cirrhosis in Mexico: Similarities and differences with other world regions. *World J Clin Cases.* 2018;6(15):922-930. doi: 10.12998/wjcc.v6.i15.922.
23. Kardashian A, Serper M, Terrault N, Nephew LD. Health disparities in chronic liver disease. *Hepatology.* 2023;77(4):1382-1403. doi: 10.1002/hep.32743.1.
24. Younossi ZM, Stepanova M, Al Shabeeb R, Eberly KE, Shah D, Nguyen V, et al. The changing epidemiology of adult liver transplantation in the United States in 2013-2022: The dominance of metabolic dysfunction-associated steatotic liver disease and alcohol-associated liver disease. *Hepatal Commun.* 2023;8(1):e0352. doi: 10.1097/HCG.0000000000000352.
25. Trivedi PS, Jensen AM, Kriss MS, Brown MA, Morgan RL, Lindrooth RC, et al. Ethnoracial Disparity in Hospital Survival following Transjugular Intrahepatic Portosystemic Shunt Creation for Acute Variceal Bleeding in the United States. *J Vasc Interv Radiol.* 2021; 32(7):941-949.e3. doi: 10.1016/j.jvir.2021.02.027.
26. Almomani A, Kumar P, Onwuzo S, Boustany A, Krishtopaytis E, Hitawala A, et al. Epidemiology and prevalence of lean nonalcoholic fatty liver disease and associated cirrhosis, hepatocellular carcinoma, and cardiovascular outcomes in the United States: a population-based study and review of literature. *J Gastroenterol Hepatol.* 2023;38(2):269-273. doi: 10.1111/jgh.16049.
27. Abougergi MS, Avila P, Saltzman JR. Impact of Insurance Status and Race on Outcomes in Nonvariceal Upper Gastrointestinal Hemorrhage: A Nationwide Analysis. *J Clin Gastroenterol.* 2019;53(1):e12-e18. doi: 10.1097/MCG.0000000000000909.
28. Mattock R, Tripathi D, O'Neill F, Craig J, Tanner J, Patch D, et al. Economic evaluation of covered stents for transjugular intrahepatic portosystemic shunt in patients with variceal bleeding and refractory ascites secondary to cirrhosis. *BMJ Open Gastroenterol.* 2021;8(1): e000641. doi: 10.1136/bmjgast-2021-000641.

Increased incidence of symptomatic venous thrombosis associated with peripherally inserted central catheter in COVID-19 patients

Miguel A. Hinostrroza-Sanchez^{1,2}, Ricardo Oliva-Enriquez^{1,2}, Sofía Hurtado-Arellano³,
Francisco E. Puente-Gallegos^{1,2}, and Miguel A. Carrillo-Martinez^{1,2}

¹Department of Radiology and Imaging, Hospital San Jose; ²Department of Radiology and Imaging, Hospital Zambrano Hellion, TecSalud Hospitals; ³School of Medicine and Health Sciences, Tecnológico de Monterrey, Monterrey, Nuevo Leon, Mexico

ABSTRACT

Introduction: The identification of catheter-associated symptomatic thrombosis in COVID-19 patients has not received sufficient attention. This study compared the incidence of peripherally inserted central catheter-associated symptomatic venous thrombosis (PICC-ASVT) in COVID-19 and non-COVID-19 patients. **Materials and Methods:** This was a historical cohort of non-COVID-19 patients treated from April 2018 to December 2019 and a retrospective cohort of COVID-19 patients treated from April 2020 to December 2021. A positive PICC-ASVT case was defined based on clinical manifestations of obstruction of intravenous solution flow confirmed by ultrasound. The incidence of PICC-ASVT was based on the total number of PICCs with venous thrombosis divided by the total number of PICCs placed. **Results:** COVID-19 patients had a higher incidence of PICC-ASVT: 38 of 617 cases had an incidence of 6.2%, while an incidence of 2.03% was found in 12 of 592 non-COVID-19 patients. The association of risk of PICC-ASVT in COVID-19 patients was up to sixfold (OR 3.1, 95% CI, 1.6–6.1). The most common area of hospital admission was the intensive care unit (ICU) in patients with PICC-ASVT in 24 (63.2%) of 38 cases, followed by the intermediate care unit (IMCU) in 11 cases (28.9%) ($p < 0.001$). No PICC-ASVT cases were found in the ward or the respiratory therapy unit (RTU). **Conclusion:** This study highlights the increased incidence of PICC-ASVT in COVID-19 patients. Thrombosis was associated with hospitalizations in the ICU and IMCU.

Keywords: Severe acute respiratory syndrome-related coronavirus. Peripheral venous catheterization. Deep vein thrombosis. Radiology. Interventional.

INTRODUCTION

Central catheters are essential for effective, long-term patient care. A peripherally inserted central catheter (PICC) is preferred as it can be placed at the patient's bedside and is associated with fewer serious complications¹. Symptomatic venous thrombosis due to PICC-associated symptomatic venous thrombosis (PICC-ASVT) is a clinical condition that occurs when a

thrombus forms in an indwelling venous catheter². It can manifest as deep (DVT) or superficial vein thrombosis (SVT). DVT is usually asymptomatic, but when it is symptomatic, the patient presents edema and pain in the arm or forearm². On the other hand, SVT patients typically complain of redness, pain, and swelling at the puncture site. Both complications can lead to catheter malfunction and may cause further issues such as pulmonary embolism or post-thrombotic syndrome^{3,4}.

*Corresponding author:

Miguel A. Hinostrroza-Sanchez
E-mail: *doc.hinostrroza@gmail.com

Received for publication: 13-02-2024

Accepted for publication: 24-04-2024

DOI: 10.24875/JMEXFRI.M24000079

Available online: 03-10-2024

J Mex Fed Radiol Imaging. 2024;3(3):182-188

www.JMeXFRI.com

2696-8444 / © 2024 Federación Mexicana de Radiología e Imagen, A.C. Published by Permanyer. This is an open access article under the CC BY-NC-ND (<https://creativecommons.org/licenses/by-nc-nd/4.0/>).

PICCs have a higher risk of venous thrombosis, with an incidence ranging from 2.4% to 25.7%^{1,4-12}. Several PICC-ASVT risk factors related to prothrombotic conditions, such as cancer, infections, hematologic conditions, and stasis, have been described in the literature^{1,4,8,10,13-16}. Catheter size, number of lumens, and tip location influence the incidence of venous thrombosis^{1,4,6-9,11-15,17,18}.

The outbreak of the COVID-19 pandemic increased the demand for PICCs in hospitalized patients and led to an increased incidence of venous thrombosis cases¹⁹. This increase was due to the virus's inflammatory mechanisms and alterations in the coagulation cascade²⁰. These disease mechanisms likely impacted the incidence of PICC-ASVT, but there is controversial data on the topic²¹. This study compared the incidence of PICC-ASVT in COVID-19 and non-COVID-19 patients.

MATERIALS AND METHODS

This was a historical cohort study of non-COVID-19 patients treated from April 2018 to December 2019¹² and a retrospective cohort study of COVID-19 patients treated from April 2020 to December 2021 at the San Jose Hospital and the Zambrano Hellion Hospital of the TecSalud System in Monterrey, Nuevo Leon, Mexico. Hospitalized adult patients of both sexes with a PICC placed by an interventional radiologist under ultrasound guidance were included. Catheters placed by other specialties, cases with incomplete information, and out-patient PICCs were excluded. Eligible patients provided consent by accepting the patient's privacy statement. The Institutional Ethics and Research Committees approved the study.

Study development and variables

The variables included were age, gender, hospitalization area, number of PICC lumens, catheter caliber (Fr), catheter duration in days (from placement to removal), vessel patency in days, catheter insertion site, and catheter tip location in the venous system.

A positive PCR-RNA test of SARS-CoV-2 confirmed COVID-19 patient status. The patients were recruited before COVID-19 vaccines were available in our community, so none had been vaccinated.

The attending physician suspected a positive PICC-ASVT case based on the patient's clinical manifestations (pain, edema, elevated local temperature, erythema along the catheter course, or obstruction of intravenous solution flow)²⁻⁴. Venous thrombosis was confirmed by ultrasound performed and interpreted by

Table 1. Comparison of characteristics of non-COVID-19 patients (historical cohort)^a and COVID-19 patients

Characteristic	Non-COVID-19 patients (n = 592)	COVID-19 patients (n = 617)
Age, years, mean ± SD	68.0 ± 35.1	65.0 ± 17.9
Gender		
Male	311 (52.5)	320 (51.9)
Female	281 (47.5)	297 (48.1)
Hospital admission area, n (%)		
ICU	243 (41.1)	240 (38.9)
Ward	279 (47.1)	180 (29.2)
Operating room ^b	-	21 (3.4)
IMCU	70 (11.8)	96 (15.5)
RTU ^c	-	80 (13.0)
Catheter insertion site, n (%)		
Right basilic	391 (66.5)	404 (65.5)
Left basilic	124 (20.9)	136 (22.0)
Right cephalic	21 (3.5)	18 (2.9)
Left cephalic	6 (1.0)	9 (1.5)
Right humeral	32 (5.4)	40 (6.5)
Left humeral	16 (2.7)	10 (1.6)
Catheter tip location		
Right auricle	52 (8.8)	54 (8.7)
Superior vena cava	482 (81.5)	503 (81.5)
Left subclavian vein	12 (2.0)	13 (2.1)
Right subclavian vein	35 (5.9)	36 (5.8)
Right jugular vein	3 (0.6)	3 (0.5)
Left jugular vein	1 (0.2)	3 (0.5)
Left axillary vein	2 (0.4)	1 (0.2)
Right axillary vein	3 (0.6)	3 (0.5)
Inferior vena cava	0	1 (0.2)
Vein caliber (mm) mean ± SD	NA	4.15 ± 0.90
Catheter caliber, Fr, n (%)		
5	NA	599 (97.1)
6	NA	18 (2.9)
Lumen number		
3	591 (99.8)	617 (100.0)
2	1 (0.2)	0
Catheter duration, days ^d	9 (1-56)	17 (1-162)

^aHinostrroza-Sanchez et al.¹²; ^bThis area was not included in non-COVID-19 before the pandemic; ^cThis area was created during the COVID-19 pandemic outbreak.

COVID-19: coronavirus disease 2019; Fr: French; all values are absolute frequencies and percentages unless otherwise stated; ICU: intensive care unit; IMCU: intermediate care unit; NA: not available; PICC: Peripherally inserted central catheter; RTU: respiratory therapy unit.

radiology specialists with 24 (MCM) and 12 (FPG) years of experience using a HealthCare Venue™ (General Electric Co. Chicago, IL, USA) with a linear L4-12t-RS transducer.

Data were collected from the catheter records of the RIS/PACS (Radiology Information System/Picture Archiving and Communication System) of the Interventional Radiology team and the Epidemiological Surveillance Unit/Catheter Clinic database.

Statistical analysis

The incidence of symptomatic venous thrombosis associated with PICC (PICC-ASVT) was calculated using the total number of PICCs with venous thrombosis divided by the total number of PICCs placed. Central tendency and dispersion were used to describe numerical variables, which were analyzed with the Kolmogorov–Smirnov test to determine their parametric or nonparametric distribution. If the distribution was parametric, the relationship between numerical and categorical variables was analyzed with Student’s t-test or the ANOVA for two or more groups, respectively. For non-parametric distribution, the relationship between numerical and categorical variables was analyzed with the Mann–Whitney U-test or the Kruskal–Wallis test for two or more groups. The categorical variables were described as absolute numbers and percentages. The association between categorical variables was analyzed using the chi-square test. Odds ratios were defined to determine differences in the risk of symptomatic thrombosis associated with PICC when two or more variables were compared with a 95% confidence interval. A p-value <0.05 was significant. Statistical analysis was performed using SPSS version 25.0 (IBM Corp., Armonk, NY, USA).

RESULTS

Table 1 shows the study population of 592 non-COVID-19 patients (historical cohort) and 617 COVID-19 patients. The age and gender distribution were comparable between the groups, and 243 and 240 patients (41.1% and 38.9%, respectively) were admitted to the intensive care unit (ICU). Ward admission was higher for non-COVID-19 patients, 279 (47.1%), than for COVID-19 patients, 180 (29.2%). The operating room and the respiratory therapy unit were only included in the COVID-19 cohort. The predominant catheter insertion sites in both cohorts were the right basilic (391, 66.5% and 404, 65.5%) and the left basilic (124, 20.9%

Table 2. Comparison of the PICC-ASVT incidence of COVID-19 patients and non-COVID-19 patients^a

Description	Total, n	PICC-ASVT		Incidence %
		Yes n (%)	No n (%)	
COVID-19 patients	617	38 (76.0) ^b	579 (49.9)	6.2
Non-COVID-19 patients	592	12 (24.0)	580 (50.1)	2.03

^aHinojosa-Sanchez et al.¹²; ^bp < 0.001.

COVID-19: coronavirus disease 2019; PICC-ASVT: Peripherally Inserted Central Catheter-Associated Symptomatic Venous Thrombosis.

Table 3. PICC-ASVT type and location in COVID-19 patients

Description	n (%)
Deep thrombosis	27 (71.1)
Superficial thrombosis	7 (18.4)
Deep and superficial thrombosis	4 (10.5)
Location of thrombosis ^a	
Right axillary vein	4 (10.5)
Left axillary vein	4 (10.5)
Right basilic axillary vein and cephalic vein	1 (2.6)
Right basilic axillary vein and subclavian vein	1 (2.6)
Right basilic vein	5 (13.1)
Left basilic vein	3 (7.9)
Right cephalic vein	2 (5.3)
Right humeral vein	2 (5.3)
Left humeral vein	2 (5.3)
Left subclavian axillary vein and basilic vein	1 (2.6)
Left subclavian axillary vein and cephalic vein	1 (2.6)
Right subclavian vein	2 (5.3)
Right subclavian vein and axillary vein	1 (2.6)
Right subclavian vein and basilic vein	2 (5.3)
Right subclavian vein and cephalic vein	1 (2.6)
Right jugular vein	3 (7.9)
Right internal jugular vein	1 (2.6)
Right jugular, axillary, subclavian and cephalic veins	1 (2.6)
Left jugular vein and subclavian vein	1 (2.6)

^aThe percentage in these rows was calculated using data from 38 patients with thrombosis. All values are given as absolute frequencies and percentages.

PICC-ASVT: Peripherally Inserted Central Catheter-Associated Symptomatic Venous Thrombosis.

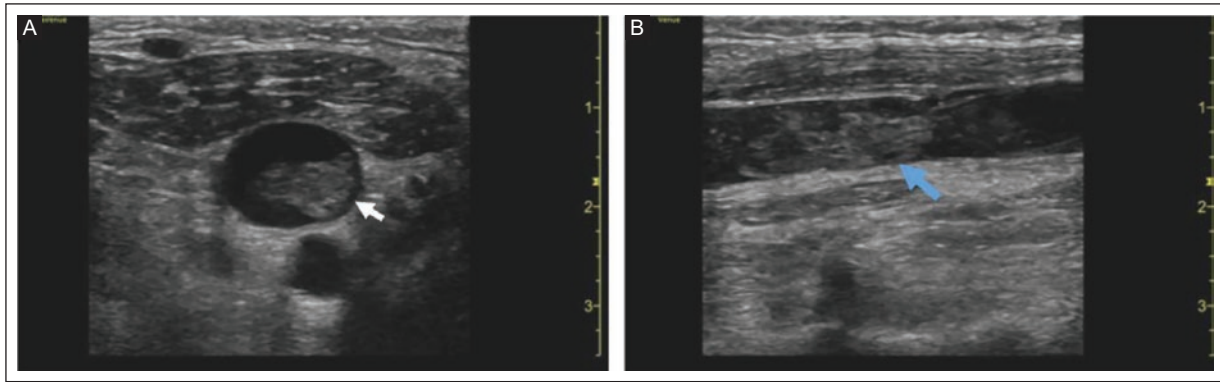


Figure 1. Grayscale US of right upper extremity veins of a 61-year-old female patient with COVID-19. **A:** acute deep venous PICC-ASVT with partial luminal obstruction (white arrow) in the right jugular vein. **B:** total luminal occlusion of the right basilic vein (blue arrow). COVID-19: coronavirus disease 2019; US: ultrasound; PICC-ASVT: peripherally inserted central catheter-associated symptomatic venous thrombosis.

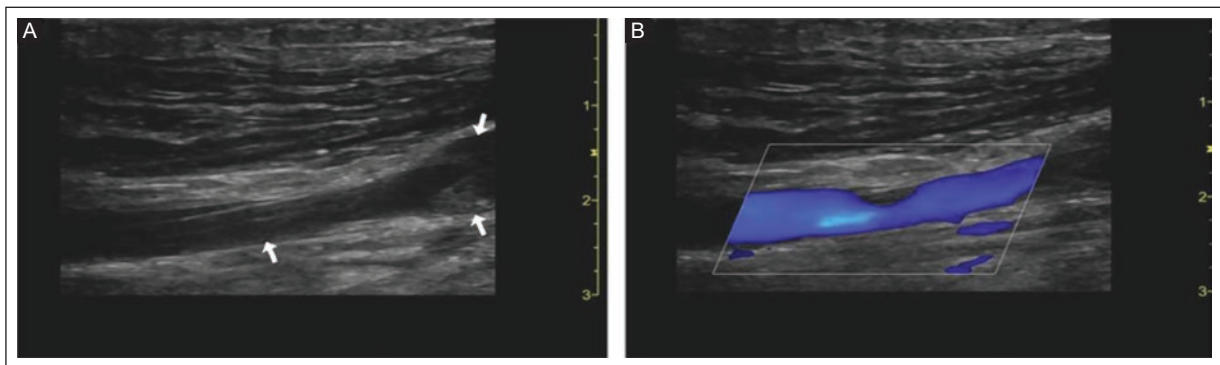


Figure 2. Grayscale (left) and color Doppler US (right) of a 49-year-old male patient with COVID-19. There is acute deep PICC-ASVT of the right upper extremity veins. **A:** several small thrombi are visible on the walls of the right axillary vein (white arrows). **B:** the vein is still permeable, and blood flow is normal. COVID-19: coronavirus disease 2019; PICC-ASVT: peripherally inserted central catheter-associated symptomatic venous thrombosis; US: ultrasound.

and 136, 22.0%) veins. Most catheter tips were in the superior vena cava (482, 81.5% and 503, 81.5%), followed by the right atrium (52, 8.8% and 54, 8.7%). The mean vein diameter in the COVID-19 group was 4.1 mm (SD = 0.90 mm). During the pandemic, catheters were mainly 5 Fr in diameter (599, 97.1%), and a minority were 6 Fr (18, 2.9%), all with three lumens. The mean catheterization duration was 9 days in the non-COVID-19 cohort and 17 days in the COVID-19 cohort, with a range of 1-56 and 1-162 days, respectively.

Comparison of the incidence of PICC-ASVT between COVID-19 and non-COVID-19 patients

The PICC-ASVT incidence was higher in COVID-19 patients. It was found in 38 of 617 cases with an

incidence of 6.2% and in 12 of 592 non-COVID-19 patients with an incidence of 2.03% (Table 2). The estimated incidence of PICC-ASVT in COVID-19 patients was 6159 cases of venous thrombosis per 100,000 patients per year. The odds ratio to quantify this risk in patients with COVID-19 was 3.172, with a 95% confidence interval of 1.641-6.132. Figure 1 shows thrombosis of the right jugular and basilic veins in a patient with COVID-19.

Type and location of PICC-ASVT in COVID-19 patients

Table 3 provides an overview of the type and location of thrombosis in patients with catheters hospitalized for COVID-19. Among them, thrombotic episodes occurred in 38 (6.2%). The majority of cases were deep vein

Table 4. Association between catheter caliber and PICC-ASVT in COVID-19 patients

Description	Total (n = 617)	PICC-ASVT	
		Yes (n = 38)	No (n = 579)
Catheter caliber, 5 Fr ^a	599 (97.1)	34 (89.5)	565 (97.6)
Catheter caliber, 6 Fr	18 (2.9)	4 (10.5)	14 (2.4)

^ap = 0.017.

Fr: French. All values are absolute frequencies and percentages; PICC-ASVT: Peripherally Inserted Central Catheter-Associated Symptomatic Venous Thrombosis.

Table 5. Association between catheter tip location and PICC-ASVT in COVID-19 patients

Description	Total (n = 617)	PICC-ASVT	
		Yes (n = 38)	No (n = 579)
Right auricle	54 (8.7)	4 (10.5)	50 (8.6)
Superior vena cava	503 (81.5)	29 (76.3)	474 (81.8)
Left subclavian vein	13 (2.1)	1 (2.6)	12 (2.1)
Right subclavian vein	36 (5.8)	2 (5.3)	34 (5.9)
Right jugular vein	3 (0.5)	0	3 (0.5)
Left jugular vein	3 (0.5)	2 (5.3)	1 (0.2)
Left axillary vein	1 (0.2)	0	1 (0.2)
Right axillary vein	3 (0.5)	0	3 (0.5)
Inferior vena cava	1 (0.2)	0	1 (0.2)

All values are absolute frequencies and percentages.

COVID-19: coronavirus disease 2019; PICC-ASVT: Peripherally Inserted Central Catheter-Associated Symptomatic Venous Thrombosis.

thrombosis (n = 27, 71.1%), followed by superficial thrombosis (n = 7, 18.4%) or a combination of both (n = 4, 10.5%). The location of the thrombosis varied widely, with the right basilic, right axillary, and left axillary veins most commonly affected. Figure 2 shows a thrombosis with partial blood flow in the right axillary vein.

Association between catheter caliber and PICC-ASVT in COVID-19 patients

Table 4 shows a significant association between catheter caliber and the occurrence of thrombosis (p = 0.017). Most patients, with and without thrombosis, had 5 Fr catheters. In contrast, the use of 6 Fr catheters was minimal but slightly higher in patients with thrombosis.

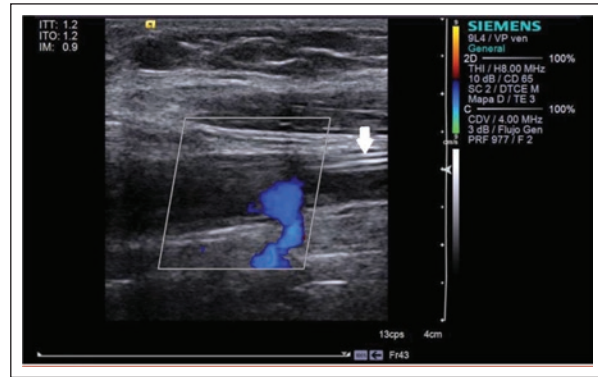


Figure 3. Color Doppler US of a 75-year-old male patient with COVID-19. The right upper extremity veins show acute deep PICC-ASVT, the catheter tip (white arrow), and partial blood flow occlusion in the right subclavian vein.

COVID-19: coronavirus disease 2019; PICC-ASVT: peripherally inserted central catheter-associated symptomatic venous thrombosis; US: ultrasound.

Association of catheter tip location and PICC-ASVT in COVID-19 patients

The catheter tip was most frequently in the superior vena cava (n = 503, 81.5%), followed by the right auricle (n = 54, 8.7%) and the right subclavian vein (n = 36, 5.8%) (Table 5). The analysis showed that in patients transitioning from a thrombosis-free to a thrombosis-affected category, the right atrium (from 8.6% to 10.5%), the left subclavian vein (from 2.1% to 2.6%), and the left jugular vein (from 0.2% to 5.3%) increased, while the superior vena cava (from 81.8% to 76.3%) decreased (p = 0.011). This finding suggests a potential risk associated with tip placement in specific locations, such as the right atrium, the left subclavian vein, and the left jugular vein. Figure 3 shows a venous thrombus adjacent to the PICC tip in the right subclavian vein.

Association of the hospital admission area with PICC-ASVT in COVID-19 patients

In PICC-ASVT patients, the most common hospital admission area was the ICU in 24 (63.2%) of 38 cases, followed by the IMCU (n = 11, 28.9%) (p < 0.001) (Table 6). No cases of PICC-ASVT were found in the wards and RTU.

DISCUSSION

Our study showed an increased incidence of PICC-ASVT in COVID-19 patients compared to non-COVID-19 patients (6.2% and 2.03%, respectively). This report

Table 6. Association of hospital admission area and PICC-ASVT in COVID-19 patients

Description	Total (n = 617)	PICC-ASVT	
		Yes (n = 38)	No (n = 579)
ICU ^a	240 (38.9)	24 (63.2)	216 (37.3)
Ward	180 (29.2)	0	180 (31.1)
Operating room	21 (3.4)	3 (7.9)	18 (3.1)
IMCU ^a	96 (15.5)	11 (28.9)	85 (14.7)
RTU	80 (13.0)	0	80 (13.8)

All values are absolute frequencies and percentages. ^ap < 0.001.

ICU: intensive care unit; IMCU: intermediate care unit; PICC-ASVT: Peripherally Inserted Central Catheter Associated Symptomatic Venous Thrombosis; RTU: respiratory therapy unit.

represents the first instance in Mexico that quantifies the incidence of PICC-ASVT in COVID-19-positive patients and identifies SARS-CoV-2 infection as a risk factor for developing thrombosis in PICC vascular accesses. These findings are relevant for vascular access monitoring and thromboprophylaxis protocols for hospitalized COVID-19 patients.

PICC is a recognized risk factor for venous thrombosis. A retrospective, multicenter cohort study of 1,228 hospitalized COVID-19 patients, 30 of whom received PICC, found an incidence of venous thromboembolism of 6.7%²². This finding suggests a higher rate of venous thromboembolism in COVID-19 patients who receive vascular access compared to those who do not. In contrast, a retrospective cohort study found that none of the 227 COVID-19-positive patients had a PICC-ASVT, suggesting that the risk of catheter-related thrombosis is close to zero when a PICC is placed according to international guidelines²¹. The differences between the results above are mainly because 100% of the participants in the study by Frondizi et al.²¹ were hospitalized patients who were not treated in the ICU, whereas 38.9% of our study participants were treated in the ICU and IMCU (28.9%); admission to these areas is a risk marker for thrombosis. Finally, another source of contention could be due to differences in the health status of patients with a PICC, particularly diseases associated with an increased risk of thrombosis, such as obesity, hypertension, dyslipidemia, diabetes mellitus, metabolic syndrome, and tobacco use²³. Our results highlight the thrombotic impact of COVID-19 and its impact on intra-venous device placement by interventional radiology by comparing pre- and post-pandemic scenarios.

Critically ill patients have an increased risk of thrombosis. Our study showed significant differences between the patient groups in ICUs, the operating rooms, and ward area, with the proportion of patients with thrombosis increasing up to 63.2% in the ICU, in contrast with none in the ward. These results are consistent with Sebolt et al.²², where the majority of patients in the ICU (n = 340, 98%) experienced thrombotic events. A study by Kang et al.²⁴ examined complications in patients with a PICC placed in a COVID-19 unit, considering the technical factors involved in performing the procedure. This study highlighted the limitations in vision and mobility caused by personal protective equipment, such as poor or no vision, the inability to adjust the light intensity in the rooms, and blurring and reflections in the face shields and masks, to name a few. It is important to clarify that these findings identify ICU and IMCU stays as undeniable risk markers rather than risk factors per se. This is because these areas reflect the critical condition, the severity, the clinical relevance of the patient's proinflammatory state, and the technical difficulties of personal protective equipment in all medical procedures during the pandemic.

The robustness of our study stems from the elements of cohort design and the standardized placement technique, equipment, and operator. Moreover, the cases of PICC-ASVT in COVID-19 and non-COVID-19 patients were all confirmed by ultrasound. Nevertheless, there are limitations to our study: clinical diagnoses of comorbidities as risk factors were not recorded and analyzed. Ultrasound was not performed to identify asymptomatic PICC-associated venous thrombosis.

CONCLUSION

In our study, SARS-CoV-2 infection was found to be a risk factor for PICC-ASVT, increasing the probability of thrombotic event hospitalizations in the ICU and IMCU, which were associated with thrombosis and reflected the clinical condition of the patient and the severity of COVID-19. This study contributes to interdisciplinary decision-making regarding thromboprophylaxis, screening, and treatment of catheter-associated thrombosis in patients with SARS-CoV-2 infection. Further studies are needed to develop a protocol for screening high-risk patients with indwelling catheters.

Acknowledgments

The authors thank Professor Ana M. Contreras-Navarro for her guidance in preparing and writing this

scientific paper. This original research in the Radiology Specialty field was awarded as a thesis at the Segunda Convocatoria Nacional 2023-2024, "Las Mejores Tesis de Radiología para Publicar en el JMEXFRI."

Funding

This research received no external funding.

Conflict of interest

The authors declare no conflicts of interest.

Ethical disclosures

Protection of individuals. This study complied with the Declaration of Helsinki (1964) and subsequent amendments.

Confidentiality of data. The authors declare they followed their center's protocol for sharing patient data.

Right to privacy and informed consent. Informed consent was not required for this observational study of information collected during routine clinical care.

Use of artificial intelligence. The authors did not use generative artificial intelligence to prepare this manuscript and/or create tables, figures, or figure legends.

REFERENCES

- Evans RS, Sharp JH, Linford LH, Lloyd JF, Tripp JS, Jones JP, et al. Risk of Symptomatic DVT Associated with Peripherally Inserted Central Catheters. *Chest*. 2010;138(4):803-810. doi: 10.1378/chest.10-0154.
- Grant JD, Stevens SM, Woller SC, Lee EW, Kee ST, Liu DM, et al. Diagnosis and management of upper extremity deep-vein thrombosis in adults. *Thromb Haemost*. 2012;108(6):1097-1108. doi: 10.1160/TH12-05-0352.
- Greene MT, Flanders SA, Woller SC, Bernstein SJ, Chopra V. The Association Between PICC Use and Venous Thromboembolism in Upper and Lower Extremities. *Am J Med*. 2015;128(9):986-993.e1. doi: 10.1016/j.amjmed.2015.03.028.
- Ong B, Gibbs H, Catchpole I, Hetherington R, Harper J. Peripherally inserted central catheters and upper extremity deep vein thrombosis. *Australas Radiol*. 2006;50(5):451-454. doi: 10.1111/j.1440-1673.2006.01623.x.
- Biffi R, Orsi F, Pozzi S, Pace U, Bonomo G, Monfardini L, et al. Best choice of central venous insertion site for the prevention of catheter-related complications in adult patients who need cancer therapy: a randomized trial. *Ann Oncol*. 2009;20(5):935-940. doi: 10.1093/annonc/mdn701.
- Abdullah BJJ, Mohammad N, Sangkar JV, Abd Aziz YF, Gan GG, Goh KY, et al. Incidence of upper limb venous thrombosis associated with peripherally inserted central catheters (PICC). *Br J Radiol*. 2005;78(931):596-600. doi: 10.1259/bjir/32639616.
- Chemaly RF, de Parres JB, Rehm SJ, Adal KA, Lisgaris M V, Katz-Scott DS, et al. Venous thrombosis associated with peripherally inserted central catheters: a retrospective analysis of the Cleveland Clinic experience. *Clin Infect Dis*. 2002;34(9):1179-1183. doi: 10.1086/339808.
- Grove JR, Pevec WC. Venous thrombosis related to peripherally inserted central catheters. *J Vasc Interv Radiol*. 2000;11(7):837-840. doi: 10.1016/S1051-0443(07)61797-7.
- Trerotola SO, Stavropoulos SW, Mondschein JI, Patel AA, Fishman N, Fuchs B, et al. Triple-lumen peripherally inserted central catheter in patients in the critical care unit: prospective evaluation. *Radiology*. 2010;256(1):312-320. doi: 10.1148/radiol.10091860.
- Cortezzi A, Fracchiolla NS, Maisonneuve P, Moia M, Luchesini C, Ranzi ML, et al. Central venous catheter-related complications in patients with hematological malignancies: a retrospective analysis of risk factors and prophylactic measures. *Leuk Lymphoma*. 2003;44(9):1495-1501. doi: 10.3109/10428190309178770.
- Chen P, Zhu B, Wan G, Qin L. The incidence of asymptomatic thrombosis related to peripherally inserted central catheter in adults: A systematic review and meta-analysis. *Nurs Open*. 2021;8(5):2249-2261. doi: 10.1002/nop.2.811.
- Hinojosa-Sanchez MA, Martinez-Aparicio JS, Franco-Estrada M, Escobar-Luna A, Carrillo-Martinez MA, Puente-Gallegos FE. Low incidence of symptomatic venous thrombosis associated with peripherally inserted central catheter. *J Mex Fed Radiol Imaging*. 2022;1(2):111-118. doi: 10.24875/JMEXFRI.M22000015.
- Dubois J, Rypens F, Garel L, David M, Lacroix J, Gauvin F. Incidence of deep vein thrombosis related to peripherally inserted central catheters in children and adolescents. *CMAJ*. 2007;177(10):1185-1190. doi: 10.1503/cmaj.070316.
- Periard D, Monney P, Waeber G, Zurkinden C, Mazzolai L, Hayoz D, et al. Randomized controlled trial of peripherally inserted central catheters vs. peripheral catheters for middle duration in-hospital intravenous therapy. *J Thromb Haemost*. 2008;6(8):1281-1288. doi: 10.1111/j.1538-7836.2008.03053.x.
- Nash EF, Helm EJ, Stephenson A, Tullis E. Incidence of deep vein thrombosis associated with peripherally inserted central catheters in adults with cystic fibrosis. *J Vasc Interv Radiol*. 2009;20(3):347-351. doi: 10.1016/j.jvir.2008.11.018.
- Liem TK, Yanit KE, Moseley SE, Landry GJ, DeLoughery TG, Rumwell CA, et al. Peripherally inserted central catheter usage patterns and associated symptomatic upper extremity venous thrombosis. *J Vasc Surg*. 2012;55(3):761-767. doi: 10.1016/j.jvs.2011.10.005.
- Lobo BL, Vaidean G, Broyles J, Reaves AB, Shorr RI. Risk of venous thromboembolism in hospitalized patients with peripherally inserted central catheters. *J Hosp Med*. 2009;4(7):417-422. doi: 10.1002/jhm.442.
- Ge X, Cavallazzi R, Li C, Pan SM, Wang YW, Wang FL. Central venous access sites for the prevention of venous thrombosis, stenosis and infection. *Cochrane Database Syst Rev*. 2012;2012(3):CD004084. doi: 10.1002/14651858.CD004084.pub3.
- Smit JM, Lopez Matta JE, Vink R, Müller MCA, Choi KF, van Baarle FEHP, et al. Coronavirus disease 2019 is associated with catheter-related thrombosis in critically ill patients: A multicenter case-control study. *Thromb Res*. 2021;200:87-90. doi: 10.1016/j.thromres.2021.01.013.
- Panigada M, Bottino N, Tagliabue P, Grasselli G, Novembrino C, Chantarangkul V, et al. Hypercoagulability of COVID-19 patients in intensive care unit: A report of thromboelastography findings and other parameters of hemostasis. *J Thromb Haemost*. 2020;18(7):1738-1742. doi: 10.1111/jth.14850.
- Frondizi F, Dolcetti L, Pittiruti M, Calabrese M, Fantoni M, Biasucci DG, et al. Complications associated with the use of peripherally inserted central catheters and midline catheters in COVID-19 patients: An observational prospective study. *Am J Infect Control*. 2023;51(11):1208-1212. doi: 10.1016/j.ajic.2023.05.002.
- Sebolt J, Buchinger J, Govindan S, Zhang Q, O'Malley M, Chopra V. Patterns of vascular access device use and thrombosis outcomes in patients with COVID-19: a pilot multi-site study of Michigan hospitals. *J Thromb Thrombolysis*. 2022;53(2):257-263. doi: 10.1007/s11239-021-02559-4.
- Piazza G, Goldhaber SZ. Venous thromboembolism and atherothrombosis an integrated approach. *Circulation*. 2010;121(19):2146-2150. doi:10.1161/circulationaha.110.951236.
- Kang MC, Lee K. Feasibility of peripherally inserted central catheter placement in covid-19 patients isolated in the intensive care unit of a small volume center (291-bed hospital). *J Acute Care Surg*. 2022;12(3):125-131. doi:10.17479/jacs.2022.12.3.125.

Abnormal US findings of the shoulders in Mexican patients with end-stage renal disease: association with long-term hemodialysis

J. Gerardo Gutierrez-Compean^{1,2,*}, Jesús I. Nafarrate-Rivera³, and Eliseo Monroy-Alvarado¹

¹Radiology Department, Unidad Médica de Alta Especialidad, Hospital de Especialidades Num. 71, Instituto Mexicano del Seguro Social, Torreon, Coahuila; ²Radiology Department, UMF 31, Instituto Mexicano del Seguro Social, San Nicolas de los Garza, Nuevo Leon; ³Nephrology Department, Unidad Médica de Alta Especialidad, Hospital de Especialidades Núm. 71, Instituto Mexicano del Seguro Social, Torreon, Coahuila. Mexico

ABSTRACT

Introduction: Ultrasound (US) findings of the shoulders of end-stage renal disease (ESRD) patients on hemodialysis therapy have been insufficiently researched. This study aimed to describe the abnormal US findings in Mexican patients with ESRD and their relationship with long-term hemodialysis treatment. **Material and Methods:** In this cross-sectional study, we performed US grayscale examination of the shoulders of adult ESRD patients. We assessed qualitative abnormal US findings, such as non-homogeneous and loss of the regular fibrillar pattern and hyperechogenic or hypoechogenic material in the tendons and/or bursae. We also quantitatively assessed the thickening of the supraspinatus, subscapularis, and long head biceps (LHB) tendons of the rotator cuff (RC). **Results:** One hundred seventy shoulders from 85 ESRD patients on hemodialysis were examined. At least one US shoulder abnormality was found in 51 (60.0%) of the 85 patients. RC thickening was the most common abnormality ($n = 49, 96.0\%$). The diameters of the supraspinatus, subscapularis, and LHB tendons were significantly thicker in ESRD patients with abnormal shoulder US findings. RC thickening was found in 44 (51.8%) of 85 right shoulders and 27 (31.8%) left shoulders. Eleven (27.0%) of the patients with less than 1 year of hemodialysis had no RC thickening in the right shoulders, while only 2 (5.0%) had thickening ($p = 0.001$). In the 1 to 3-year range of hemodialysis, 24 (59.0%) did not have RC thickening, while 18 (41.0%) had thickening. After 4 to 6 years of dialysis, 5 (12.0%) had no thickening, while 16 (36.0%) had thickening. In patients with more than 7 years of hemodialysis, only one (2.0%) had no RC thickening compared to 8 (18.0%) with thickening ($p < 0.001$). In the left shoulders, RC thickening was also significant with long-term hemodialysis ($p < 0.004$). **Conclusion:** This study showed a high frequency of abnormal US findings in the shoulders of ESRD patients on hemodialysis. Longer duration of hemodialysis was associated with RC thickening.

Keywords: Ultrasound. Shoulder. End-stage renal disease. Hemodialysis. Rotator cuff.

INTRODUCTION

Arthropathy associated with chronic hemodialysis or continuous ambulatory peritoneal dialysis is a complication in end-stage renal disease (ESRD) patients^{1,2}. Pain and stiffness in large joints, such as the shoulders, wrists, hips, knees, and spine, are clinical manifestations. The shoulders are the most affected joints in almost half of all patients on hemodialysis for more than

10 years². The gold standard for shoulder assessment is magnetic resonance imaging (MRI)³. However, it is time-consuming, expensive, and not always available. Therefore, ultrasound (US) has been proposed as a useful morphologic and functional assessment tool for shoulder pathologies.

The US findings of the shoulder include rotator cuff (tendon tears, tendinosis, and bursitis) and non-rotator cuff (RC) abnormalities (e.g., synovial joint disorders

*Corresponding author:

J. Gerardo Gutierrez-Compean
E-mail: Gera.compean@gmail.com

Received for publication: 22-01-2024

Accepted for publication: 25-04-2024

DOI: 10.24875/JMEXFRI.M2400082

Available online: 03-10-2024

J Mex Fed Radiol Imaging. 2024;3(3):189-196

www.JMeXFRI.com

2696-8444 / © 2024 Federación Mexicana de Radiología e Imagen, A.C. Published by Permanyer. This is an open access article under the CC BY-NC-ND (<https://creativecommons.org/licenses/by-nc-nd/4.0/>).

and nerve entrapment syndromes)^{2,4}. Abnormal US findings in RC tendons have been described as non-homogeneous tendons with loss of the regular fibrillar pattern and hyperechogenic or hypoechogenic material in the tendons and/or bursae^{1,4,5,6}. Other US findings include subacromial-subdeltoid bursa effusion and subacromial impingement. In some cases, this finding is associated with extensive ruptures of the supraspinatus tendon^{1,4,5}.

The normal tendon thickness of the subscapularis and supraspinatus tendons of the RC in ESRD patients has been reported as ≤ 7 mm^{4,5,7}, and the long head biceps (LHB) tendon as ≤ 4 mm⁵. RC thickening is the most common abnormality in hemodialysis-related shoulder arthropathy^{1,4,8}. Histopathologic studies have demonstrated β_2 -microglobulin amyloid deposition in the musculoskeletal tissue in association with RC thickening^{4,7}. There are a few reports of abnormal US findings of the shoulder in patients with ESRD on hemodialysis^{1,2,4,5,7,8}. The aim of this study was to describe the abnormal US findings in Mexican ESRD patients and their relationship with long-term hemodialysis.

MATERIAL AND METHODS

This cross-sectional study was conducted from December 2021 to February 2022 in the Department of Imaging and the Department of Nephrology of the Unidad Medica de Alta Especialidad, Hospital de Especialidades N° 71 of the Instituto Mexicano del Seguro Social, in Torreon, Coahuila, Mexico. Adult patients of both sexes on hemodialysis with a diagnosis of ESRD were included. Patients with a history of shoulder surgery or trauma, acute nephropathy on hemodialysis, or rheumatic diseases and who were uncooperative during the dynamic US examination were excluded. Study participants signed an informed consent form. The institutional research ethics committee and the research committee approved the study protocol.

Study development and variables

Age, sex, and occupation were recorded. The etiology of ESRD, diabetes, systemic arterial hypertension (SAH), or other causes, such as preeclampsia, autosomal dominant polycystic kidney disease, systemic lupus erythematosus, nephrotic syndrome, and urolithiasis, was obtained from the electronic clinical file. The type of vascular access and duration of hemodialysis (in years) were also recorded.

US acquisition protocol and analysis

Shoulder US grayscale was performed with a CHISON Echo 2 system (CHISON Medical Technologies Co., LTD, Xinwu District, China) using a high-resolution linear transducer (8 MHz-12MHz). US examinations of both shoulders were performed according to a previously described protocol by Beggs⁹.

The assessment was performed with dynamic maneuvers, starting with the LHB tendon. The patient rests with the hand palm up on the thigh and the elbow flexed at 90°. Next, the patient is asked to hold the arm in external rotation with the elbow flexed at 90° to scan the short-axis subscapularis tendon. The supraspinatus tendon was examined with the shoulder internally rotated with the palm outward behind the lower back, in the "hand-in-back pocket" position, palm facing backwards.

The thin, hypoechoic subdeltoid bursa lies draped over the supraspinatus tendon. Finally, the patient was asked to abduct his arm while internally rotating it. With this maneuver, the supraspinatus tendon and the bursa can be seen passing deep to the coracoacromial arch. The thickness of the supraspinatus and subscapularis tendons of the RC was assessed. The longitudinal axis was measured 1.5 cm from its insertion⁴. The LHB tendon was measured in its transverse axis, inside its bicipital groove.

Qualitative abnormal US findings assessed were non-homogeneous tendons with loss of the regular fibrillar pattern and hyperechogenic or hypoechogenic material in the tendons and/or bursae. The quantitative thickening diameter of the RC tendons was recorded in millimeters.

Statistical analysis

The qualitative variables were expressed as frequencies and percentages. The normality of distribution was defined using Levene's test. Numerical variables were expressed as means \pm standard deviation (SD). A stratified analysis was performed according to hemodialysis duration using the chi-square test or Fisher's exact test to determine the association between hemodialysis duration and abnormal ultrasonographic shoulder findings. A p-value ≤ 0.05 was considered significant. The statistical analysis was performed with SPSS version 29 (IBM Corp., Armonk, NY, USA).

RESULTS

One hundred seventy shoulders from 85 ESRD patients on hemodialysis were examined. The mean age was 57.7 ± 12.9 years; there were 38 (44.7%)

Table 1. Characteristics of 85 Mexican patients with ESRD on hemodialysis

Description	Parameter
Age, years, mean ± SD	57.7 ± 12.9
Sex	
Women, n (%)	38 (44.7)
Men, n (%)	47 (55.3)
Occupation, n (%)	
Active employee	30 (35.3)
Home	25 (29.3)
Business	10 (11.8)
Retiree	10 (11.8)
Other	10 (11.8)
Etiology of ESRD ^a , n (%)	
Diabetes	4 (4.7)
SAH	12 (14.1)
Diabetes and SAH	32 (37.7)
Others ^a	37 (43.5)
Type of vascular access, n (%)	
Mahurkar catheter	67 (78.8)
Arteriovenous fistula	18 (21.2)
Time in hemodialysis, n (%)	
< 1 year	13 (15.3)
1-3 years	42 (49.4)
4-6 years	21 (24.7)
> 7 years	9 (10.6)

^aPreeclampsia, autosomal dominant polycystic kidney disease, systemic lupus erythematosus, nephrotic syndrome, and urolithiasis. All values are absolute frequencies and percentages unless otherwise stated.

ESRD: end-stage renal disease; SAH: systemic arterial hypertension.

women and 47 (55.3%) men (Table 1). Thirty-two (37.7%) patients had diabetes and SAH, followed by 37 (43.5%) with another etiology. A Mahurkar catheter was the most commonly used vascular access (n = 67, 78.8%). Forty-two (49.4%) patients had been on hemodialysis for 1 to 3 years, followed by 21 (24.7%) patients with 4 to 6 years. In the smallest group of 9 (10.6%) patients, the duration was > 7 years. Thirty-four (40.0%) of 85 patients had no shoulder abnormalities on US (Table 2). Figure 1 shows a US grayscale of the right subscapularis tendon with a normal fibrillar pattern.

Table 2. Frequency of normal or abnormal US in relation to shoulder laterality of 85 Mexican patients with ESRD on hemodialysis

Description	n (%)
Normal US findings	34 (40.0)
Abnormal US findings	51 (60.0)
Unilateral right shoulder	22 (43.2)
Unilateral left shoulder	4 (7.8)
Bilateral shoulder	25 (49.0)

ESRD: end-stage renal disease; US: ultrasound.

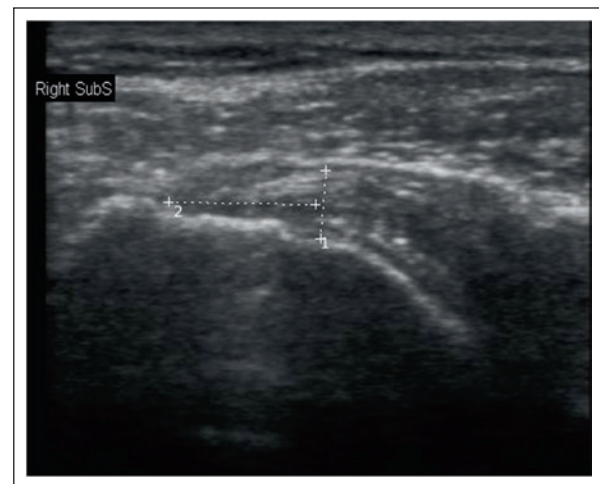


Figure 1. US grayscale of the shoulder of a 69-year-old woman with ESRD who has been on hemodialysis for two years. The longitudinal view shows the right subscapularis tendon of the RC with homogeneous echogenicity and a thickness of 4.9 mm (dashed lines). Diagnosis of a normal right subscapularis tendon.

ESRD: end-stage renal disease; RC: rotator cuff; SubS: subscapularis tendon. US: ultrasound

Figures 2 and 3 show the grayscale US of the supraspinatus tendon and the LHB with a normal fibrillar pattern. At least one US abnormality was detected in 51 (60.0%) of 85 patients: 22 (43.2%) with unilateral involvement of the right side, 4 (7.8%) with unilateral involvement of the left side, and 25 (49.0%) with bilateral involvement.

Qualitative US abnormalities of the shoulders

Thickening of the RC tendons was observed in 49 (80.3%) patients, while only 5 (8.2%) had bursal effusion and 7 (11.5%) subacromial impingement (Table 3).

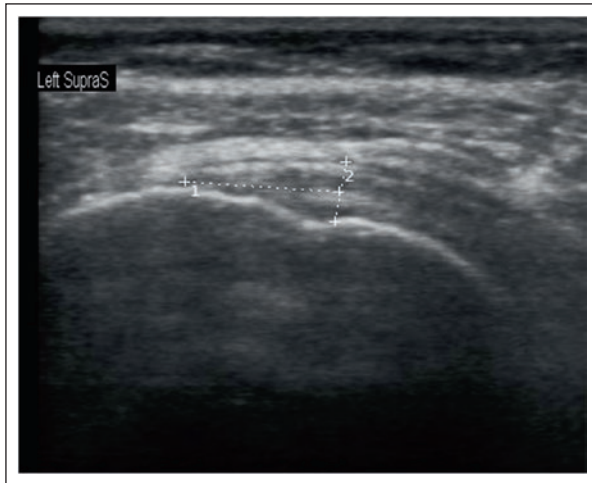


Figure 2. US grayscale of the shoulder of a 30-year-old woman with ESRD with two years of hemodialysis. The longitudinal view shows the left supraspinatus tendon of the RC with homogeneity and a thickness of 4.4 mm (dashed lines). Diagnosis of a normal left supraspinatus tendon.

ESRD: end-stage renal disease; SupraS: supraspinatus tendon; RC: rotator cuff; US: ultrasound.

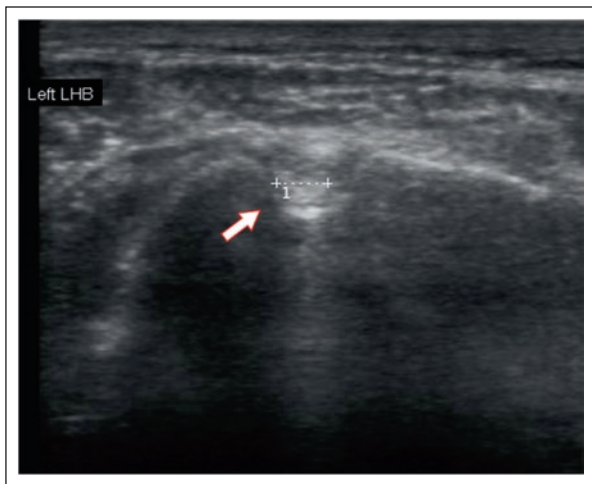


Figure 3. US grayscale of the shoulder of a 57-year-old woman with ESRD with three months of hemodialysis. The transversal view shows the LHB tendon (dashed lines) homogeneous and inside the bicipital groove (arrow). Diagnosis of a normal left LHB tendon.

ESRD: end-stage renal disease; LHB: long head biceps tendon; US: ultrasound.

Some patients had more than one abnormal US finding. No nodular images were found in any shoulder. The subscapularis, supraspinatus, and LHB tendons were included in the RC assessment. Qualitative US abnormalities were non-homogeneous tendons with loss of a regular fibrillar pattern and hyperechogenic or hypoechogenic material in the tendons.

Quantitative assessment of RC tendons thickness in shoulder US

There was a significant difference in RC tendon thickness in patients with abnormal US findings compared to the group with normal findings (Table 4). The abnormal US thickness of the right (5.7 ± 1.2 mm) and left (5.7 ± 1.2 mm) subscapularis tendon differed from the normal US findings of the right (4.8 ± 0.7 mm) and left (4.7 ± 0.6 mm) subscapularis tendon by almost one millimeter ($p < 0.001$). The difference between the abnormal right (5.6 ± 1.2) and left (5.4 ± 1.0) supraspinatus tendon differed from the normal US findings of the right (4.9 ± 0.6) and left (4.9 ± 0.6) supraspinatus tendon ($p < 0.002$). In patients with normal US findings, the mean thickness of the right LHB was 3.8 ± 0.4 mm, and the left LHB was 3.9 ± 0.4 mm; in patients with abnormal US, the mean right LHB was 5.1 ± 0.9 mm and the left LHB with a mean of 5.4 ± 1.1 mm ($p < 0.001$). Figures 4, 5, 6, and 7 show the qualitative and quantitative US abnormalities of the subscapularis, supraspinatus, and LHB tendons of the RC in a grayscale US examination.

Association between abnormal US findings in the shoulder and long-term hemodialysis

Table 5 shows a comparison of 170 right and left shoulder RCs of ESRD patients and the duration of hemodialysis. RC thickening was found in 44 (51.8%) of 85 right shoulders and 27 (31.8%) left shoulders. In the right shoulders, 11 (27.0%) of the patients with less than 1 year of therapy had no RC thickening, while only 2 (5.0%) of these patients had thickening ($p = 0.001$). In the 1 to 3-year range of hemodialysis duration, 24 (59.0%) had no RC thickening, compared to 18 (41.0%) with thickening. After 4 to 6 years, 5 (12.0%) had no thickening, while 16 (36.0%) had thickening. Finally, in patients with more than 7 years of therapy, only one (2.0%) had no RC thickening compared to 8 (18.0%) with thickening ($p < 0.001$).

In the left shoulders, 10 (16.4%) patients with less than 1 year of hemodialysis duration had no RC thickening compared to 3 (13.0%) who did ($p < 0.004$). At 1 to 3 years, 35 (57.3%) showed no RC thickening, while 7 (29.0%) had thickening; at 4 to 6 years, 9 (18.1%) showed no thickening, while 12 (42.0%) had thickening. In patients with more than 7 years, 4 (8.2%) had no RC thickening compared to 5 (16.0%) who did ($p < 0.004$). These results show a significant association between RC thickening and longer hemodialysis time.

Table 3. Qualitative US abnormalities in shoulders of 51 Mexican patients with ESRD on hemodialysis

Description ^a	Total, n	Right shoulder involvement, n (%)	Left shoulder involvement, n (%)	Bilateral n (%)
RC thickened tendons ^{a,b,c}	49	22 (44.9)	5 (10.2)	22 (44.9)
Bursal effusion	5	3 (60.0)	2 (40.0)	0
Subacromial impingement	7	3 (42.8)	4 (57.2)	0

^aSome patients had more than one abnormal US finding; ^bQualitative abnormal US findings were non-homogeneous tendons with loss of a regular fibrillar pattern with hyperechogenic or hypoechogenic material in tendons. ^cSubscapularis, supraspinatus, and long head of the biceps (LHB) tendons included.

ESRD: end-stage renal disease; RC: Rotator cuff; US: ultrasound.

Table 4. Quantitative assessment of RC tendon thickness in shoulder US in patients with ESRD on hemodialysis

Description	Right shoulder US			Left shoulder US		
	Normal (n = 41)	Abnormal (n = 44)	p-value	Normal (n = 58)	Abnormal (n = 27)	p-value
Subscapularis tendon thickness, mm	4.8 ± 0.7 (3.3, 4.8, 6.1)	5.7 ± 1.2 (4.0, 6.1, 7.9)	0.001	4.7 ± 0.6 (3.5, 4.7, 6.0)	5.7 ± 1.2 (3.9, 5.7, 7.9)	0.001
Supraspinatus tendon thickness, mm	4.9 ± 0.6 (2.7, 5.0, 6.0)	5.6 ± 1.2 (2.3, 5.8, 7.8)	0.002	4.9 ± 0.6 (3.0, 5.0, 6.0)	5.4 ± 1.0 (2.8, 5.4, 6.6)	0.015
LHB tendon thickness, mm	3.8 ± 0.4 (2.8, 3.9, 4.7)	5.1 ± 0.9 (2.9, 4.0, 7.1)	0.001	3.9 ± 0.4 (2.4, 4.0, 4.6)	5.4 ± 1.1 (3.5, 5.2, 7.4)	0.001

Values are means ± SD (minimum, median, maximum).

ESRD: end-stage renal disease. RC: rotator cuff; US: ultrasound.

DISCUSSION

Our study showed a high frequency of abnormal US findings in the shoulders of Mexican patients with ESRD on hemodialysis. RC tendon thickening was the most frequent finding significantly associated with a longer duration of hemodialysis. This study is the first to describe the qualitative and quantitative features of RC tendon US assessments in Mexican patients with ESRD on hemodialysis.

The shoulders are the most affected joints in ESRD patients on hemodialysis^{2,7,8}. US examination has been proposed as a diagnostic, non-invasive, less expensive, and more useful method for morphologic and functional assessment of the shoulder². Our study found at least one abnormal US finding in the shoulders in 51 (60.0%) of 85 ESRD patients on hemodialysis. Tharwat et al.² assessed 28 patients with ESRD to determine the validity of US to properly detect shoulder disorders in ESRD patients on hemodialysis with shoulder pain by identifying US abnormalities and comparing them with those identified on MRI, with MRI serving as the gold standard. US

abnormalities were present in almost all patients. Supraspinatus tendinopathy was the most common abnormality in symptomatic shoulders (92.1%). The percentage agreement between shoulder US and MRI in detecting biceps tenosynovitis was 82.14% (kappa, 0.64), subscapularis tendinopathy 83.93% (kappa, 0.654), and supraspinatus tendinopathy 91.07% (kappa, 0.617). The authors concluded that shoulder US has high sensitivity and specificity compared to MRI. Shoulder US is a valuable imaging examination in the diagnosis of hemodialysis-associated shoulder arthropathy in ESRD patients. Therefore, histologic examination of the shoulder, as the “gold standard,” may be unnecessary².

In shoulder arthropathy secondary to chronic hemodialysis, a significant difference in RC tendon thickness was found compared to patients without hemodialysis exposure^{4,5,7}. Cardinal et al.⁴ compared shoulder US findings from 19 shoulders of 11 American patients with ESRD on chronic hemodialysis (average time 14 years) with a control group of 20 shoulders of asymptomatic patients without renal disease. The mean RC thickness was significantly greater (7 mm,

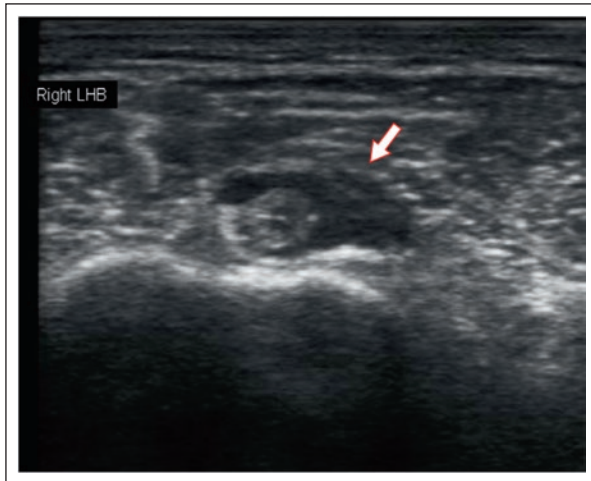


Figure 4. US grayscale of the shoulder of a 63-year-old man with ESRD with 21 years of hemodialysis and a limited range of motion of both shoulders. The transverse view of the right LHB tendon and its sheath showed a thickening of 6.8 mm and non-homogeneous echogenicity (arrow). The diagnosis was tendinosis of the right LHB tendon. ESRD: end-stage renal disease; LHB: long head biceps; US: ultrasound.

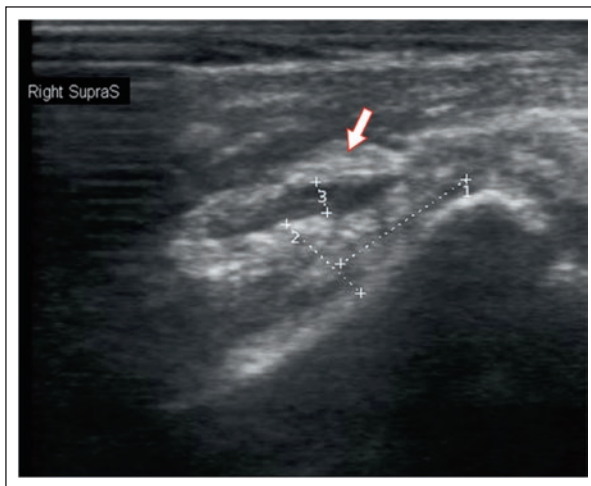


Figure 5. US grayscale of the shoulder of a 78-year-old woman with ESRD with three years of hemodialysis. She reported morning pain in the right shoulder. A longitudinal view shows right subacromial bursa effusion (arrow). The adjacent supraspinatus tendon of the RC is non-homogeneous with loss of the fibrillar pattern (dashed lines). The diagnosis was subdeltoid bursitis and tendinosis of the right supraspinatus tendon of the RC.

US: ultrasound; ESRD: end-stage renal disease; RC: rotator cuff; SupraS: supraspinatus tendon.

range 3-10 mm) than the control group (5 mm, range 3-6 mm) ($p < 0.001$). Sommer et al.⁵ assessed 14 shoulders of 12 Israeli patients with ESRD with > 10 years of hemodialysis. The most common finding was a non-homogeneous thickening of the RC tendons

with a mean thickness of 7.6 mm of the supraspinatus tendon compared to a normal supraspinatus tendon thickness of 3 to 6 mm. The LHB had a mean thickness of 5.5 ± 1.9 mm in contrast to the normal group, with a thickness of 2.7 to 3.5 mm. The most significant difference between the thickened and normal groups was found in the LHB, where differences of up to 4 mm in thickness were observed. Hyperechoic and hypoechoic material was also seen in tendons. On the other hand, Kay et al.⁷ reported the shoulder US findings in 38 patients who had been on hemodialysis for more than 6 years. Shoulder US abnormalities were found in 28 (74%) of 38 patients. Fourteen patients with joint shoulder and histologically confirmed amyloidosis had an RC thickening > 8 mm. They reported a US sensitivity of 60-87% and a specificity of 81-100% for diagnosing RC tendon arthropathy related to hemodialysis in ESRD patients. In our study, supraspinatus, subscapularis, and LHB tendon thickening of the RC was the most common finding. However, the mean values of the diameters in these Mexican patients were smaller than those reported by other authors^{4,5,7}. The difference in the diameters of thickened RC tendons in our study and other reports could be due to the longer duration of hemodialysis and perhaps to anthropometric differences in the study populations.

Chronic hemodialysis treatment is a known risk factor for developing shoulder arthropathy, especially RC thickening⁷. Our study showed that the longer the duration of hemodialysis, the greater the likelihood of RC tendon thickening. In comparison, Coari et al.⁸ reported RC tendon thickening in 16 (24%) of 66 shoulders and 20 (30%) with bursal effusion in 33 ESRD patients with an average hemodialysis time of 7.3 years. The authors concluded that the duration of dialysis treatment is the most important factor for shoulder arthropathy. According to our results, the longer the duration of hemodialysis, the higher the incidence of shoulder involvement. In particular, RC thickening.

The strengths of this study include a large sample size and an imaging modality that is affordable and dynamic. In addition, the RC tendons were evaluated qualitatively and quantitatively. There are some study limitations. First, US examination has the disadvantage of being operator-dependent, and usually, radiologists in charge of performing it are not experts in musculoskeletal imaging. Second, the data on shoulder arthropathy clinical manifestations were not reported. Third, the diagnosis of shoulder hemodialytic arthropathy was not histopathologically confirmed. Fourth, only a few

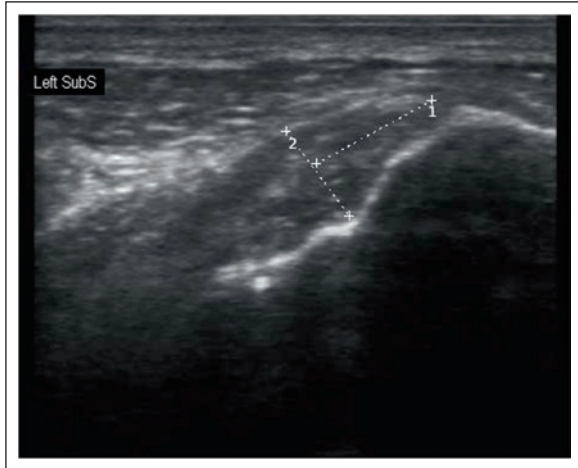


Figure 6. US grayscale of the shoulder of a 45-year-old man with ESRD with 14 years of hemodialysis. He reported pain in both shoulder joints, especially in the morning. The longitudinal view shows a thickening of 7.9 mm of the left subscapularis tendon of the RC with a loss of its usual fibrillar pattern (dashed lines). Diagnosis of tendinosis of the left subscapularis muscle.
US: ultrasound; SubS: subscapularis tendon; ESRD: end-stage renal disease; RC: rotator cuff.

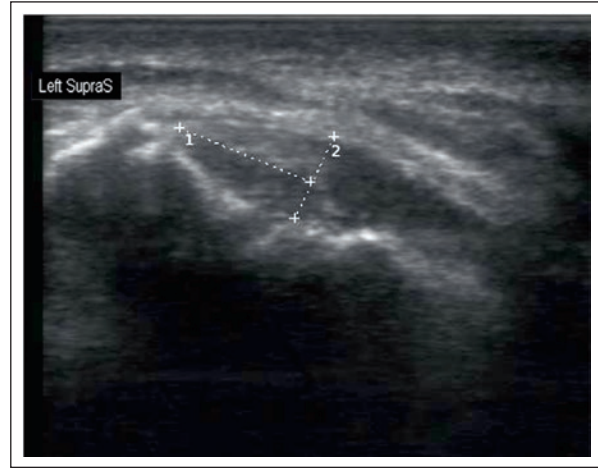


Figure 7. US grayscale of the shoulder of a 64-year-old man with ESRD with six years of hemodialysis. The longitudinal view shows a non-homogeneous and thickened 6.4 mm left supraspinatus tendon (dashed lines). Diagnosis of tendinosis of the left supraspinatus muscle of the RC.
US: ultrasound; SupraS: supraspinatus; ESRD: end-stage renal disease; RC: rotator cuff.

Table 5. Association between duration of hemodialysis and US thickening of the RC tendons^a of 170 shoulders in patients with ESRD

Description	Right shoulder US			Left shoulder US		
	without RC thickening, n (%)	with RC thickening, n (%)	p-value	without RC thickening, n (%)	with RC thickening, n (%)	p-value
< 1 year	11 (27.0)	2 (5.0)	0.001	10 (16.4)	3 (13.0)	0.004
1-3 years	24 (59.0)	18 (41.0)		35 (57.3)	7 (29.0)	
4-6 years	5 (12.0)	16 (36.0)		9 (18.1)	12 (42.0)	
≥ 7 years	1 (2.0)	8 (18.0)		4 (8.2)	5 (16.0)	
Total	41	44		58	27	

^aSubscapularis, supraspinatus, and long head of the biceps (LHB) tendons included.
ESRD: end-stage renal disease; RC: rotator cuff; US: ultrasound.

patients were on hemodialysis for more than 7 years. Fifth, interobserver and intraobserver concordance were not evaluated. Sixth, tendon thickness can sometimes be overestimated, especially when associated with an inflammatory process.

CONCLUSION

This study showed a high frequency of abnormal US findings in the shoulders of ESRD patients on hemodialysis. RC tendon thickening was the most frequent and showed a significant association with a longer duration of hemodialysis. US examination is a useful

diagnostic tool for detecting US abnormalities in the shoulder caused by prolonged hemodialysis. As the longevity of hemodialysis patients continues to increase, there is little doubt that these findings will become more prevalent⁵. There is a need for cohort studies with more patients to validate the quantitative US findings of RC tendons in Mexican patients with ESRD compared to patients with normal renal function. US examination is a relatively sensitive and highly specific non-invasive imaging modality that can be used as an aid in the early detection and diagnosis of shoulder arthropathy associated with hemodialysis.

Acknowledgments

The authors thank Professor Ana M. Contreras-Navarro for her guidance in preparing and writing this scientific paper. This original research in the Radiology Specialty field was an awarded thesis at the Segunda Convocatoria Nacional 2023-2024, "Las Mejores Tesis de Radiología para Publicar en el JMEXFRI."

Funding

This research received no external funding.

Conflicts of interest

The authors declare that they have no conflicts of interest.

Ethical disclosures

Protection of individuals. This study was conducted in compliance with the Declaration of Helsinki (1964) and its subsequent amendments.

Confidentiality of data. The authors declare they followed their center's protocol for sharing patient data.

Right to privacy and informed consent. Informed consent was not required for this observational study of information collected during routine clinical care.





Use of artificial intelligence for generating text.

The authors did not use generative artificial intelligence to prepare this manuscript and/or create tables, figures, or figure legends.

REFERENCES

1. Slavotinek JP, Coates PT, McDonald SP, Disney AP, Sage MR. Shoulder appearances at MR imaging in long-term dialysis recipients. *Radiology*. 2000;217(2):539-543. doi:10.1148/radiology.217.2.r00nv05539.
2. Tharwat S, Nagy E, Mohsen M, Nassar MK. Ultrasound Versus Magnetic Resonance Imaging in the Evaluation of Shoulder Pain in End Stage Renal Disease Patients on Chronic Hemodialysis. *Int J Clin Pract*. 2022; 28;2022:1315446. doi:10.1155/2022/1315446.
3. Ando A, Hagiwara Y, Sekiguchi T, Koide M, Kanazawa K, Watanabe T, et al. Magnetic resonance imaging classification of haemodialysis-related amyloidosis of the shoulder: risk factors and arthroscopic treatment. *Knee Surg Sports Traumatol Arthrosc*. 2017;25(7):2217-2224. doi:10.1007/s00167-016-4033-1.
4. Cardinal E, Buckwalter KA, Braunstein EM, Raymond-Tremblay D, Benson MD. Amyloidosis of the shoulder in patients on chronic hemodialysis: sonographic findings. *AJR Am J Roentgenol*. 1996;166(1):153-156. doi: 10.2214/ajr.166.1.8571867.
5. Sommer R, Valen GJ, Ori Y, Weinstein T, Katz M, Hendel D, et al. Sonographic features of dialysis-related amyloidosis of the shoulder. *J Ultrasound Med*. 2000;19(11):765-770. doi: 10.7863/jum.2000.19.11.765.
6. Habas E, Rayani A, Khammaj A. Long-term Complications of Hemodialysis Long-term Complications of Hemodialysis. *Sebha Med J*. 2012;11(1): 1-15.
7. Kay J, Benson CB, Lester S, Corson JM, Pinkus GS, Lazarus JM, et al. Utility of high-resolution ultrasound for the diagnosis of dialysis-related amyloidosis. *Arthritis Rheum*. 1992;35(8):926-932. doi:10.1002/art.1780350812.
8. Coari G, Iagnocco A, Maggi S, Bracci M, De Cata A, Mastantuono M, et al. Sonographic findings in haemodialysis-related chronic arthropathy. *Eur Radiol*. 1996;6(6):890-894. doi: 10.1007/BF00240698.
9. Beggs I. Shoulder ultrasound. *Semin Ultrasound CT MR*. 2011;32(2): 101-113. doi:10.1053/j.sult.2010.10.003.

Imaging findings in synchronous bilateral breast cancer: a case report

Jorge A. Montero-Torres^{1,a*}, Sofia Salas-Aguirre^{2,b}, Sergio O. Meza-Chavolla^{2,c} and Elizabeth Alvarez-Gonzalez^{3,d}

¹Departamento de Radiología e Imagen, Hospital de Especialidades, Centro Medico Nacional del Bajío, Instituto Mexicano del Seguro Social, Leon, Guanajuato; ²Unidad de Detección y Diagnóstico de Cáncer de Mama, Instituto Mexicano del Seguro Social, Guadalajara, Jalisco; ³Unidad Médica de Alta Especialidad Hospital de Gineco-Obstetricia, Centro Medico Nacional de Occidente, Guadalajara, Jalisco. Mexico

ABSTRACT

Bilateral breast cancer is when malignant lesions are present in both breasts; synchronous bilateral breast cancer is rare. We report the case of a 74-year-old woman who sought medical attention due to a palpable lump in her left breast. A mammogram and ultrasound (US) were performed. The mammogram showed an irregular isodense mass with an indistinct margin in the right breast without other associated findings. Focal asymmetry was detected in the left breast. US showed an irregular hypoechoic mass with parallel orientation and an indistinct margin in the periareolar region of the right breast, BI-RADS category 5. US showed a hypoechoic irregular mass, not parallel orientation with an indistinct angular margin in the left breast. BI-RADS category 5. Lymph nodes with normal US features were found in both axillary regions. Core needle biopsies of both masses showed an invasive mucinous carcinoma in the right breast and a microinvasive ductal carcinoma in the left breast. This case report highlights the critical role of mammography and US in identifying and characterizing synchronous bilateral breast cancer. This case report is for educational purposes since distinguishing synchronous and metachronous bilateral breast cancer is critical for diagnosis and treatment.

Keywords: Bilateral breast cancer. Synchronous breast cancer. Case report.

INTRODUCTION

Breast cancer is the most common malignant neoplasm in women worldwide¹. In 2020, approximately 2.3 million women were newly diagnosed¹. It is considered bilateral when malignant lesions affect both breasts and occurs in up to 12% of cases. It is usually asynchronous²⁻⁴ with synchronous cancer comprising 3%². Contralateral synchronous breast cancer can occur simultaneously or over time after remission³. Bilateral synchronous cancer occurs within 1 month to 1 year. In contrast, if cancer is detected in the contralateral breast more than one year after treatment, it is considered metachronous cancer^{3,5-8}.

Synchronous bilateral breast cancer has a higher mortality risk, while metachronous cancer has a similar prognosis to unilateral breast cancer if no lymph nodes are involved⁸. Synchronous bilateral breast cancer has a poor prognosis with low survival and a higher rate of distant metastasis⁹. Vuoto et al.⁹ reported that the 5-year survival rate was 85.9% for unilateral breast cancer, 94.6% for metachronous breast cancer, and 63.3% for synchronous breast cancer. The distinction between synchronous and metachronous bilateral breast cancer is critical for diagnosis and treatment. This case report is of a 74-year-old woman who sought medical attention due to a palpable lump in her left breast and underwent a mammogram and ultrasound (US).

*Corresponding author:

Jorge A. Montero-Torres
E-mail: jorge_montero08@hotmail.com

Received for publication: 10-03-2024

Accepted for publication: 20-07-2024

DOI: 10.24875/JMEXFRI.24000010

Available online: 03-10-2024

J Mex Fed Radiol Imaging. 2024;3(3):197-201

www.JMeXFRI.com

2696-8444 / © 2024 Federación Mexicana de Radiología e Imagen, A.C. Published by Permanyer. This is an open access article under the CC BY-NC-ND (<https://creativecommons.org/licenses/by-nc-nd/4.0/>).

CASE DESCRIPTION

The patient is a 74-year-old woman with a palpable lump in her left breast. Her family history revealed that her mother and a sister had had breast cancer. A mammogram performed at another clinic one month before revealed an irregular mass at 12 o'clock in the left breast.

Imaging findings

Mammography

A mammogram was performed using a Selenia™ Dimensions Mammography System (Hologic, Inc., Marlborough, MA, USA). The right breast showed an irregular, isodense mass in the anterior third of the central region, with an indistinct margin and no other associated findings. Focal asymmetry was detected in the left breast in the middle third of the interline of the upper quadrant with no change in the mediolateral oblique view with BIRADS category 5 (Figures 1 and 2).

Ultrasound

US examination was performed with a MyLab Seven™ device (Esaote Co. Genoa, Italy) with a 14 MHz multifrequency linear transducer. US grayscale showed an irregular hypoechoic mass in the periareolar region of the right breast between 8 and 9 o'clock, with parallel orientation and an indistinct margin, BI-RADS category 5. Color Doppler US showed no flow signal, and real-time elastography strain (E-Strain) showed intermediate hardness (Figure 3).

An US grayscale of the left breast showed an irregular, not parallel orientation, hypoechoic mass at 11 and 12 o'clock, 1 cm from the nipple with an indistinct and angular margin. BI-RADS category 5. Peripheral vascularity was found on color Doppler, and the mass was rigid on elastography (Figure 4). Lymph nodes with normal US features were found in both axillary regions.

Histopathological findings

A core needle biopsy of each mass was performed. The right breast mass was an invasive mucinous

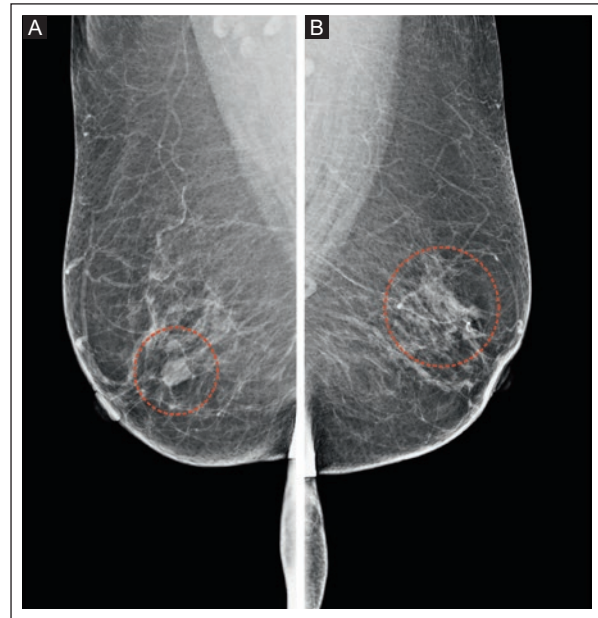


Figure 1. Bilateral mammogram of a 74-year-old woman with synchronous bilateral breast cancer. **A:** a mediolateral oblique view shows an irregularly shaped mass in the right breast with an indistinct margin and equal density (dotted circle). No other features. **B:** the left breast with focal asymmetry (dotted circle).

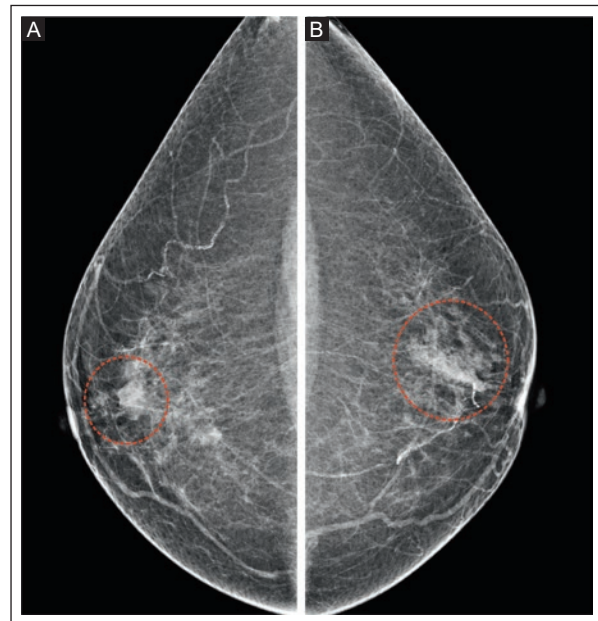


Figure 2. Bilateral mammogram of a 74-year-old woman with synchronous bilateral breast cancer. **A:** the craniocaudal view shows an irregularly shaped mass in the right breast with an indistinct margin and equal density (dotted circle). **B:** the left breast with focal asymmetry (dotted circle).

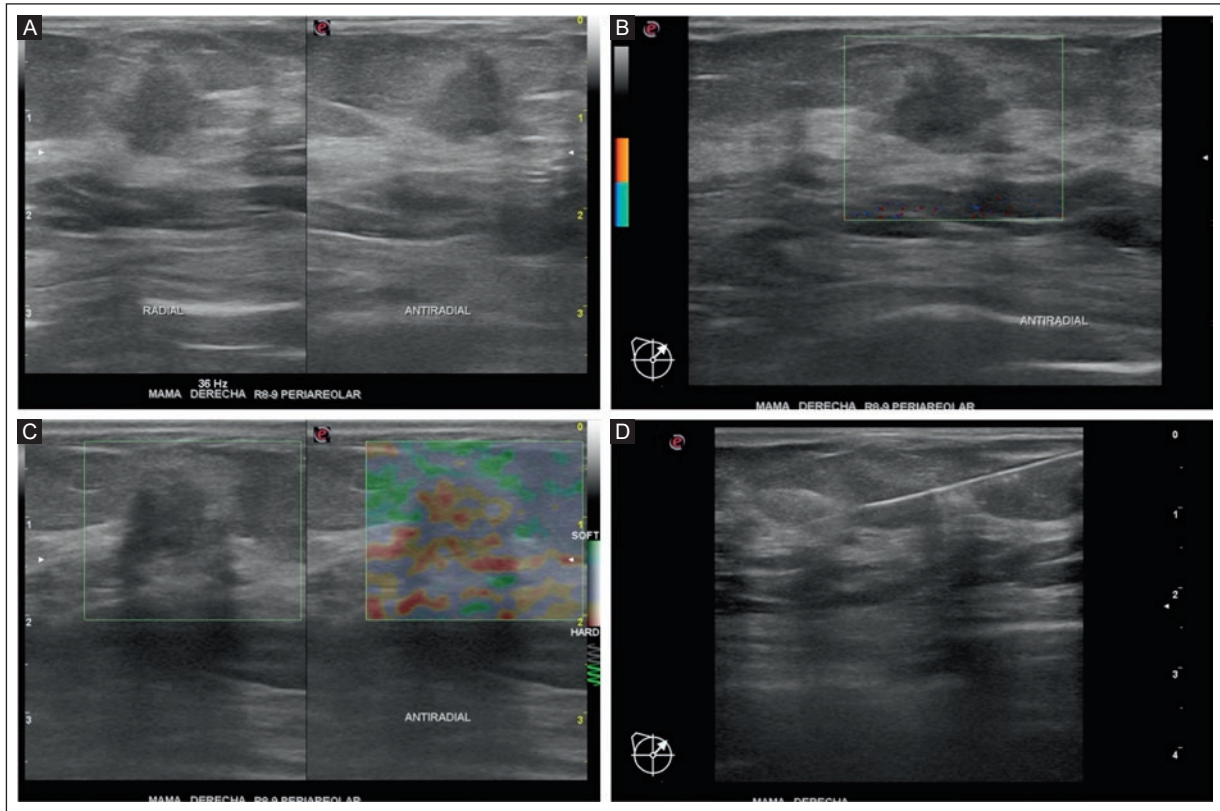


Figure 3. US of a 74-year-old woman with synchronous bilateral breast cancer. **A:** grayscale US of the right breast in radial and antiradial view shows an irregular hypoechoic mass with parallel orientation and an indistinct margin. **B:** there is no flow signal on color Doppler US. **C:** there is intermediate hardness on qualitative elastography. **D:** a hyperechoic needle is seen in the mass during the biopsy, BI-RADS 5. US: ultrasound.

carcinoma, and the left breast mass was a microinvasive ductal carcinoma with molecular subtype luminal A in both.

Clinical outcome

The patient underwent a bilateral total mastectomy and a bilateral sentinel lymph node biopsy, which was normal. The pathologic findings were consistent with the biopsies. Chemotherapy and radiotherapy were administered.

DISCUSSION

This case report is about a woman with synchronous bilateral breast cancer in whom mammography showed a mass in the right breast and focal asymmetry in the left breast. US examination showed masses

in both breasts with different histopathologic diagnoses. This case report is published for educational purposes because a diagnosis of synchronous bilateral breast cancer should always be considered when bilateral malignant suspicious lesions are found on breast imaging.

The development of a second primary cancer in the contralateral breast, especially if it occurs synchronously, is associated with worse survival and is an independent risk factor for mortality⁸. The lesion in the contralateral breast in our patient was a focal asymmetry detected on mammography. Subsequent US showed an irregular hypoechoic mass with non-parallel orientation and angular margins classified as BIRADS 5. Vuoto et al.⁸ found that contralateral synchronous cancer was a nonpalpable breast lesion in 21 (26.2%) of 80 women and was detected by imaging, as was the case in our patient. Naik

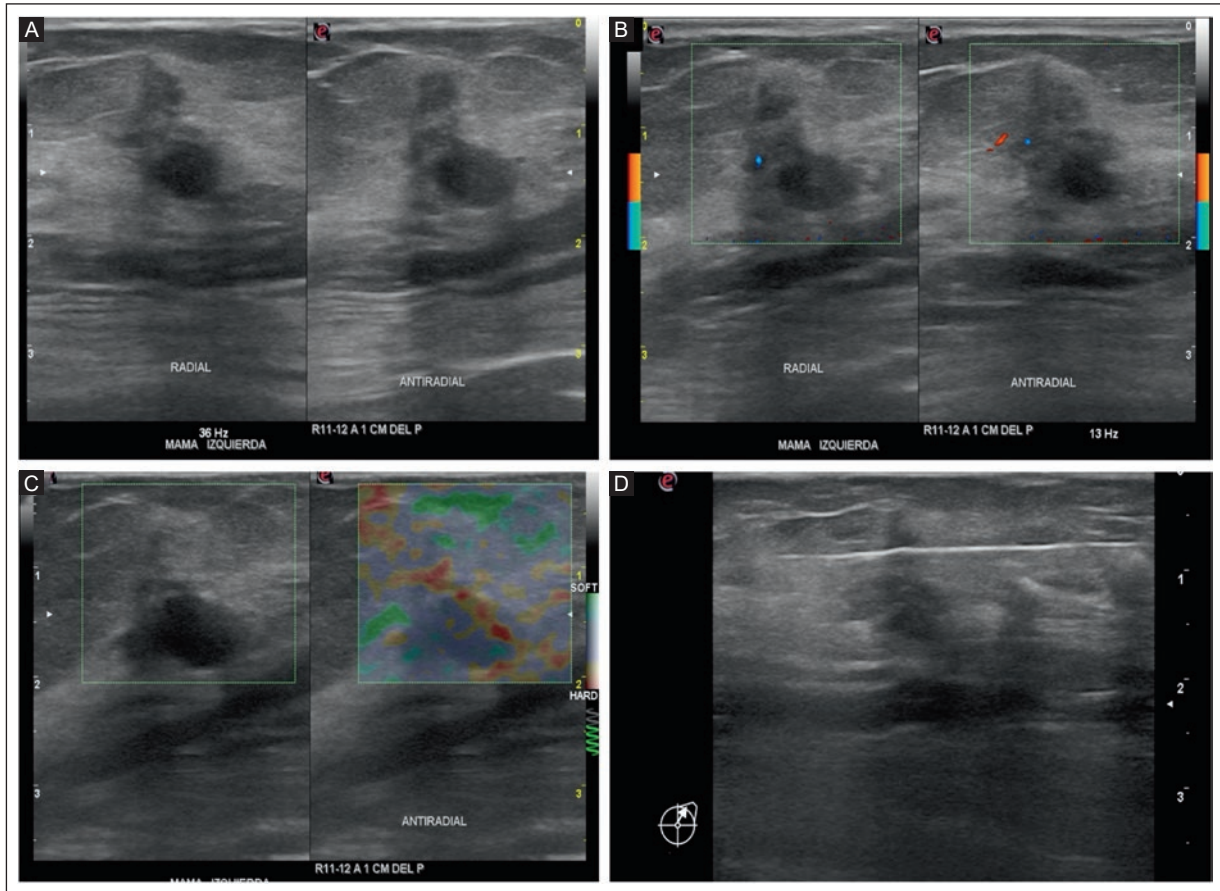


Figure 4. US of a 74-year-old woman with synchronous bilateral breast cancer. **A:** a grayscale US of the left breast in radial and antiradial view shows a hypoechoic, non-parallel, irregular mass with an angular margin. **B:** peripheral vascularity on color Doppler US. **C:** rigid qualitative elastography, BI-RADS 5. **D:** a hyperechoic needle is seen in the mass during the biopsy. Lymph nodes with normal US features were found in both axillary regions.

US: ultrasound.

et al.² reported the case of a 58-year-old woman with a palpable lump in the right breast. Mammography and US revealed a 4.5 cm suspicious mass in the mid-posterior upper outer quadrant of the right breast. In contrast, no significant suspicious lesions were initially detected in the left breast. Mammography and US play a critical role in identifying synchronous bilateral breast cancer^{7,8,10}.

Risk factors for bilateral cancer include age at diagnosis, with a higher risk under 40 years of age, a family history of breast cancer, lobular carcinoma in situ, invasive lobular carcinoma, and a multifocal or multicentric malignant neoplasm^{5,7,8,11}. In our case, the patient had a family history of breast cancer in first-degree relatives. In contrast, Vuoto et al.⁸ showed a statistically non-significant trend in the group of synchronous cancer in women with a positive family history of breast cancer.

Imaging examination involving the axillary lymph nodes provides valuable information for prognosis and staging. The sentinel lymph node remains the standard of care for early breast cancer, but preoperative US examination has become increasingly important for staging. Kijima et al.¹² reported an US accuracy of 79.7 % in detecting axillary lymph node metastases in 380 patients. They found a statistically significant correlation between US assessment of lymph node levels and histopathologic findings and suggested US characterization of lymph nodes at the axillary level to establish the relationship between the risk of distant metastasis and treatment. In this case report, the lymph nodes appeared normal on US with histopathologic confirmation. Overall, an individualized, patient-specific, multidisciplinary approach remains essential for the comprehensive treatment of bilateral breast cancer.

Treatment options for synchronous bilateral breast cancer include breast-conserving surgery, mastectomy, radiotherapy, systemic chemotherapy, endocrine therapy, or targeted therapy². In our patient the treatment approach was bilateral total mastectomy followed by chemotherapy and radiotherapy. It is recommended to determine the stage and treatment based on the primary breast cancer criteria, as there is still no consensus on the approach for treating synchronous bilateral breast cancer. The prognosis and treatment options for synchronous bilateral breast cancer depend on several factors, including the stage, histologic grade, and other prognostic factors of each tumor².

CONCLUSION

This case report showed synchronous bilateral breast cancer with different histopathologic diagnoses. Abnormal mammographic and US findings suspected of malignancy were found in both lesions. It is important to define the timing of synchronous bilateral breast cancer clearly and to differentiate between metachronous and synchronous lesions.

Acknowledgments

The authors thank Professor Ana M. Contreras-Navarro for her guidance in preparing and writing this scientific paper.

Funding

This paper received no external funding.

Conflicts of interest

The authors declare no conflicts of interest.

Ethical disclosures

Protection of individuals. This paper complies with the Declaration of Helsinki (1964) and its subsequent amendments.

Data confidentiality. The authors declare they followed their center's protocol for sharing patient data.

Right to privacy and informed consent. Informed consent was not required to analyze and publish routinely acquired clinical and imaging data.

Use of artificial intelligence: The authors state that they did not use generative artificial intelligence to prepare this manuscript and/or create figures or figure legends.

REFERENCES

1. Sung H, Ferlay J, Siegel RL, Laversanne M, Soerjomataram I, Jemal A, et al. Global Cancer Statistics 2020: GLOBOCAN Estimates of Incidence and Mortality Worldwide for 36 Cancers in 185 Countries. *CA Cancer J Clin.* 2021;71(3):209-249. doi:10.3322/caac.21660.
2. Naik HR, Prather AD, Gurda GT. Synchronous Bilateral Breast Cancer: A Case Report Piloting and Evaluating the Implementation of the AI-Powered Large Language Model (LLM) ChatGPT. *Cureus.* 2023; 15(4):e37587. doi: 10.7759/cureus.37587.
3. Boufettal H, Samouh N. Synchronous bilateral breast cancer in Morocco: epidemiological and clinical characteristics. *Pan Afr Med J.* 2015;20:118. doi:10.11604/pamj.2015.20.118.6136.
4. Lim GH, Hoo JX, Shin YC, Choo RZT, Wong FY, Allen JC. Is Metastatic Staging Needed for All Patients with Synchronous Bilateral Breast Cancers? *Cancers (Basel).* 2023;16(1):17. doi: 10.3390/cancers16010017.
5. Kim MJ, Kim EK, Kwak JY, Park BW, Kim SI, Oh KK. Bilateral synchronous breast cancer in an Asian population: mammographic and sonographic characteristics, detection methods, and staging. *AJR Am J Roentgenol.* 2008;190(1):208-213. doi:10.2214/AJR.07.2714.
6. Gollamudi SV, Gelman RS, Peiro G, Schneider LJ, Schnitt SJ, Recht A, et al. Breast-conserving therapy for stage I-II synchronous bilateral breast carcinoma. *Cancer.* 1997;79(7):1362-1369. doi: 10.1002/(sici)1097-0142(19970401)79:7.
7. McCredie JA, Inch WR, Alderson M. Consecutive primary carcinomas of the breast. *Cancer.* 1975 ;35(5):1472-1477. doi: 10.1002/1097-0142(197505)35:5.
8. Vuoto HD, García AM, Candás GB, Zimmermann AG, Uriburu JL, Isetta JA, et al. Bilateral breast carcinoma: clinical characteristics and its impact on survival. *Breast J.* 2010;16(6):625-632. doi: 10.1111/j.1524-4741.2010.00976.x.
9. Bellanger M, Zeinomar N, Tehranifar P, Terry MB. Are Global Breast Cancer Incidence and Mortality Patterns Related to Country-Specific Economic Development and Prevention Strategies? *J Glob Oncol.* 2018; 4:1-16. doi:10.1200/JGO.17.00207.
10. Janschek E, Kandioler-Eckersberger D, Ludwig C, Kappel S, Wolf B, Taucher S, et al. Contralateral breast cancer: molecular differentiation between metastasis and second primary cancer. *Breast Cancer Res Treat.* 2001;67(1):1-8. doi:10.1023/a:1010661514306.
11. Lopez-Mendez JI, Delgadillo-Cristerna R, Rodriguez-Pulido G. Unifocal, multifocal, or multicentric breast cancer distribution patterns on multiplanar breast MRI: a technical note. *J Mex Fed Radiol Imaging.* 2024;3(1):56-61. doi: 10.24875/JMEXFRI.24000001.
12. Kijima Y, Yoshinaka H, Hirata M, Mizoguchi T, Ishigami S, Nakajo A, et al. Number of Axillary Lymph Node Metastases Determined by Preoperative Ultrasound is Related to Prognosis in Patients with Breast Cancer. *Cancers (Basel).* 2010;2(1):20-31. doi:10.3390/cancers2010020.

Contrast-enhanced CT: aortocaval fistula secondary to a ruptured abdominal aortic aneurysm

Amit Shrivastava¹ , Gottumukkala Maichael Goodwin² , and Gunjan Jindal^{2*} 

¹Department of Interventional Radiology; ²Department of Radiodiagnosis. Maharishi Markandeshwar Institute of Medical Sciences and Research, Mullana, Haryana, India

An aortocaval fistula (ACF) secondary to spontaneous rupture of an abdominal aortic aneurysm (AAA) into the inferior vena cava (IVC) was first reported in 1831 by James Syme¹. ACF is a rare complication of infrarenal AAA, accounting for 3-6% of all rupture cases, and it is associated with a mortality rate of 40%^{2,3}. AAA expansion/erosion is responsible for 80% of ACFs. Trauma accounts for 15%, and 5% are iatrogenic. Less

common causes include mycotic aneurysms, arteritis, and connective tissue disease^{4,5}. Contrast-enhanced CT typically shows a large infrarenal abdominal aortic aneurysm with equal aorta and IVC enhancement

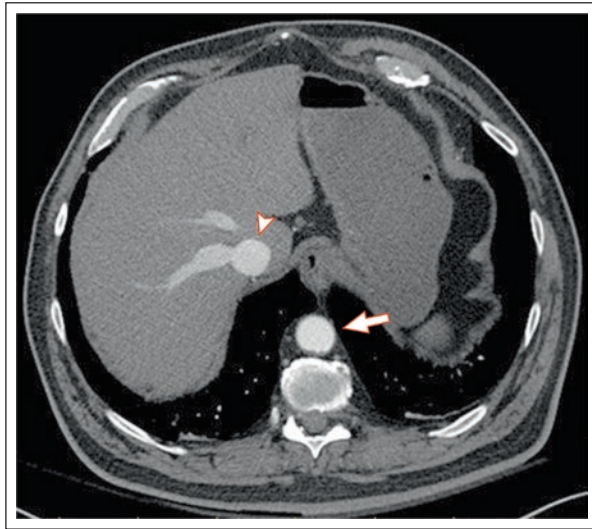


Figure 1. Axial arterial phase contrast-enhanced CT shows equal enhancement in the aorta (arrow) and IVC (arrowhead). The contrast medium flowing back into the hepatic veins indicates possible venous hypertension.

CT: computed tomography; IVC: inferior vena cava.



Figure 2. Coronal arterial phase contrast-enhanced CT shows an infrarenal AAA (arrow), an arterially enhanced compressed IVC (arrowhead), and an ACF (dashed circle).

AAA: abdominal aortic aneurysm; ACF: aortocaval fistula; IVC: inferior vena cava.

Corresponding author:

*Gunjan Jindal
E-mail: dr.gunjanvjindal@gmail.com

Received for publication: 06-07-2023

Accepted for publication: 20-07-2024

DOI: 10.24875/JMEXFRI.23000011

Available online: 03-10-2024

J Mex Fed Radiol Imaging. 2024;3(3):202-203

www.JMeXFRI.com

2696-8444 / © 2024 Federación Mexicana de Radiología e Imagen, A.C. Published by Permanyer. This is an open access article under the CC BY-NC-ND (<https://creativecommons.org/licenses/by-nc-nd/4.0/>).

(Figure 1). A fistulous communication between the aorta and the IVC is usually identified (Figure 2).

Symptoms and signs can vary greatly in severity and are often of relatively recent onset. Abdominal and/or back pain are common. Signs include high-output heart failure, liver congestion, and kidney failure. Rapid diagnosis and treatment are critical to survival. Fistula closure by open surgery (which takes longer) or an endovascular approach is necessary. The endovascular approach is faster, but is complicated in up to 50% by endoleaks (persistent blood flow within the aneurysm sac). This entity is difficult to diagnose, contrast-enhanced CT is the diagnostic modality of choice.

Funding

This paper received no external funding.

Conflicts of interest

The authors declare no conflicts of interest.

Ethical disclosures

Protection of individuals. This report complies with the Declaration of Helsinki (1964) and subsequent amendments.

Data confidentiality. The authors declare they followed their center's protocol for sharing patient data.

Right to privacy and informed consent. Informed consent was not required to analyze and publish routinely acquired clinical data.

Use of artificial intelligence. The authors did not use generative artificial intelligence in preparing this manuscript or creating figures or figure legends.

REFERENCES

1. Syme J. Case of Spontaneous Varicose Aneurism. *Edinb Med Surg J.* 1831;36(108):104-105.
2. Schmidt R, Bruns C, Walter M, Erasmi H. Aorto-caval fistula—an uncommon complication of infrarenal aortic aneurysms. *Thorac Cardiovasc Surg.* 1994;42(4):208-211. doi: 10.1055/s-2007-1016489.
3. Woolley DS, Spence RK. Aortocaval fistula treated by aortic exclusion. *J Vasc Surg.* 1995;22(5):639-642. doi: 10.1016/s0741-5214(95)70053-6.
4. Orion KC, Beaulieu RJ, Black JH, 3rd. Aortocaval Fistula: Is Endovascular Repair the Preferred Solution? *Ann Vasc Surg.* 2016; 31:221-228. doi: 10.1016/j.avsg.2015.09.006.
5. Lorenzati B, Perotto M, Bottone S, Tenconi G, Gazzina G, Cataldi W. Aortocaval fistula. *Intern Emerg Med.* 2014;9(8):895-896. doi: 10.1007/s11739-014-1076-5.